GROWTH OF SAMS ON GAAS FOR OPTICAL BIOSENSING APPLICATIONS

GROWTH AND CHARACTERIZATION OF ALKANETHIOL SELF-ASSEMBLED MONOLAYERS ON GaAs FOR USE IN OPTICAL BIOSENSING APPLICATIONS

By

HANNA BUDZ, B.Eng.Mgt.

A Thesis

Submitted to the School of Graduate Studies

In Partial Fulfilment of the Requirements

for the Degree

Doctor of Philosophy

McMaster University

DOCTOR OF PHILOSOPHY (2010)
(Engineering Physics)

McMaster University
Hamilton, Ontario

TITLE:	Growth and Characterization of Alkanethiol Self-Assembled Monolayers on GaAs for use in Optical Biosensing Applications
AUTHOR:	Hanna Budz, B.Eng.Mgt. (McMaster University)
SUPERVISOR:	Professor Ray R. LaPierre
NUMBER OF PAGES:	xv, 153

Abstract

The first part of this study details the formation and characterization of octadecanethiol (ODT) self-assembled monolayers (SAMs) on GaAs (100) substrates from solution and vapor phases. The liquid-phase-deposited monolayers were prepared by immersing the substrate in an ethanolic solution, while vapor-deposited monolayers were prepared by the vapor phase transport of ODT in an ultrahigh vacuum (UHV) environment. The structural and optical properties of the resulting SAMs were examined with contact angle (CA) analysis, photoluminescence (PL) spectroscopy, atomic force microscopy (AFM), high-resolution x-ray photoelectron spectroscopy (HRXPS), and spectroscopic ellipsometry. Although well-ordered films were formed by both preparation routes, PL, AFM, CA analysis, HRXPS, and ellipsometry measurements revealed that the overall quality, structure, and durability of the monolayers depend on the deposition technique. Collectively, the results suggested that more robust monolayers exhibiting greater surface coverage and therefore, increased passivation and stability characteristics are assembled from vapor phase.

The second part of this work describes the development of a hybrid GaAs-aptamer biosensor for the label-free detection of analytes. The implemented sensing strategy relies on the use of functional alkanethiol SAMs as biorecognition elements as well as the sensitivity of the GaAs PL emission to the local environment at its surface. Specifically, GaAs substrates were modified with thiol-derivatized aptamers and exposed to the target biomolecules. The resulting modification in the PL intensity is attributed to a specific aptamer-target biorecognition interaction and the accompanying ligand-induced structural change in the aptamer conformation. Modeling the performance data by means of Poisson-Boltzmann statistics in combination with the dead layer model indicates a

good correlation between the structural conformation of the aptamers and the GaAs PL yield. The results demonstrate the potential of the prospective luminescence-based GaAs-SAM biosensor in real-time sensing assays requiring a simple and effective means of direct analytical detection.

Preface

The work presented in this thesis has been previously published in the form of two refereed journal articles and one submitted manuscript currently under review (permission for the reproduction of published work is given in Appendix A).

Articles Published in Refereed Journals:

1. H. Budz and R. LaPierre, J. Vac. Sci. Technol. A 26, 1425 (2008).
2. H. Budz, M. Biesinger, and R. LaPierre, J. Vac. Sci. Technol. B 27, 637 (2009).

Articles Accepted for Publication in a Refereed Journal:

1. H. A. Budz, M. Ali, Y. Li, and R. R. LaPierre, accepted for publication on Apr. 7, 2010 in J. Appl. Phys.

Acknowledgements

I would like to acknowledge the support and guidance of a number of key people who over the years have contributed to my progress as a researcher as well as to my overall experience at McMaster University.

First and foremost, I would like to thank my thesis advisor, Dr. Ray LaPierre, for introducing me to the concept of self-assembly and giving me the opportunity to work on this interesting research project. His valuable insight and support throughout the course of this work are directly responsible for my success as a graduate student. He allowed me the freedom to challenge myself academically while providing me with the guidance necessary to achieve my research goals.

I would also like to extend my thanks and appreciation to my supervisory committee members, Dr. Peter Mascher and Dr. Peter Kruse, for reviewing my progress, providing constructive advice, and sharing their unique perspectives.

During my graduate studies at McMaster University, I have had the pleasure of working with a number of colleagues who deserve special mention. I would most like to thank my closest group members Chris, Subir, and Parsian for providing a fun and stimulating environment both inside the lab and out, as well as for their scientific opinion and kind help with technical issues. Likewise, I would especially like to thank Martin Plante for the emotional support, friendship, and sheer entertainment that he provided.

I wish to thank several researchers associated with the CEDT. First, thanks extend to Doris Stevanovic, for her genuine concern regarding my well-being and for her compassion towards others. Next, I must thank Dr. Jacek Wojcik for sharing his vast knowledge of ellipsometry and for supplying countless pieces of

spare equipment necessary to keep this research project going. I would also like to express my sincere gratitude to Dr. Brad Robinson. His practical, hands-on approach to research coupled with his untiring work ethic is exemplary and inspirational. He has patiently taught me the value of thinking on one's feet. I would have been lost without the input that he provided through many hours of pertinent discussion and technical assistance on several aspects of this project.

Much appreciation goes out to the staff of the CCEM. In particular, I would like to acknowledge Andy Duft and Steve Koprich for their instructive assistance with the microscopy-related instrumentation. Also, I must recognize Dr. Glynis de Silveira for helping me to establish a collaboration with Dr. Yingfu Li's group, which resulted in the biological component of this work. Moreover, I would like to thank Dr. Yingfu Li and his post-doctoral fellow, Dr. Monsur Ali, for supplying the biological materials and expertise needed to produce the hybrid biosensors discussed in this thesis.

For their financial support, I would also like to acknowledge the various funding agencies that sustained this work either through grants or scholarships, including the Ontario Photonics Consortium, and the Natural Sciences and Engineering Research Council of Canada.

From the bottom of my heart, I wish to thank my parents, Krzysztof and Hanna Bohdanowicz, who have both sacrificed so much throughout their lives to bring us to this country in the hopes of giving us a brighter future. Without their unconditional love and encouragement, I would not have had the courage to pursue a higher education. Special thanks also go to my brother, Michal, for his keen sense of humor and my babcia, Janina Mergo, for showing me the power of true spirituality.

Most importantly, I would like to thank my husband, Andrew, and our furry friend, Snickers, for the love, support, and snuggles that you provide on a daily basis. You have enriched my life in immeasurable ways and I look forward

to spending the rest of it with you. Finally, I wish to thank the newest soon-to-be-member of our family, who I dearly hope will decide to wait until after this thesis is defended to make his/her debut into the world. Although we do not know each other very well yet, you have given a new, wonderful perspective on life that can only be gained through impending motherhood. For that, I thank you, *little one*.

Contents

List of Figures

List of Tables

Chapter 1 Introduction

1.1 Outline

The modern field of materials science and engineering has greatly broadened over the past decades with renewed interest of researchers in the interactions between molecules and surfaces. One of the most intensively studied areas of surface science is the spontaneous self-organization of atoms and molecules on surfaces into highly ordered, two-dimensional arrays [1]. Since the theme of molecular self-assembly is at the core of numerous naturally occurring biological, physical, and chemical processes such as in the formation of living cells, it is not surprising that this phenomenon has attracted considerable attention [2]. A major driving force behind this research trend involves the development of novel bottom-up fabrication techniques which have the potential to overcome the limitations of traditional top-down approaches and revolutionize the emerging field of nanoscience. The spontaneous self-assembly of active surfactant molecules adsorbed on various solid substrates has been widely examined in recent years because of the ability of the resulting films to homogenously modify the physical and chemical properties of the substrate surfaces. Self-assembled monolayers (SAMs) are particularly relevant from the perspective of their significance to a multitude of scientific and technological applications. The ability to tune the structure and thickness of SAMs at the molecular level has facilitated the development of ultrathin film coatings as well as optical and electronic devices [3]. For example, organosulfur monolayers have been found to minimize

friction in microelectromechanical systems (MEMS) and thus provide an attractive means of lubrication and wear protection [4], [5]. As a result of their closely packed and stable structure, SAMs are also suitable in corrosion inhibition [6], adhesion enhancement [7], [8], and as passivating layers [9], [10]. Likewise, as SAMs can be laterally patterned [11], the films can be used as resist materials to produce ultra-fine nanopatterns on substrates using nanoimprinting [12], microcontact printing [13], or other lithographic techniques [14], [15]. Furthermore, the biomimetic and biocompatible properties of these organic monolayers makes them suitable for chemical and biosensing applications [1], [16]-[19]. In particular, by controlling the chemical functionalities displayed at the exposed interface, SAMs can be used as active layers for the attachment of biorelated molecules in biochemical sensors [20]-[23].

Several different SAM-substrate systems have been investigated since the concept of a monolayer was first introduced in 1917 by Langmuir, encompassing a range of substrates and a wide variety of adsorbates [24]. Some of the more noteworthy chemistries include organosilicon compounds and their derivatives on hydroxylated surfaces, alkyl monolayers on silicon, fatty carboxylic acids on metal oxides, and organosulfur adsorbates on metals and semiconductor [1]. However, the most intensely investigated assembly to date has been that of alkanethiols ($CH_3(CH_2)_{n-1}SH$) on Au since the chemisorption of these hydrocarbon-chained molecules leads to the formation of stable and well-defined monolayers on the metallic surface. For these reasons considerable progress has been made in the investigation of SAMs on Au surfaces (see, for example, [25]-[27]). In comparison, relatively few studies of SAM deposition on compound semiconductors such as III-V surfaces have been reported ([9], [28]-[31]) despite the prospective benefits of hybrid organic-semiconductor systems. In particular, SAMs on III-V semiconductors are promising in the development of innovative technologies ranging from metal-molecule-semiconductor junctions for memory applications and nanowire functional networks to novel biosensors [32]-[34]. A

prominent semiconductor in the III-V family for the synthesis of SAMs is GaAs on account of its unique optical and electronic properties as well as other important criteria necessary for many of the intended applications outlined above [35].

To exploit the opportunities that are presented by the unique combination of organic thin films with III-V materials for a variety of prospective applications, it is necessary to first prepare and characterize the properties of the SAMs on these surfaces. Over the years, many thin film characterization techniques have been developed to analyze the structure and growth dynamics of the supramolecular assemblies. Likewise, two distinct growth methods have been employed to deposit monolayers on solid substrates, namely solution deposition and vapor phase deposition.

The present work investigates the structural and chemical differences between alkanethiol SAMs deposited from solution and from vapor phase on GaAs substrates as well as describes the development of a hybrid aptamer-GaAs optical biosensor. The remaining sections of this chapter provide a concise historical review of the major achievements in the field of SAMs, provide the motivation behind the research, describe the fundamental aspects of the self-assembly process, and illustrate the basic principles behind one of the more noteworthy applications of these systems, namely, biosensors. In the first half of Chapter 2, the methods used to prepare the alkanethiol SAMs on GaAs wafers are discussed in terms of the key growth parameters, experimental conditions, and required laboratory equipment. The advantages and disadvantages of each preparation technique are stressed along with the underlying growth mechanisms. Likewise, the central material constituents needed for the formation of SAMs are briefly summarized. The second half of the chapter is dedicated to the principal characterization tools used in the study of the monolayers along with the relevant instrumental considerations. The pertinent aspects of each analytical method are examined with the intent to introduce the reader to these experimental techniques,

and to establish the groundwork for a better understanding of the models and results discussed in subsequent chapters. Chapter 3 describes the effects of the preparation route on the structural and chemical properties of alkanethiol SAMs deposited on GaAs substrates. In particular, the chapter details the formation of octadecanethiol (ODT) monolayers on the semiconductor surfaces from ethanolic solution and from vapor phase as well as the analysis of the resultant films using contact angle (CA) analysis, photoluminescence (PL) spectroscopy, atomic force microscopy (AFM), and spectroscopic ellipsometry. The experimental results discussed in the chapter provide insight into the overall quality of the monomolecular assemblies on GaAs surfaces and describe the specific differences and similarities between the structural, electronic, and chemical properties of the SAMs obtained by each deposition method. In addition, the discussion in Chapter 3 illustrates the particular aspects of the monolayers highlighted by each analytical tool with respect to the sensitivity of each technique to different features of the film. Chapter 4 is devoted to a supplementary investigation of the chemical bonding characteristics and stability of the SAMs deposited from vapor and liquid phases. Specifically, the durability and optoelectronic characteristics of the resultant ODT monolayers were evaluated over the course of several months by means of CA analysis and PL spectroscopy. Complementary studies using spectroscopic ellipsometry and high-resolution x-ray photoelectron spectroscopy (HRXPS) were conducted to correlate the chemical and structural properties of the films to the efficacy of the resulting passivation. The fabrication and operation of a hybrid aptamer-GaAs luminescence biosensor are described in Chapter 5. The biosensing approach combines a number of useful properties of the thiolated monolayer-GaAs system discussed in the previous chapters with the high affinity and biorecognition specificity of single-strand nucleic acid receptors. A quantitative theoretical model of the stimulated optical response is included. The results presented in this chapter demonstrate the feasibility of the proposed biorecognition method in providing a simple and effective means of label-free

identification of specific biological analytes. Chapter 6 concludes this work and outlines a few of the more fruitful opportunities that remain for future progress in this interdisciplinary research area.

1.2 Historical Review

Although the study of SAMs has only attracted considerable interest in the last few decades, the general concept of a monolayer is centuries old. While Langmuir was credited with performing the first systematic study on the formation of monolayers on the surface of a liquid with his work on the spreading of amphiphiles on water [36], monolayers have been prepared at the air-water interface since the 19th century by Pockels, Rayleigh, Hardy, Deveaux, and others [37], [38]. In 1935, Blodgett demonstrated that a Langmuir monolayer formed at the air-water interface could be physically transferred onto a glass surface leading to the creation of the first Langmuir-Blodgett (LB) film [39]. Although the procedure underlying the formation of LB films is simple, the monolayers obtained are thermodynamically unstable on account of the fact that the molecules are only physisorbed to the solid surface [24]. Consequently, exposure to various solvents or temperature changes can significantly deteriorate the two-dimensional structure of the films [24]. Subsequently in 1946, the first seminal paper documenting the successful chemisorption of a monolayer was published by Zisman and colleagues who spontaneously formed a SAM from a dilute solution of long-chain alcohols in hexadecane on a glass support [40]. The wetting characteristics of the chemisorbed monolayer mimicked those of LB films while the structural properties exhibited well-defined orientation. Three years later, Zisman and Shafrin confirmed that ligating chemical interactions between a metal surface and the headgroup of an adsorbing molecule could produce a closed-

packed monolayer during their study of SAM formation through the immersion of a Pt substrate in an aqueous solution of alkyl amines [41]. The hydrophobic nature and wetting properties of the resulting monolayers were similar to those of films obtained in nonpolar hexadecane [42]. The realization of well-oriented SAMs from a polar solvent proved the preferential adsorption of one chemical moiety over another. Specifically, a preference of ~106 was shown by the amine group for the Pt surface in comparison to the hydroxyl groups of water [41], [42]. Following the initial experiments, Zisman and coworkers investigated a wide range of adsorbate-substrate combinations for the formation of SAMs including long-chain amines, carboxylic acids, and primary amides on metal and metal oxide surfaces [43], [44]. However, the majority of the developed systems displayed low energies of adsorption (in the range of 5 to 15 kcal/mol), were relatively unstable, and only produced low-energy hydrophobic interfaces [42]. It was not until the preparation of S-terminated SAMs on Au that the field of self-assembly witnessed tremendous growth. In 1983 Nuzzo and Allara extended the work of Zisman and first reported the process of self-assembly in alkanethiol-Au systems with the formation of a monolayer of dialkyl disulfide on a Au surface [45]. Subsequently, as a result of a number of related studies on the systems, it was shown that thiols preferentially adsorb on Au forming stable, well-ordered, and densely packed monolayers for two reasons: first, Au is a reasonably inert substrate which does not form a stable oxide and thus can withstand contamination when handled in ambient conditions [46]. Second, Au undergoes an intense and highly specific interaction with the sulfur headgroup, which enables the exclusive formation of organosulfur assemblies in the presence of other chemical species [46]. By employing different organosulfur compounds, it was later shown that energy of the exposed surface could be varied from high to low depending on the chain terminus of the adsorbing molecules [42].

Upon further investigation, the adsorption of S-based chemical functionalities to form two-dimensional monolayers was not restricted to Au as

extensive studies since the initial work performed by Nuzzo and Allara have revealed. Numerous types of substrates used to support the SAMs including Ag, Cu, Ni, Fe, Pt, Hg, Ge, InP, InAs, and GaAs have been explored [1], [38], [47]-[53]. Although the formation of SAMs on compound semiconductor substrates has been demonstrated in earlier studies, the surface coverage, stability, and structural characteristics of the resulting monolayers have not been completely determined and remain somewhat a matter of controversy. Consequently, organosulfur SAMs on coinage metals continue to be the most investigated systems to date. Nevertheless, modification of semiconducting III-V materials with organothiolate SAMs has captured the interest of several researchers in recent years, likely stimulated by the potential applications in pioneering technologies. The majority of current work in this area has focused on the properties of these systems from a fundamental materials science perspective. In particular, studies performed in the last few years by McGuiness et al. have investigated the structural characteristics of solution-deposited n-alkanethiol monolayers on GaAs (100) for a series of chain lengths ($12 \leq n \leq 19$) with an attempt to control the organization and packing density of the monomolecular films [52]-[54]. The group examined the bonding preferences of the monolayers by means of XPS as well as the electron-hole recombination velocities at the GaAs surface [53], [54]. While the results revealed an increase in the degree of organization with the length of the alkyl chains, the data demonstrated only a weak relationship between the SAMs and the surface electronic states of the underlying substrate. In contrast, recent work by Dubowski and coworkers indicates the improved passivation performance of long-chain alkanethiol monolayers prepared from liquid phase on GaAs substrates [10], [55], [56]. Other studies by the group have focused on the ordering process of the thiol molecules on the semiconductor surface during the chemisorption process as well as on the influence of the SAMs on the chemical stability of the material [57], [58]. Likewise, a recent publication by Jun et al. details the dependence of the

monolayer thickness on the molecular length of alkanethiols and alkanedithiols, and investigates the mechanism responsible for the SAM formation on GaAs [28]. The experimental findings presented by the authors show a drastic difference in the thicknesses of the SAMs deposited on GaAs compared to metallic surfaces [28].

In addition to understanding the properties of thiolated SAMs on semiconductor surfaces from a fundamental perspective, current researchers in the field have been actively involved in the development of a number of applications based on these material systems. For example, a recent report by Hang et al. details the surface passivation of InAs nanowire field effect transistors (NWFETs) with ODT SAMs [59]. The authors describe the fabrication procedure of the NWFETs as well as the characterization of their electrical transport properties. The results of the electrical analysis established that the I-V transfer characteristics and the electron mobility of passivated devices are superior to the respective values of unpassivated NWFETs [59]. Likewise, Dassa and coworkers have recently shown the reduction of the base-collector dark current in SAM-functionalized InP/InGaAs heterojunction bipolar transistors by three orders of magnitude [51]. Similarly, Lodha et al., in a study of the electrical behavior of metal/molecule/semiconductor devices in which an alkanethiol monolayer was incorporated between Au and GaAs, demonstrated strongly coupled molecular charge transport through the structures to the bulk GaAs layer [60].

Another current area of applied research in the field of hybrid SAM-semiconductor devices deals with the development of biomolecular detection systems for a variety of bioanalytical applications. Recent experimental work in this area has, for the most part, been preliminary in nature and has focused on the immobilization of the biorecognition elements on the semiconducting platform [61], [62]. For instance, a recent publication by Ye et al. describes the immobilization of SAMs consisting of thiol terminated single-stranded DNA on GaAs [61]. The authors assessed the homogeneity and surface morphology of the

films by means of AFM and fluorescence methods. The data presented by the authors indicate the assembly of the DNA into evenly packed, homogenous films, and thus the feasibility of using different thiolated biomoieties as probes on the semiconductor surface [61]. A similar study conducted by Dubowski's group evaluated the anchoring of avidin on a variety of thiol-GaAs (001) interfaces by means of PL and fluorescence microscopy measurements [62]. The results of the study confirm that the highest efficiency of avidin immobilization occurs on a GaAs surface coated with a loosely packed layer of biotinylated thiol interwoven with another diluent thiol [62].

1.3 Motivation

While a number of scientific groups are currently examining the properties of solution-deposited alkanethiol SAMs on III-V surfaces, research on monolayers prepared from vapor phase has been neglected for the most part. Although the synthesis of organic monolayers is most readily achieved at the bench-scale through the use of conventional solution-based techniques, this type of chemical processing is difficult to execute in industrial manufacturing situations on account of the sensitivity of the reaction to the environmental conditions [63]. Consequently, the use of SAMs deposited from liquid phase in technological applications is often limited due to the quality, reproducibility, and scalability of the resultant films [63]. For the aforementioned reasons, vapor phase deposition of organic thin films appears to be an attractive alternative in the development and manufacturing of novel technologies that rely on the assembly of high quality coatings. To enable the widespread use of these materials in commercial applications, there exists a need for modern systematic studies on the

characteristics of vapor-deposited alkanethiol SAMs on compound semiconductor surfaces.

One of the most intriguing applications for which organic SAMs are particularly well suited is in the design of innovative biosensors that combine the recognition capabilities of biofunctional membranes with the detection sensitivity of semiconducting transducers. While Si has been the most commonly utilized base material for traditional electronic devices, GaAs is an attractive candidate for high performance technologies for several reasons. First, the direct bandgap structure of GaAs results in efficient optical absorption and emission, and thus makes the semiconductor extremely effective in optical and optoelectronic applications [35]. Second, the larger bandgap of GaAs in comparison to Si (1.4 eV vs. 1.1 eV) yields a much lower intrinsic carrier concentration and a much higher intrinsic resistivity than those of Si [64]. The combination of these properties makes GaAs suitable for devices requiring a high degree of isolation and low parasitics [64]. Third, the significantly higher electron mobility of GaAs when compared to that of Si (> 6000 cm^2/V-s vs. > 1300 cm^2/V-s) favors the high-speed performance of GaAs-based devices over Si-based devices [64]. In spite of these benefits, a severe hindrance to the mainstream use of GaAs in established devices is the existence of a large surface state density, which tends to pin the Fermi level of the material at the midgap. Therefore, in addition to actively immobilizing the signaling moieties in a well-distributed fashion, the monolayer must successfully passivate the GaAs surface in order to take full advantage of its useful properties. Although previous studies on the passivation efficacy of alkanethiol SAMs on GaAs (100) have been conducted, the results have been somewhat debatable, especially in terms of the stability of the treatment. Accordingly, more detailed experimental investigations could provide insight into the physical basis of the passivation mechanism as well as the reasons for its success or failure. Moreover, since the majority of recent publications concerning the use of SAM-GaAs systems for biosensing applications have

focused on the immobilization of self-assembled probes on the substrate surface, studies devoted to providing a proof-of-concept of the biosensing capability of this adsorbate-substrate system are essential.

This work addresses pertinent engineering issues of vapor phase synthesis, passivation stability, and bioanalytical application of organothiolate SAMs on GaAs substrates. As outlined earlier, the first part of this thesis examines the properties of vapor-deposited alkanethiol monolayers and compares them to those of solution-deposited films. The second part investigates the characteristics and stability of the passivation provided by the SAMs under industrially relevant conditions. Finally, the third part of this study details the design and analyte detection capability of a hybrid SAM-GaAs optical biosensor in an effort to showcase the potential of these types of devices for revolutionizing the field of biological sensing.

1.4 Fundamental Principles of Self-Assembly

In general, SAMs are best described as two-dimensional arrays that are formed on a solid support through the adsorption of an active surfactant [1]. As the system approaches equilibrium, order in the resultant assemblies is achieved by a spontaneous chemical reaction at the interface which drives the SAM synthesis [1]. To initiate this process, the adsorbate with a specific affinity of its terminus chemisorbs to the substrate surface, as illustrated in Figure 1.1. The inherent simplicity of the self-assembly technique and the robust nature of the resulting surface coatings make this method extremely viable in the fabrication of hierarchical supramolecular structures [38].

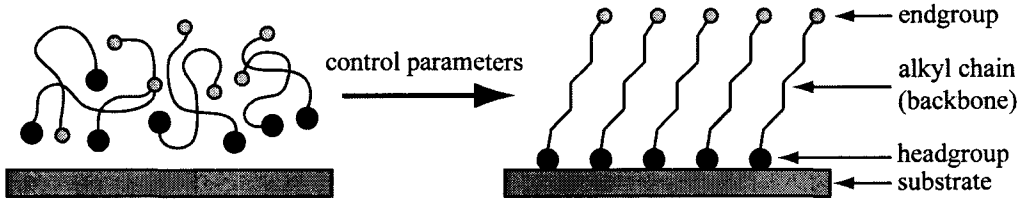

Figure 1.1: Schematic illustration of SAM formation on a solid surface. The main components of a SAM molecule are also outlined.

As depicted in Figure 1.1, the adsorbing SAM molecules can be separated into three distinguishing constituents based on the energetics of each component with respect to the self-assembly process [38]. The first part, referred to as the headgroup, is the defining feature of the molecule and is responsible for its attachment to the substrate. The ensuing intermolecular interaction anchors the headgroup to a particular site on the solid surface through a strong chemical bond [38]. The bond energies related to chemisorption are on the order of a few eV depending on the particular adsorbate-substrate system [38]. For example, the bonding energies of a thiolate monolayer are in the range of 1.63-2.3 eV on Au (111), 2.1 eV on GaAs (100), and 2.19 eV on Cu (111) [65]. On account of the exothermic nature of the chemisorption process, the adsorbing molecules attempt to occupy every available binding site on the surface, filling in the unoccupied spaces between the previously absorbed molecules, thus forming a well-defined domain [38].

The second component of the surfactant molecules is the alkyl chain or backbone (C_nH_{2n+1}). This section of the molecule interacts with the other alkyl chains as the molecules are brought closer together by means of dispersive van der Waals forces that have energies on the order of a few tenths of an eV [38]. Although the short-range van der Waals forces are the primary interactions associated with alkyl chains, polar groups can be incorporated into the chains giving rise to more substantial long-range electrostatic forces that take precedence over the elementary van der Waals interactions [38].

The last molecular constituent of the SAM molecule is the terminal endgroup. In the case of simple alkanethiols, this moiety is a methyl group (CH_3). At room temperature, these external groups are usually thermally disordered and energies related to this process are on the order of a few kTs, where k is Boltzmann's constant and T is the temperature in kelvins [38]. Since a variety of different chemically and biologically relevant functionalities can be used to terminate the alkyl chains (e.g. -OH, -COOH), the endgroup imparts a convenient flexibility on the SAMs that allows the surface properties of the films to be tuned to suit various applications. For instance, the endgroup can be selected such that the monolayer is hydrophilic or hydrophobic [37].

Kinetic studies concerning the preparation of alkanethiol SAMs on III-V semiconductors from solution have demonstrated that monolayers form in two distinct steps [28], [37]. The first step involves the absorption of the thiolate molecules to the substrate surface through a dissociation of the S-H bonds [66], [67]. It is believed that during this stage the molecules are only physisorbed to the surface in a disordered state and are stabilized by van der Waals interactions with the substrate [28], [66]. At an increasing thiolate coverage, the second step of the growth process starts as the molecules begin to self-assemble into an ordered array and transition from the lying down physisorbed state to the standing up chemisorbed state [28], [37]. During this stage, the SAM formation is driven in part by the van der Waals interactions (and in some instances hydrogen bonds [49]) occurring between adjacent alkyl chains. From a kinetics perspective, the time scales on which the two steps take place are very similar with the entire assembly process lasting over 36 hours on semiconductor surfaces [37].

1.5 Basic Principles of Biosensing

As discussed earlier, the prospect of modifying a III-V semiconductor surface with biologically relevant functionalities for the detection of specific analytes is one of the most stimulating applications of SAMs. However, in order to fully appreciate the true potential of these systems in the design of state-of-the-art biosensors, it is instructive to first highlight the fundamental aspects of a biosensor.

A biosensor is typically described as an integrated self-contained analytical device that can be used to detect and monitor the presence of a wide variety of chemical and biological analytes [68]. The detection response is generated through a combination of two key components: a biorecognition element that is responsible for sensing the analyte and producing an appropriate chemical or physical response, and a signal conversion unit or transducer that subsequently converts the response to a measureable output signal [69]. The overall scheme necessary for biosensing is illustrated in Figure 1.2 [69]. As depicted in the diagram, prior to detection, a sampling unit functions to bring the analyte within the vicinity of the bioreceptors. Subsequently, a biochemical reaction between the bioreceptors and analyte occurs which creates the recognition event. Since the bioreceptors are explicitly adapted to react with a certain analyte, they impart a detection specificity and selectivity on the system [70]. To obtain the response from the system, external stimulation in the form of an electrical, optical, or another type of force field is required [69]. With the application of the external stimulus, the physical or chemical response associated with the biorecognition is converted to a quantifiable electrical or optical signal via a transduction mechanism. Examples of some of the more common transduction mechanisms include electrochemical, optical, mass sensitive, and

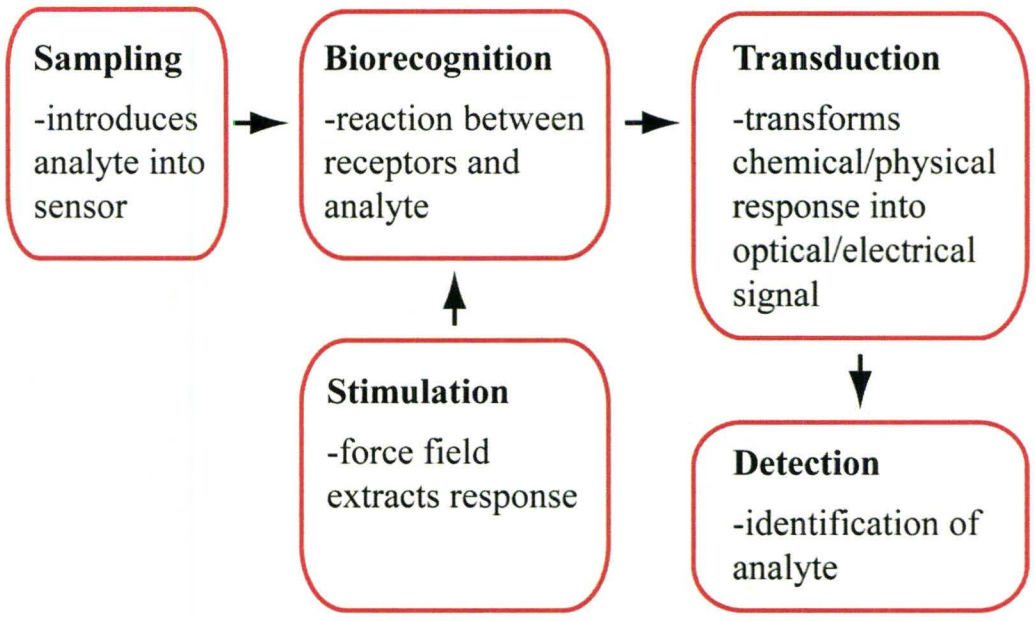

Figure 1.2: Block diagram of the typical functions involved in biosensing [Adapted from [69]].

acoustic wave [70]. Finally, the resultant signal is processed by a detection unit, which includes a suitable scheme for identifying the analyte.

Among the various transduction schemes outlined above, optical transducers that rely on the use of optical phenomena for the detection and identification of different analytes offer a number of key advantages. In particular, these types of sensors exhibit high selectivity and specificity, isolation from electromagnetic interference, fast response, possibility of substantial miniaturization, as well as have the inherent ability to be used in remote sensing applications [69]. Likewise, optical biosensors are capable of taking advantage of unique biorecognition strategies that allow the devices to be tailored for explicit laboratory and point-of-care applications. An important subset of optical-based systems is direct integrated biosensors which possess increased mechanical stability owing to a reduction in the complexity normally associated with conventional labeled techniques [71].

In optical sensing methods, the most commonly used form of stimulation is electromagnetic radiation in the visible or near-infrared spectrum. With the physiological or chemical response that occurs as a result of biorecognition, a change in the amplitude, phase, wavelength, or polarization state is induced in the input light wave by the transduction process [69]. To improve the selectivity and sensitivity of recognition, the biorecognition elements are often immobilized on the surface of the main optical component. Immobilization of the biorecognition elements in the detection region can be accomplished by physical confinement or chemical attachment [69]. While physical methods present a simple means of adsorption, chemical techniques offer specific binding, a defined spatial density distribution, and the minimization of unintentional desorption. Among the various chemical immobilization schemes, thiolated coupling SAMs are a convenient way of providing functionality to biorecognition elements in order to minimize nonspecific binding and promote label-free detection [70]. As mentioned previously, the sulfur headgroup of the monolayers shows a high affinity for a wide range of substrates which facilitates the detection of target analytes in the absence of a label by utilizing the intrinsic properties of the biomolecules [71]. For these reasons, SAMs can be considered as optimal systems for the formation of biosensor layers, in which the biomolecules preserve a high functional activity and are readily accessible by analyte molecules during the assay process [70].

Chapter 2 SAM Deposition and Characterization Techniques

The deposition of chemisorbed molecular films on solid substrates can be achieved by two distinct methods: solution deposition and vapor phase deposition. While the assembly of monolayers has been most frequently performed by immersion of the substrate in a dilute surfactant solution, the deposition of organic thin films from vapor phase presents numerous benefits. In this chapter, the preparation techniques as applied to the deposition of alkanethiol SAMs on GaAs are discussed in terms of the main growth parameters, experimental conditions, and necessary laboratory equipment. The advantages and disadvantages of each growth method are highlighted along with the fundamental growth mechanisms. In addition, the key material constituents needed for the preparation of SAMs are briefly outlined. The specific differences and similarities between the structural, electronic, and chemical properties of the SAMs obtained by each deposition method are examined in greater detail in Chapter 3 and Chapter 4.

Although the focus of the discussion will be limited to the specific case of alkanethiol-based SAMs on GaAs, the general growth methodology can be applied to most of the other related molecule-substrate systems that have been used to form supported monolayers. However, it should be noted that the structure, packing density, and stability of the resultant films on these surfaces may differ from those formed on III-Vs due to the specific geometries and electronic characteristics of the other substrates.

A broad category of characterization techniques has been applied to the analysis of organic monolayers ranging from microscopy-based (such as AFM and scanning tunneling microscopy (STM)) [72], [73] and spectroscopy-based techniques (such as XPS and spectroscopic ellipsometry) [72], [74], to diffraction-based techniques (such as grazing incidence x-ray diffraction and low energy electron diffraction (LEED)) [72]-[74]. As a result of the different spatial averaging behavior of each method, as well as sensitivity to specific material properties, a clear picture of the SAM structure can only be acquired by combining a number of complementary techniques.

The second half of this chapter will focus on the main experimental tools that were used in the investigation of the SAMs. The aspects of each characterization technique pertinent to this study will be presented with the intent to introduce the reader to these analytical methods, and to establish the groundwork for an enhanced understanding of the models and results presented in subsequent chapters. For a more rigorous description of each technique the reader is referred to the relevant technical references provided throughout.

2.1 Substrate Characteristics

Aside from the chemical nature of the substrate, which is often chosen based on the intended application of the resultant SAM-substrate system, the crystallographic orientation, electronic characteristics, and quality play an important role when choosing a substrate for the assembly of organic monolayers. By selecting a substrate with a specific set of parameters, the properties of the monolayer films can be fully realized.

For the experiments described within this work, care was taken to select epiready single-side polished crystalline GaAs substrates with a low defect

density. The single crystal substrates (2-inches in diameter) were purchased from Wafer Technology Ltd [75]. As a result of the growth technique and the high purity of the starting material used by the vendor, the wafers exhibited low dislocation densities and etch pit densities of less than 2000 cm^{-2} [75].

(100)-oriented GaAs substrates were used exclusively in the study. This specific crystallographic orientation was chosen for three practical reasons. First, conventional (100)-oriented surfaces are the most commonly used in device fabrication due to their ease of cleaving and aptness for good quality epitaxial growth [76]. Second, atomically smooth (100)-oriented surfaces lack the structural features (i.e. steps and terraces) present on non-planar high-index semiconductor surfaces which can complicate the adsorption of impinging molecules [51]. Finally, (100)-oriented surfaces are more stable and exhibit well-defined surface reconstructions which can help to simplify the post-growth characterization of the ensuing structures and improve reproducibility between the growths [77]. Therefore, in an attempt to conduct a systematic analysis and reduce the number of experimental variables, only (100)-oriented GaAs substrates were used in the preparation of the SAM samples.

To maximize the sensitivity of the electronic and optical properties at the GaAs surface to modification by organic surfactants, undoped semi-insulating GaAs wafers were used throughout the study, except where otherwise noted. The use of undoped semiconductors is preferable in experiments where an optical response is indicative of the efficacy of a passivation treatment as the influence of the resultant passivation on the optical characteristics is more pronounced for surfaces with low carrier densities [78].

2.2 Growth of SAMs

2.2.1 Liquid Phase Deposition

Depositing organic molecules from liquid phase has been the most widely used means of preparing SAMs on solid surfaces mainly due to the convenience and low cost of the technique. Despite the aforementioned advantages, solution growth of SAMs has some serious technological drawbacks, such as the long timescale of the growth, possible incorporation of organic solvents, and the need for careful control of the cleanliness of the growth environment. The latter concern is of particular importance in growth and characterization studies where the formation of highly ordered SAMs greatly depends on the ability to achieve clean and reproducible conditions [72]. Consequently, rigorous cleaning procedures used to ensure the removal of contaminants from the surface of the substrates and any glassware used in the deposition process are crucial to the successful growth of ultra-thin organic films, which may be a shortcoming in smaller laboratories lacking a suitable infrastructure. Another important consideration in the deposition of SAMs on GaAs and other III-V semiconductors deals with the removal of the native oxide layer that is present on the surface of the substrates under ambient conditions. As the native oxide layer is chemically inert it prevents the adsorption of organic molecules on the surface of the semiconductors [79]. Therefore, to form alkanethiol monolayers on GaAs, the chemical inertness of the substrates has to be overcome prior to the film growth.

In the deposition of SAMs from liquid phase as described within this work, numerous measures were taken to attain a clean environment and reproducible conditions. One of the first precautious taken was to use only high purity chemicals and materials. All of the solvents (acetone, methanol, isopropanol, chloroform, and anhydrous ethanol) used during the growth process were HPLC grade and were used as obtained from Sigma-Aldrich [80]. Likewise,

the ODT (purity: 98+%) was purchased from Sigma-Aldrich [80] and was used without further purification in the solution deposition process. The ultrapure deionized water (resistivity $\geq$ 18 MΩ-cm) used during the rinsing steps was supplied by a Milli-Q purification system manufactured by Millipore [81].

Further elimination of undesirable contaminants from the solution deposition process was achieved through a variety of elaborate pretreatment methods that were employed to carefully clean the laboratory equipment and substrates, as well as to provide a highly reactive surface ideal for anchoring the thiolated molecules. Prior to the deposition, all of the glassware used to prepare the monolayers was cleaned in an ultrasonication bath of anhydrous ethanol and chloroform (1:1 mixture) for 1 hour, followed by exhaustive rinsing with deionized water, and a final rinse in anhydrous ethanol, before being dried under streaming nitrogen. Similarly, the first few steps of the solution deposition procedure (outlined in Figure 2.1) were dedicated to preparing the surface of the samples. As shown in Figure 2.1, the GaAs samples were first degreased with consecutive ultrasonication in three organic solvents (acetone, methanol, and isopropanol) for 15 minutes. To remove residual hydrocarbons and to produce an oxide-free surface, each sample was exposed to a 20-minute dry UV-ozone treatment followed by a 2.5-minute wet-chemical etch in 10% buffered HF. The combination of the UV irradiation with the ozone results in the formation of a thin oxide layer (approximately 3.5 nm thick [82]) on the semiconductor surface that traps the organic and non-organic contaminants. By subsequently immersing the sample in the aqueous HF solution, the UV-ozone created oxide film along with the incorporated contaminants and native oxide layer are selectively removed leaving a clean and reactive surface suitable for SAM growth [83].

In an effort to control the cleanliness of the growth environment by minimizing the exposure of the samples to impurities in the ambient atmosphere, the HF-etch as well as the subsequent SAM deposition process were carried out in

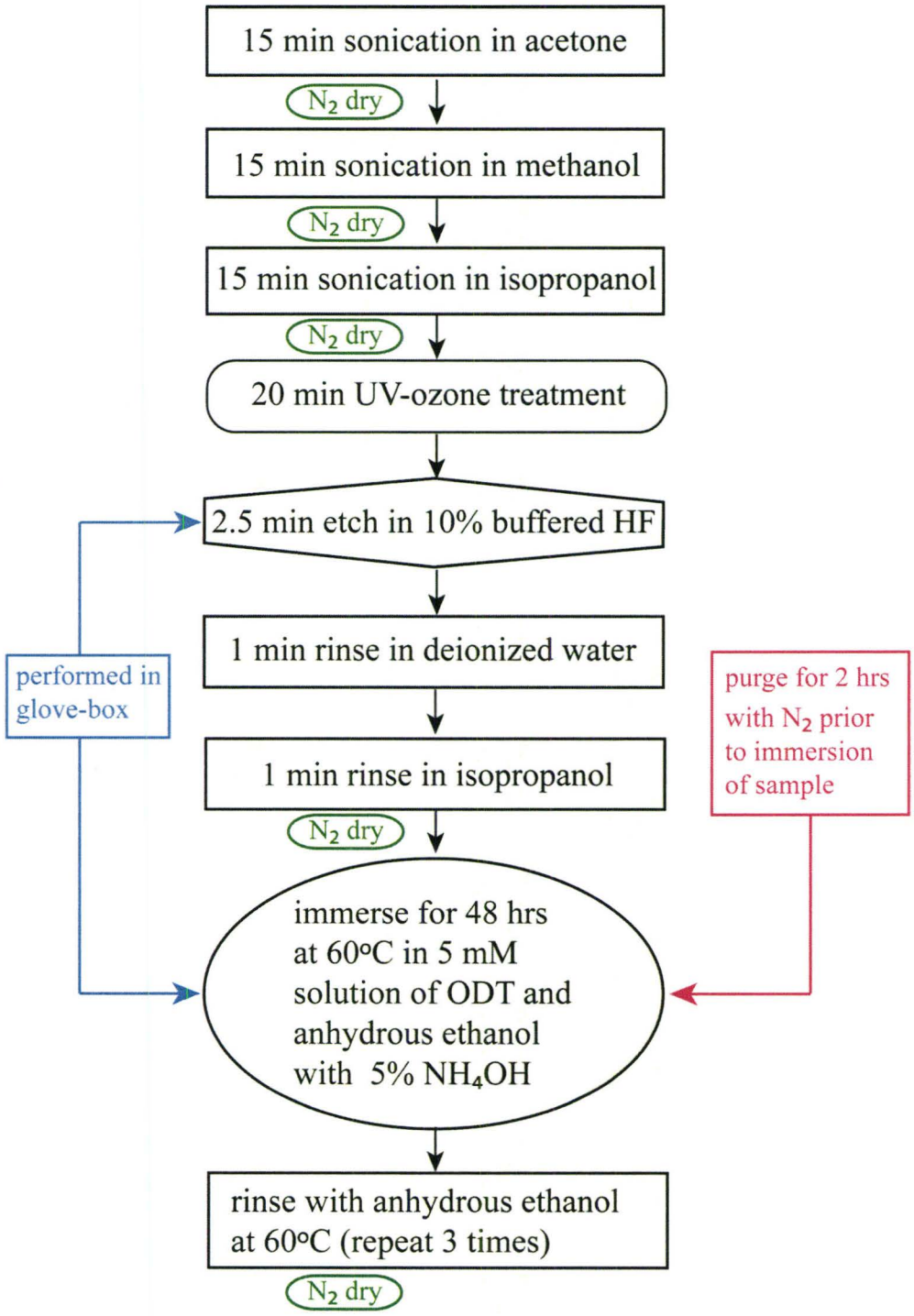

Figure 2.1: **Flow chart indicating the sequence of processing steps applied to the GaAs substrates used to deposit SAMs from solution.**

a nitrogen purged Omni-Lab glove-box manufactured by Vacuum Atmospheres Company [84], with oxygen and moisture levels below 1 part per million. Performing the growth of the monolayers in an anaerobic chamber helps to prevent the reoxidation of the freshly etched sample surface, which would otherwise occur in an air ambient.

The solution-based growth of single component alkanethiol SAMs on GaAs is affected by a number of growth parameters, such as the aliphatic chain length, solution concentration, nature of the solvent, growth time, and temperature. Past studies of this system have shown that the quality of the monolayers strongly depends on the length of the alkyl chains with films composed of short-chain thiolates being more disorganized with lower packing densities and surface coverages [52], [79]. The structural disturbances and defects found in monolayers composed of shorter hydrocarbon chains can be attributed to the reduced van der Waals interactions between the adjacent chains due to the decreased length of the molecules [46]. As the goal of the present work was to produce pseudo-crystalline monolayers, longer-chain SAMs were used on the GaAs substrates (ODT specifically).

The ODT monolayers were deposited from a 5 millimolar concentration in an ethanolic solution. The choice of solvent and concentration of the adsorbate species were based on a survey of relevant literature, the results of which indicated that smoother, more ordered and stable films are obtained from dilute ethanolic solutions as opposed to those from higher thiol concentrations [79], [85]. The chemical nature of ethanol makes it a preferred solvent for the formation of alkanethiol-based SAMs for several reasons. First, the short length of ethanol molecules allows for an increased rate of thiol adsorption at the onset of the growth. The initial rate of chemisorption has been found to be related to the length of the solvent molecules used in the growth, with a slower growth rate observed for longer-chain solvents [86]. The influence of the solvent chain length on the SAM growth rate is related to the interaction between the solvent and the

substrate surface, as well as to the mobility of the molecules in the solution [72]. Since solvents with a longer molecular length interact more strongly with the substrate and have a reduced mobility, they are more difficult to displace from the sample surface by the adsorbing alkanethiols. Second, the nonpolar terminus of the alkanethiols limits their solubility in a polar solvent like ethanol, thereby increasing the likelihood of SAM formation as adsorption of less soluble species is favored [46], [87]. Third, the geometrical mismatch between ethanol and long-chain alkanethiols lowers the tendency of solvent incorporation into the final monolayer structure [46].

The self-assembly of the monolayers from liquid phase was achieved by incubating the cleaned, freshly etched GaAs substrates in the ODT-ethanol solution for a period of 48 hours at a temperature of 60°C. Previous time-dependent spectroscopic investigations of the growth of alkanethiol SAMs on III-V surfaces have established that deposition times in excess of 36 hours are needed to achieve dense and well-ordered films [37]. To ensure a high probability of forming good quality monolayers, an assembly time of 48 hours was selected for the liquid phase growths. As mentioned previously, the long time scales associated with SAM formation from dilute solutions account for two distinct steps of the growth process. The first step involves the initial spontaneous chemisorption of the thiol headgroup to the surface, and the second deals with the structural self-alignment of the adsorbed aliphatic chains into a stable, predominantly all-trans conformation [87].

Due to a lack of comprehensive studies concerning the temperature dependence of the solution phase process, the temperature of 60°C used during the SAM growth was chosen based on that reported by other research groups in the field [29], [56], [58], [62], [79], [88]. Although the deposition temperature was selected without detailed knowledge of its effects on the characteristics of the resultant films, limited thermodynamic data available for comparable alkanethiol-

Au systems indicated only a weak relationship between the temperature and the rate of self-assembly [87].

For the deposition of high quality monolayers, the purity of the growth solution is another important parameter as it can have a strong impact on the growth behavior and film uniformity. Consequently, care must be taken to remove solid contaminants and moisture from the growth environment, as the presence of these impurities can affect the formation kinetics by delaying the onset of the self-assembly process [72]. Since ethanol is hygroscopic, the amount of water in the thiol solution and surrounding environment has to be carefully controlled during the deposition process. To mitigate the adverse effects of impurities on the solution-grown SAMs, high-purity anhydrous ethanol was used as the organic solvent from which the films were adsorbed.

Another factor that has been found to influence SAM growth is the oxygen content of the solution, which is believed to hinder the formation of the films, particularly in the case of growth on III-V semiconductor surfaces that readily oxidize. Therefore, performing proper deoxygenation procedures to minimize the amount of dissolved oxygen in the solution is crucial to attaining densely packed monolayers. To prevent the regrowth of the native oxide layer during the self-assembly process, the thiol solution was purged with nitrogen for 2 hours (per every 250 mL) to remove the dissolved oxygen before the samples were introduced. A second precautionary measure taken to maintain the reactive nature of the substrate surface was the addition of 5% (by volume) ammonium hydroxide (NH_4OH) to the ODT-ethanol solution. Addition of ammonium hydroxide to the thiol solution has been shown to provide in-situ etching of the semiconductor surface during the deposition process, thus minimizing reoxidation of the sample and improving the binding of the ODT molecules to the sample surface [79].

Following the SAM deposition, the samples were rinsed with copious amounts of warm ethanol and were blown dry with nitrogen. The use of a suitable rinsing procedure following the monolayer growth is critical to the effective removal of physisorbed molecules from the sample surface.

2.2.2 Vapor Phase Deposition

In addition to the deposition of SAMs from liquid phase, the functionalization of III-V semiconductors can be accomplished by exposing the precleaned surfaces to a flux of the impinging molecules in vapor phase. The deposition of SAMs from vapor phase is an attractive alternative to the traditional solution-based method for several reasons. First, the preparation of the films in an ultrahigh vacuum (UHV) environment allows for the in-situ characterization of the growth kinetics as well as the resultant SAM structure by a variety of surface science tools [72]. Second, the formation of SAMs from vapor phase permits better control of the experimental conditions and growth parameters, such as the cleanliness of the environment and substrate, which, as discussed previously, has been found to affect the quality of the SAMs [72]. Finally, the assembly of monolayers from vapor phase eliminates any caustic influence the solvent may have on the structure and properties of the films due to the competition of the solvent for binding sites on the surface or through the incorporation of the solvent into the two-dimensional structures [20]. Nevertheless, vapor phase deposition has remained a less explored avenue for the growth of SAMs due in part to the more extensive and costly experimental equipment required for this technique.

Figure 2.2 shows a schematic of the custom-made UHV deposition system employed in this work to deposit the SAMs from vapor phase directly onto the GaAs substrates. The UHV system consisted of a growth chamber connected through a gate valve to a load-lock chamber. The isolated load-lock was backfilled with nitrogen gas to atmospheric pressure in order to introduce the

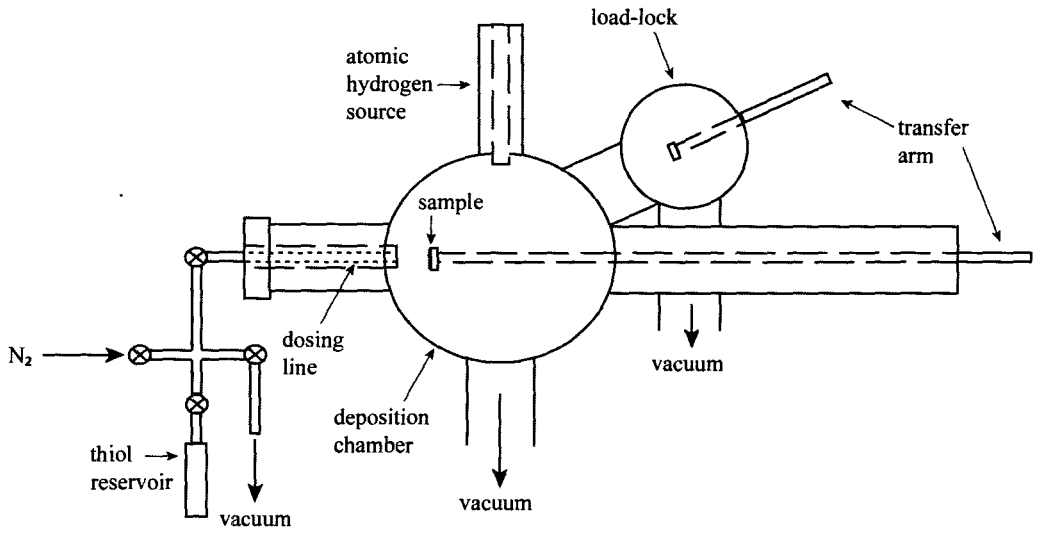

Figure 2.2: Schematic of the custom-made UHV deposition system employed to deposit the SAMs from gas phase.

samples from ambient into the UHV system. UHV conditions in the load-lock were achieved by means of a turbomolecular pump backed by a rotary vane pump. A remote manipulator was used to transfer the samples from the load-lock into the growth chamber, which was held at a base pressure of 10^{-9} Torr using a separate combination of a turbomolecular pump and rotary vane pump. The growth chamber was equipped with a Veeco Atom-H atomic hydrogen source [89] used for in-situ surface cleaning of the samples before depositing the SAMs. Atomic hydrogen was generated by cracking molecular hydrogen with a tungsten filament heated to approximately 2100°C. The pressure of the molecular hydrogen in the chamber was maintained at 5×10^{-5} Torr. During the cleaning process, the samples were heated to 500°C by means of a substrate holder equipped with a heater and exposed to atomic hydrogen for 10 minutes. A substrate temperature of 500°C was used in the presence of hydrogen to limit the extent of As desorption and thus, surface degradation, which often occurs at higher substrate temperatures commonly used in purely thermal cleaning procedures [90]. To further avoid

damaging the surface of the samples, the filament was positioned at a distance of 20 cm away and oriented parallel to the surface of the samples. In addition to the removal of surface contaminants, exposure to atomic hydrogen leads to desorption of the native oxide layer present at the surface of the GaAs, as established by real-time mass spectroscopy [91]. Removing the native oxide layer promotes the successful bonding of the adsorbing ODT molecules to the semiconductor surface, which would otherwise be hindered by the presence of the native oxide.

Prior to transferring the samples into the growth chamber, the purity of the ODT was enhanced by thorough degassing through repeated freeze-pump-thaw cycles similar to that reported elsewhere [92]. In addition to removing any volatile impurities, the degassing procedure significantly reduces the amount of dissolved oxygen in the ODT. Remaining impurities were removed from the thiols by pumping on the heated thiols (70°C) through the deposition chamber as confirmed by mass spectroscopy.

After cooling to 60°C, the samples were exposed to the molecular flux of ODT at the end of a dosing line formed by a stainless steel tube (outer diameter: ¼ inch) used to connect the exterior ODT reservoir to the deposition chamber. The substrate temperature was selected to be similar to that used for the solution deposition process. To prevent condensation of the ODT, the dosing line was heated moderately to 70°C during the deposition. The temperature of the ODT reservoir was also maintained at 70°C during the deposition to increase the vapor pressure of the thiol molecules. A variable leak valve controlled the molecular flux of ODT at the samples. By monitoring the background pressure of the thiols in the chamber, the dosing flux at the sample surface could be quantitatively regulated. The background pressure in the chamber was kept in the range of 5×10^{-6} Torr and monitored with mass spectrometry. The total exposure was controlled through a combination of the flux and the exposure time, which was limited to two hours.

From the kinetic theory of gases, the molecular flux at the surface of a sample can be determined from the following relation [93]

$$\Phi = \frac{PN_A}{(2\pi MRT)^{1/2}} \quad (2.1)$$

where P is the gas pressure (in Torr), N_A is Avogadro's number, M is the molar mass of the gas, T is the absolute temperature, and R is the gas constant. For ODT (M = 286.56 g/mol) at a pressure of 5×10^{-6} Torr and a temperature of 343 K, the molecular flux perpendicular to the surface of the sample was $\Phi = 5.61\times10^{14}$ molecules–$cm^{-2}s^{-1}$. When expressed in units typically used in the measurement of surface exposure to gases, this corresponds to an impingement rate of 5 Ls^{-1}, where 1 Langmuir (L) = 10^{-6} Torr-s. Thus, after two hours, the samples were exposed to 36000 L. The exposure time and gas pressure were chosen to obtain a high dose of ODT as doses of alkanethiols in excess of 10000 L have been shown to produce single domain monolayers on III-V surfaces [92]. Following the vapor deposition of ODT, the samples were thoroughly rinsed with high-purity anhydrous ethanol to remove any physisorbed molecules from the surface and were blown dry with nitrogen.

The characterization of the SAM samples, as discussed in Chapter 3 and Chapter 4, was performed either immediately after the preparation of the monolayers or within a couple of days. Between measurements, the samples were stored in an inert nitrogen environment in the aforementioned glove-box.

2.2.3 Biofunctionalization

Apart from the deposition of simple methyl-terminated thiolated SAMs on GaAs surfaces, research discussed in this study has also been directed towards the application of these systems in the formation of biological sensors. In this effort, alkanethiol SAMs were utilized to covalently anchor oligonucleotide sequences to

GaAs sensor platforms. Details of the sample preparation procedure are provided in Chapter 5. While the overall biofunctionalization process used is very similar to that described above for the liquid phase deposition of conventional alkanethiol monolayers, there are two main differences. First, the treatment steps were performed in buffered aqueous solutions and second, the GaAs surface modification was carried out at room temperature. The functionalization reactions were conducted in an aqueous medium at ambient temperature in order to mimic biologically relevant conditions in which biomolecules are naturally found, as well as to ensure their stability throughout the experiment.

2.3 Characterization Techniques

A wide variety of thin film characterization techniques have been applied to the study of SAMs. Since each technique is typically sensitive to a specific property of the films, a comprehensive understanding of the monolayers can only be attained through the use of several complementary techniques.

In this section, a brief overview of the various experimental techniques employed in this study is provided with emphasis on the different properties of the SAMs described by each technique. While the important technical parameters are discussed, more detailed information regarding the analytical surface science tools can be found in the references given throughout. Likewise, details regarding the specific application of each characterization technique to the study of SAMs are provided in Chapter 3 and Chapter 4.

2.3.1 Contact Angle Goniometry

Valuable insight regarding the surface properties of a particular material system can be gained from its wettability. Consequently, the measurement and interpretation of CAs is common practice in the analysis of SAMs as the quality of the films can be determined from this relatively simple experimental procedure. [94]

The CA, which forms the basis of wetting phenomena, is defined as the angle that is formed by a free-standing sessile drop between the liquid-vapor interface and the liquid-solid interface at the solid-liquid-vapor three-phase boundary (see Figure 2.3) [74]. As the shape of a liquid drop on a flat, homogeneous surface is affected by the free energy of the surface, the resultant CA is directly related to the surface tension of the solid. At equilibrium, the relationship between the free energy of the surface and the CA can be described by Young's equation, which states [74]

$$\gamma_{lv}\cos\theta_c = \gamma_{sv} - \gamma_{sl} \tag{2.2}$$

where γ is interfacial tension, θ_c is the equilibrium CA, and the subscripts *lv*, *sv*, and *sl* refer to the liquid-vapor, solid-vapor, and solid-liquid interfaces, respectively. The equilibrium CA arises due to a balance between the cohesive forces in the liquid drop and the adhesive forces between the solid and the liquid [95]. Therefore, the degree of interaction between the liquid and the solid determines the CA. For instance, under ideal conditions, if there is no interaction the CA will be 180°, as in the case of a hydrophilic liquid on a hydrophobic surface. On the other hand, if the interaction between both components is maximized the CA will be 0°, as in the case of a hydrophilic liquid on a hydrophilic surface. When a polar liquid such as water is used as the probe fluid, the resultant CA can be used to quantify the hydrophobicity of the surface and thus, the surface polarity.

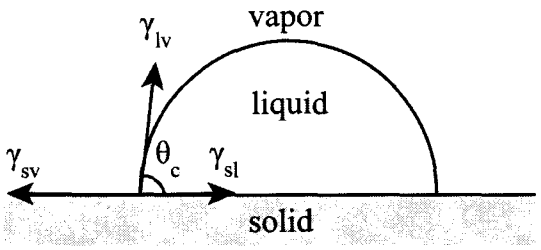

Figure 2.3: Interfacial forces acting at the three-phase boundary for a droplet of liquid placed on a solid surface. At equilibrium, the droplet assumes a CA that balances the interfacial forces.

The derivation resulting in Equation (2.2) assumes an ideal surface, which is smooth, homogeneous, isotropic, and non-deformable [74]. As SAMs rarely meet all of the above restrictions, the experimentally observed angles are not uniquely determined by the surface tensions of the given system and are affected by the inherent characteristics of the surface such as roughness. Thus, the CA that is measured is not necessarily the true thermodynamic equilibrium CA. Nevertheless, CA goniometry is frequently used in the characterization of monolayers as it provides a quick and facile means of gaining qualitative information about the chemical nature of the coated surfaces, as well as the packing density of the constituent chains [94].

A useful variant of Young's equation that applies to heterogeneous surfaces containing regions of varying surface tensions was proposed by Cassie. For a surface consisting of two distinct domains, the observed CA (referred to as the Cassie CA), θ_{ca}, is described by [74]

$$\cos\theta_{ca} = f_1 \cos\theta_{d1} + f_2 \cos\theta_{d2} \qquad \textbf{(2.3)}$$

where f_1 and f_2 are the fractional surface areas of the two domains (i.e. $f_1 + f_2 = 1$), and θ_{d1} and θ_{d2} are the intrinsic CAs of each domain. For a two-component system consisting of a surface coated with a monolayer of alkyl chains, CA

analysis can probe the quality of the outermost regions of the SAM as the wetting behavior depends on the near-surface chain-packing density. A closely packed, oriented monolayer from a methyl-terminated adsorbate will predominately present methyl groups on the surface, yielding a characteristic value for the observed water CA [74]. On the other hand, as a monolayer becomes less densely packed and more disordered, the underlying interface and the methylene groups in the alkyl chain become more exposed, thus giving rise to a different CA.

CA goniometry was used in the present work to evaluate the characteristics of the SAMs after preparation. A custom-built goniometer (Figure 2.4) was used to measure the CA of a sessile water droplet at room temperature and ambient relative humidity immediately after the deposition of the SAMs. A 5 μL drop of high-purity deionized water was dispensed through a computer-controlled microsyringe terminated with a blunt-ended needle placed on the surface of the samples. Upon retracting the needle, the drop was allowed to relax for a period of approximately 30 seconds to reach equilibrium. The static CA of the droplet was recorded with a digital camera (Moticam 1000) attached to an optical trinocular microscope (Edmund Industrial Optics). The obtained images were analyzed manually by aligning a tangent with the drop profile at both points of contact with the sample surface. Repeated measurements at three different sample locations indicated a CA precision of $\pm 2^{\circ}$.

2.3.2 Atomic Force Microscopy

The surface morphology of the substrate is vitally important in controlling the structure of SAMs as the characteristics of the substrate can have a great impact on the defect density of the films. Similarly, topographical maps of a functionalized surface can provide quantitative information regarding the structural features of the material system. Among the profilometry techniques used to assess surface properties, AFM has gained popularity in imaging surface

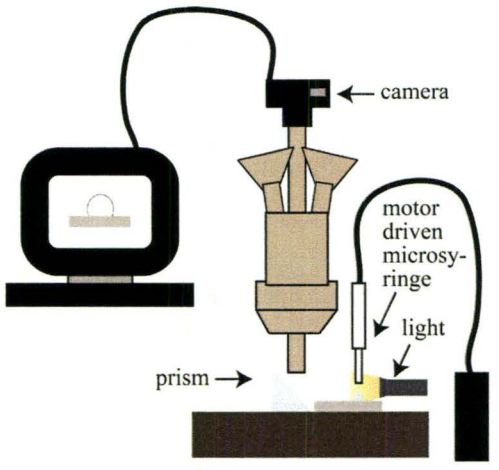

Figure 2.4: Instrumental setup used for measuring the static CAs of water on the SAM-functionalized surfaces.

topography on account of its simplicity, applicability to the study of wide variety of materials, and high resolution [96].

The general concept behind AFM involves scanning the surface of the sample with a sharp cantilever-based stylus. As the probe tip is raster-scanned across the surface, interatomic forces (van der Waals, electrostatic, and capillary) between the tip and the surface cause the cantilever to deflect [97]. A three-dimensional map of the surface topography is produced according to the magnitude of the cantilever deflection which strongly depends on the distance between the atoms on the sample surface and those on the tip. Although the AFM can operate in contact, non-contact, or in tapping mode, deformation of the monolayer can occur when the tip is brought into continuous contact with the sample surface [96]. Operation in the non-contact mode prevents SAM damage but limits the resolution of the measurement in an ambient environment. Therefore, to obtain images with a molecular resolution while minimizing the possibility of surface damage, tapping mode imaging is typically used. In this mode of operation, the cantilever probe is driven near the resonance frequency via a ceramic piezoelectric oscillator [98]. The topographical data is then compiled

from the amplitude of the cantilever oscillation, which is maintained at a constant value by means of a feedback loop that adjusts the tip-to-sample distance [97].

Useful information regarding the roughness profile of a surface can be extracted from the topographical AFM data. Two of the most frequently quoted roughness parameters are the arithmetic average roughness (R_a) and the root-mean–square roughness (R_q). R_a and R_q are both measures of the vertical roughness of a surface as given by [99]

$$R_a = \frac{1}{n}\sum_{i=1}^{n}\left|z_i - \bar{z}\right| \tag{2.4}$$

$$R_q = \left(\frac{1}{n}\sum_{i=1}^{n}\left(z_i - \bar{z}\right)^2\right)^{1/2} \tag{2.5}$$

where n is the total number of acquired data points, z_i are the data points that describe the height of the surface features, and $\bar{z}$ is the mean height. While R_a is a measure of the average absolute deviation of the surface irregularities from the mean, R_q describes the standard deviation of the distribution of surface heights taken from the mean data plane. Since R_q represents the statistical nature of the surface height profile, it is more sensitive to large deviations from the mean when compared to R_a [100].

In this work, the surface morphology and structural characteristics of the samples were evaluated by AFM over a 1×1 μm^2 scan area. The AFM measurements were carried out in air using a Digital Instruments Nanoscope III [89] in tapping mode. The tetrahedral Si tip used to acquire the images was manufactured by Olympus (AC160TS) [101]. Before each measurement, the sample surface was blown with nitrogen to remove any dust particles. AFM scans were performed prior to treatment as well as following the deposition of the SAMs. Three different areas were scanned on each sample to account for any

variability in the surface structure. From the obtained topographical images, surface roughness parameters were derived. The corresponding uncertainty in the calculated R_q and R_a was ± 0.02 nm and ± 0.03 nm, respectively.

2.3.3 Photoluminescence Spectroscopy

A sensitive, nondestructive technique for analyzing the properties of semiconductor materials is PL spectroscopy, which deals with photon emission generated by the spontaneous transition of charge carriers from a photoexcited electronic state to a lower energy state [102]. In the measurement of a PL spectrum, optical excitation provided by a pump source is used to create a high excess concentration of electron-hole pairs in the semiconductor by means of absorption. As the electron-hole pairs recombine via several radiative recombination paths involving the band extrema or bound states (excitons, impurities, or defects), photons of a characteristic energy are emitted [103].

In this study, PL spectroscopy was used to assess the passivation properties of the SAMs as well as the stability of the films. Additionally, PL measurements were also conducted to determine the suitability of optical transduction as a platform for biosensing assays based on functionalized SAM-GaAs systems. Luminescence spectra were recorded at room temperature using a custom-built apparatus shown schematically in Figure 2.5. Continuous excitation was provided by a 10 mW He-Ne laser source operating at 632.8 nm, while wavelength selection was achieved with a Sciencetech monochromator (model 9050) [104] with a resolution of approximately 1 nm. A Si pin photodiode was used to detect the sample luminescence. To increase the sensitivity of the measurement, the laser beam was modulated by a mechanical chopper (200 Hz) and monitored with a lock-in amplifier. A lens (L1) was used to focus the laser beam at the sample surface to a spot size of less than 1 mm in diameter. A second lens (L2) was used to ensure maximum light collection by focusing the PL signal

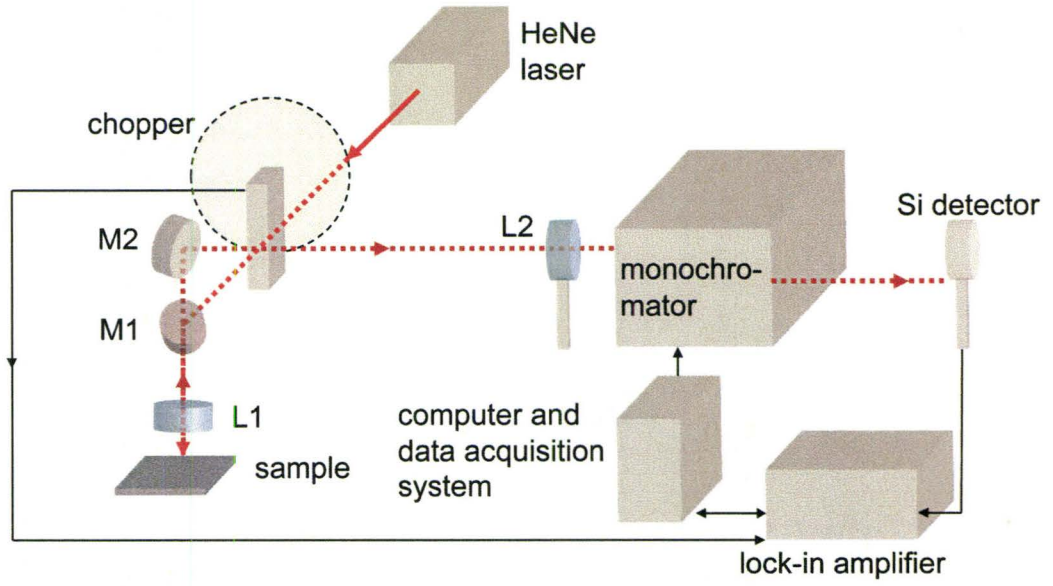

Figure 2.5: Schematic of the experimental arrangement used for measuring the PL spectra (M1/M2: mirror, L1/L2: lens).

on the entrance slit of the monochromator. As the absorption of the laser beam occurs close to the top of the sample (for 632 nm excitation the absorption depth in GaAs is approximately 250 nm) [103], the intensity of the resulting PL signal is strongly controlled by the properties of the surface and hence, is indicative of the passivation enhancement following treatment, as well as the changes in the local environment. In order to establish reproducibility between measurements, a highly doped untreated n-type GaAs sample was used as a reference against which all PL measurements were compared. The use of a reference standard strongly minimizes the influence of experimental details on the obtained PL results. On each sample, PL was collected from three different locations and averaged to account for any non-uniformity in the surface properties. The typical variation in peak PL intensity across the surface of each sample was less than 10%.

2.3.4 Variable Angle Spectroscopic Ellipsometry

Variable angle spectroscopic ellipsometry is a sophisticated, contactless method applied extensively to monitor surface phenomena as well as to determine the physical structure and optical properties of a wide variety of materials. This optical technique is predominately used to deduce the thickness and optical constants of thin films by measuring the change in polarization that a light beam incurs upon reflection from the sample surface. As conventional ellipsometry is inherently nondestructive, it has become a valuable characterization tool in the analysis of SAMs.

In an ellipsometric measurement, a well-collimated beam of polarized, monochromatic light interacts with a medium defined by a material-specific wavelength dependent dielectric function, $\hat{\varepsilon}(\lambda)$, or complex refractive index $\hat{n}(\lambda)$ where $\hat{n} = \sqrt{\hat{\varepsilon}}$ [105]. During this interaction, a polarization change occurs when the incident beam reflects from the sample surface at a non-normal angle of incidence, ϕ_1, as depicted in Figure 2.6. The reason for the observed modification in the state of the polarization deals with the distinct behavior of the two linear polarization components that comprise the incident beam; the component parallel to the plane of incidence (*p*-polarized) and the component perpendicular to the plane of incidence (*s*-polarized) [106]. As a result of the reflection, the amplitude and phase of the *s*- and *p*-polarization components change. At an interface, the characteristics of the reflected wave can be calculated by employing Fresnel's equations for the complex reflection coefficients r_s and r_p of the *s*- and *p*-polarized light, respectively, as given by [105]

$$r_{s_{12}} = \frac{\hat{n}_1 \cos\phi_1 - \hat{n}_2 \cos\phi_2}{\hat{n}_1 \cos\phi_1 + \hat{n}_2 \cos\phi_2}, \quad r_{p_{12}} = \frac{\hat{n}_2 \cos\phi_1 - \hat{n}_1 \cos\phi_2}{\hat{n}_2 \cos\phi_1 + \hat{n}_1 \cos\phi_2} \tag{2.6}$$

When more than one interface is present, such as in the case of a single isotropic thin film on a substrate, the resultant reflected wave is composed of an

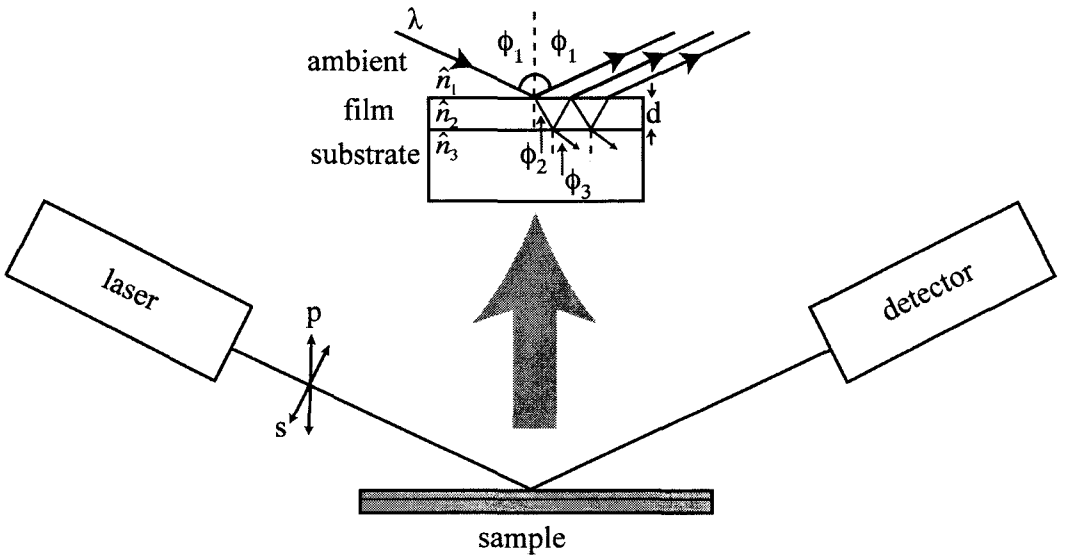

Figure 2.6: **Schematic diagram of an ellipsometry experiment used to characterize the SAMs. Polarized light from a laser source is incident upon the monolayer formed on a substrate. The interaction between the laser beam and the sample leads to a change in the polarization state of the reflected light. The detector then analyzes the polarization state of the reflected light. As depicted in the illustration, the laser beam is transmitted and reflected at multiple interfaces during the interaction.**

infinite series of partial waves that are reflected and transmitted at the two interfaces (Figure 2.6). In this case, the phase and amplitude relationships between the *s*- and *p*-polarized components of the reflected and incident beams are defined by the total reflection coefficients R_s and R_p, which are written as [105]

$$R_s = \frac{r_{s_{12}} + r_{s_{23}} e^{-i2\beta}}{1 + r_{s_{12}} r_{s_{23}} e^{-i2\beta}} \quad , \quad R_p = \frac{r_{p_{12}} + r_{p_{23}} e^{-i2\beta}}{1 + r_{p_{12}} r_{p_{23}} e^{-i2\beta}} \tag{2.7}$$

where $r_{s,p_{12}}$ and $r_{s,p_{23}}$ are the complex reflection coefficients at the ambient-film (12) and film-substrate (23) interfaces from Fresnel's equations, and β describes the phase change in the probing light wave as it propagates through the film [105]

$$\beta = 2\pi\left(\frac{d}{\lambda}\right)\hat{n}_2 \cos\phi_2 \tag{2.8}$$

In Equation 2.8, λ is the wavelength of the incident beam and d is the thickness of the film. For a layered structure consisting of multiple films, an iterative procedure must be used to determine the total reflection coefficients for the entire structure by using the relations in Equation 2.7. During this investigation, a matrix formalism within a regression analysis is often applied to compute the parameters of interest from an optical multilayer model [107].

The measured response by the ellipsometer is represented in terms of the ellipsometric angles, Δ and Ψ, as defined by the complex reflection coefficient ratio, ρ, given by the following equation [106]

$$\rho = \tan\Psi e^{i\Delta} \tag{2.9}$$

Alternative definitions for the ellipsometric angles are presented in terms of the relative amplitude and phase relationships between the *s*- and *p*-polarizations following reflection from a film-covered substrate [107]

$$\tan\Psi = \frac{|R_p|}{|R_s|} \tag{2.10}$$

$$\Delta = \delta_{rp} - \delta_{rs} \tag{2.11}$$

where δ_{rs} and δ_{rp} denote the reflection induced phase shift for the *s*- and *p*-polarization states. As suggested by Equations 2.10 and 2.11, Ψ and Δ reflect the

differential changes in the amplitude and phase, respectively, of the *s*- and *p*-polarization components upon reflection from the system under investigation. From the experimental Δ and Ψ spectra, the optical properties and the thickness of the films under study can be determined. For a bulk, film-free substrate, the optical constants can be algebraically solved directly by inverting Δ and Ψ. However, for systems with an increased degree of complexity, such as multilayer structures, ellipsometric measurements taken under an assortment of different conditions (such as wavelength and angle of incidence) are required to accurately resolve the properties of the individual layers [105]. By interpreting experimental data within the context of a model-based regression analysis, the material properties of the optical system can be extracted. At the onset of the analysis, initial estimates for the unknown free parameters are used and the values are adjusted iteratively as the regression analysis proceeds to increase the model's goodness of fit through the use of a merit function. The most commonly used merit function is the mean-square error which exhibits a minimum value when the calculated data matches the measured data as defined in terms of the following relation [105]

$$mean\text{ - }square\ error = \frac{1}{N-M}\sum_{i=1}^{N}\left(\frac{y_i - y(\bar{x},\bar{a})}{\sigma_i}\right)^2 \qquad \textbf{(2.12)}$$

where y_i represents the measured data values, $y(\bar{x},\bar{a})$ are calculated data points (where $\bar{x}$ and $\bar{a}$ contain all the known and variable parameters in the model, respectively), and σ_i is the standard deviation of the *ith* data set. In Equation 2.12, N is the total number of data points and M is the total number of adjustable parameters.

In this work, variable angle spectroscopic ellipsometry was used to determine the optical properties and the thickness of freshly prepared monolayers. The experimental data was acquired with a M2000V variable angle spectroscopic

ellipsometer manufactured by J. A. Woollam Co. [108]. The ellipsometry measurements were performed over a wide spectral range from 380 nm to 900 nm. To improve the sensitivity of the measurement to the optical properties and thickness of the film, data was collected at multiple angles of incidence, from 50° to 70°, increased systematically in 5° increments. The change in the polarization state of the light upon reflection from the sample surface was measured by means of a rotating compensator whereas the change in the amplitude was detected by a charge-coupled device (CCD) array. Combining the rotating compensator ellipsometry design with CCD detection allowed for the simultaneous measurement across the entire wavelength range. The fundamental properties of the SAMs were determined using commercial ellipsometry modeling software supplied by the manufacturer. To increase the accuracy of the results, the measurements were performed at three different locations on each sample, and the calculated parameters were averaged. The details of the parametric models used to estimate the thickness of films are described in Chapter 3 and Chapter 4.

2.3.5 X-ray Photoelectron Spectroscopy

One of the most popular and versatile surface science tools used to study the chemical properties of organic ultrathin films on solid supports is XPS [109]. In comparison to other spectroscopic techniques that aim to probe the surface of materials, XPS is inherently analytical in nature as it provides information on the elemental composition of the system being studied. Moreover, the high surface sensitivity of XPS makes it particularly attractive in the investigation of single monolayers, especially where quantitative information regarding the chemical state of the constituent elements is required.

The fundamental physical principle behind XPS involves the energy analysis of electrons emitted from a material due to a beam of soft x-rays impinging on the surface, as described by the photoelectric effect [110].

Consequently, a typical experiment begins with the irradiation of the sample with monoenergetic photons in the x-ray energy range. The important geometrical parameters in an XPS experiment are shown in Figure 2.7 a). As the x-ray radiation penetrates into the bulk of the material, it is absorbed by atoms along the way, which in turn, leads to the ejection of electrons from the near-surface region of the sample (see Figure 2.7 b)). Photoionized electrons can originate from two distinct orbitals: a tightly bound core level or a weakly bound valance level. By analyzing the energy of the emitted electrons, a spectrum of electron intensity as a function of energy is generated. Since the binding energy of core level electrons typically allows for the unambiguous identification of the atoms from which they are emitted, the spectrometer is usually arranged to convert the measured kinetic energy of the electrons to the binding energy through the following equation [110]

$$E_k = h\nu - E_B - \phi_w \tag{2.13}$$

where E_k is the kinetic energy of the emitted electron, $h\nu$ is the energy of the x-ray photon, E_B is the binding energy of the electron relative to a specific reference point (such as the Fermi level of the sample in electrical contact with the spectrometer), and ϕ_w is the characteristic work function of the spectrometer. Although the binding energy of core level electrons is usually sufficiently unique for the purpose of elemental analysis, it is not a fixed quantity and varies depending on the chemical state of the atom [95], [111]. Hence, chemical shifts in the core level binding energies of a given element can be used to determine a change in its local chemical environment.

The surface sensitivity of XPS stems from the low probability that electrons generated in the bulk of the sample will travel to the surface and escape with their original energy, thus contributing to the detected signal [110], [112]. Therefore, an important parameter in XPS studies of thin film structures is the

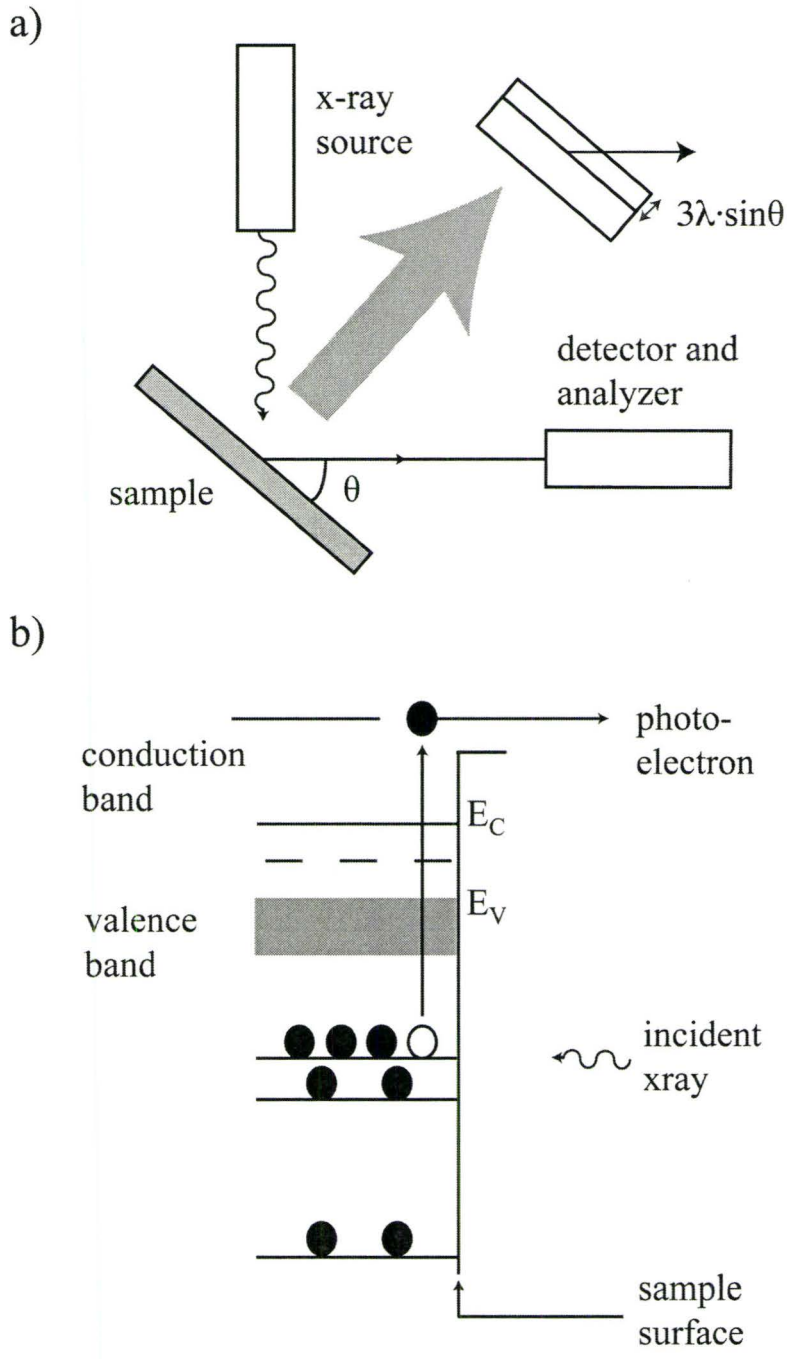

Figure 2.7: **Depiction of a) the key principles involved in a conventional angle-resolved XPS measurement, and b) the XPS process, showing the photoionization of an atom by the ejection of an electron. As illustrated in a), the sampling depth in the monolayer varies as a function of the electron take-off angle, θ.**

sampling depth, which is defined as the depth from which 95% of the detected electrons originate, as given by [110]

$$sampling\ depth = 3\lambda \sin\theta \tag{2.14}$$

where λ is the electron attenuation length and θ is the electron take-off angle measured with respect to the surface plane of the sample, as shown in the instrumental geometry presented in Figure 2.7 a). Since the sampling depth depends on the experimental geometry, it can be controlled by varying the take-off angle, by changing the angle of the analyzer relative to the sample surface. Performing the XPS measurements as a function of the take-off angle provides a convenient means of non-destructive depth profiling of the SAMs as it enables an assessment of the relative vertical distribution of the chemical species that make up the monolayers. It should be noted that the vertical ordering of the elements obtained via angle-resolved XPS provides only a qualitative description of the SAMs due to their inhomogeneous nature with depth.

In this study, XPS measurements were performed using a Kratos Axis Ultra x-ray photoelectron spectrometer equipped with a monochromatic Al Kα (1486.71 eV) source and a charge neutralization system. Broad range survey scans at a pass energy of 160 eV were performed to conduct a preliminary elemental analysis of the samples. As the intensity of each photoelectron line is directly proportional to the density of the element from which it derives, information regarding the relative atomic concentration of each element within the sampled volume is obtained [112].

High-resolution scans at a pass energy of 20 eV were performed to analyze the chemical state of each sample in more detail. The bonding chemistry at the SAM-GaAs interfacial regions was investigated by measuring the shifts in the core level binding energy of the constituent elements as a result of a variation in the chemical state. Since a number of different chemical bonding

configurations were present in each sample, a degree of overlap between the component core levels existed, thereby adding a degree of complexity to the analysis of the discrete binding energies and the peak intensities. Even though a refined non-linear least-squares algorithm was carried out to decompose the peaks in the collected spectra, a level of uncertainty still exists in the interpretation of the XPS data.

CasaXPS software [113] was used in the curve fitting of the core level spectral lines with mixed Gaussian-Lorentzian peak profiles and a Shirley background. For a quantitative estimation of the surface compositions, the integrated peak areas were used along with the standard atomic photoionization cross-sections from the software's database [113]. In an effort to avoid x-ray induced damage, the exposure time for each sample was minimized. The binding energy scale was internally referenced to the well-defined GaAs bulk As $3d_{5/2}$ peak at a binding energy of 40.95 eV, allowing for the accurate determination of the other binding energies in the spectra. In the case of the doublet photoemissions, the features were curve fitted with a pair of peaks with the same full-width at half-maximum, fixed spin-orbit splitting, and branching ratios of 2:1 ($2p_{3/2}/2p_{1/2}$) and 3:2 ($3d_{5/2}/3d_{3/2}$). To determine the elemental distribution perpendicular to the SAM-GaAs interfaces, as well as the molecular orientation, angle-dependent data was collected at photoelectron take-off angles of 30° and 90° measured from the sample surface. Both the survey and high-resolution scans were carried out across a 300×700 μm^2 sample area.

Chapter 3 Properties of ODT SAMs Deposited on GaAs from Liquid and Vapor Phases

3.1 Introduction

The success of novel hybrid organic-semiconductor devices based on the two-dimensional self-assembly of organic monolayers depends greatly on the ability to achieve close-packed layers that exhibit a high degree of lateral order [114]. In the design of these material structures, two approaches can be taken to functionalize the semiconductor surfaces. First, the monolayers can be formed on the solid supports via conventional liquid phase deposition techniques. Second, the self-organized adsorption of organic molecules can be accomplished from vapor phase. While both fabrication methods offer a means of surface modification, each has its own advantages and disadvantages, as discussed in Chapter 2. More importantly, the preparation of SAMs on semiconductors by either route may have an impact on the characteristics of the resulting films. Thus, an understanding of how the structure and material properties of the monolayers are affected by the deposition process is of practical importance.

In this chapter, the structural and chemical differences between alkanethiol SAMs deposited from an ethanolic solution and from vapor phase on GaAs substrates are investigated. ODT SAMs were formed on the semiconductor surfaces by both preparation routes and the resultant monolayers were analyzed using AFM, spectroscopic ellipsometry, CA analysis, and PL spectroscopy. The

experimental results discussed herein provide insight into the overall quality of the monomolecular assemblies on GaAs surfaces and attempt to answer the question of whether the properties of the films are indeed influenced by the deposition technique used to prepare them. In addition, the discussion in this chapter describes the particular aspects of the monolayers highlighted by each analytical tool and shows the applicability of each technique to the study of specific SAM properties. The central results reported in this chapter have been previously published by the author in [115].

In Chapter 4, a supplementary investigation of the chemical bonding characteristics and stability of the SAMs deposited from vapor and liquid phases is provided. The comprehensive results presented in both chapters indicate that the fabrication method used to functionalize the semiconductor surfaces with organic monolayers can be used to achieve a desired control of the physical and chemical properties of the resulting material system. In particular, the results imply that in the case where stability and optical properties of SAM-GaAs systems are important, vapor deposition may be the self-assembly technique of choice in the development of advanced molecular structures and devices.

3.2 Experimental Results

3.2.1 Film Quality After Formation

CA goniometry was used to evaluate the characteristics of the ODT SAMs after preparation on the GaAs substrates from liquid and vapor phases. Specifically, CA analysis was used to detect the changes in the wetting properties on the semiconductor surface resulting from the formation of the organic films, as well as to probe their near-surface chain-packing density and uniformity. Details

regarding the protocol used to deposit the monolayers, the materials utilized, and the measurement methodology are provided in Chapter 2. Briefly, the CA of a 5 μL sessile water droplet was measured under ambient laboratory conditions immediately after the formation of the SAMs. To establish a reliable reference level for the purpose of comparison, the CA was measured on an untreated oxidized semi-insulating GaAs (100) substrate. The reference water CA on a film-free surface was found to be 67°. Following the SAM deposition, the ODT monolayers prepared from liquid and vapor phases demonstrated static water CAs of 100° and 102°, respectively. The increase in the CA reflects a decrease in the surface free energy upon the adsorption of the thiolates as the contact area with the water is minimized causing it to bead up on the modified GaAs surface. Similarly, the formation of a compact droplet on the monolayer signifies an increase in the hydrophobicity of the surface due to the nonpolar nature of the methyl endgroups. According to a survey of literature, water CAs in excess of 100° indicate the formation of high quality ODT SAMs on a GaAs surface [6], [53], [116]. Consequently, the relatively equal values of the measured CAs suggest a similar structure for monolayers prepared from liquid and vapor phases. Moreover, the high magnitudes of both CAs are consistent with the existence of conformationally well-ordered uniform films chemically bonded to the GaAs surface.

3.2.2 Passivating Properties

An interesting property of organic S-based monolayers on compound III-V semiconductors is their ability to passivate the surfaces, which is of particular importance to the successful operation of electronic and optical devices based on these materials [37]. As used here, passivation refers to the technological process of reducing the adverse effects of the electronically active defect states in the presence of operating ambients [64]. PL spectroscopy was used to assess the

effectiveness of passivating semiconductor surfaces with solution and vapor-deposited alkanethiol SAMs. Since the luminescence intensity of GaAs is greatly influenced by the high density of surface states that act as nonradiative recombination centers, PL measurements are a suitable means of monitoring the passivation efficiency of thin film coatings [10]. A detailed description of the PL system used in the analysis is provided in Chapter 2. Figure 3.1 shows room temperature PL spectra of ODT monolayers on semi-insulating GaAs prepared from liquid and vapor phases, as well as that of an untreated and hydrogen-cleaned GaAs substrate. To minimize the possibility of adverse effects caused by the exposure of the samples to oxygen and moisture, the spectra were collected immediately after atomic hydrogen cleaning or deposition of the organic films. As indicated in the figure, the steady-state peak PL intensity following SAM

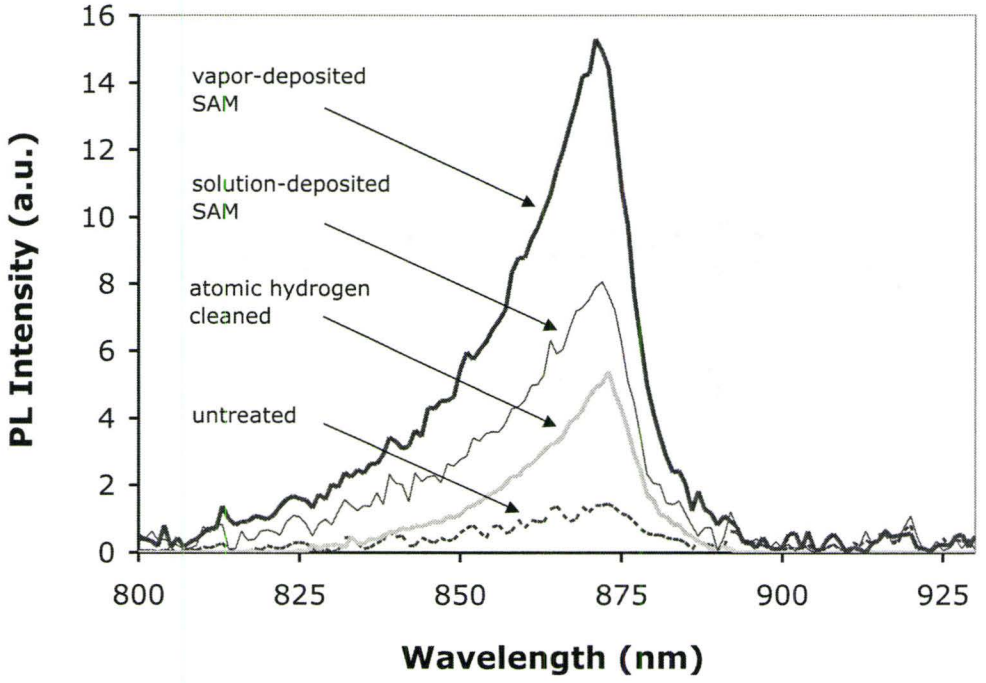

Figure 3.1: Room temperature PL spectra of various GaAs samples: untreated, after the atomic hydrogen cleaning procedure, with a solution-deposited ODT SAM, and with a vapor-deposited ODT SAM.

deposition increased compared to the untreated substrate, regardless of the method used to prepare the films. The observed enhancement in PL intensity upon exposure to the thiols is attributed to the formation of sulfur-surface bonds and the successful passivation of the midgap GaAs surface states typically present on an oxidized semiconductor surface [117]. Without an adequate means of passivation, the existence of a vast number of surface states in the vicinity of the fundamental gap depletes the charge carriers from the near-surface region of the GaAs crystal, pinning the Fermi level and bending the bulk energy bands [118]. The adsorption of the thiolate molecules onto the surface satisfies the dangling bonds and significantly reduces the density of surface states, thereby unpinning the Fermi level and unbending the bulk bands. The overall passivation effect due to the monolayer chemisorption results in an increase in the peak PL intensity of the GaAs owing to radiative recombination processes [10]. Direct comparison of the luminescence results in Figure 3.1, as well as those from numerous trials, revealed the magnitude of the PL enhancement induced by the monolayers was, on average, a factor of two greater for vapor-deposited SAMs when compared to their solution-deposited analogs. The basis behind this difference in passivation properties of the monolayers is investigated further in later sections.

An alternative reason for the improved surface passivation observed on the vapor-deposited SAMs that warrants further investigation is related to the atomic hydrogen cleaning process used to remove the native oxide layer from the semiconductor surface. As indicated in Figure 3.1, the PL intensity of the GaAs substrate increased after cleaning with atomic hydrogen. Three plausible explanations might be offered for the observed enhancement in PL yield upon exposure of the semiconductor to atomic hydrogen. The first involves the deposition of a partial ODT film on the GaAs surface resulting from residual thiols present in the growth chamber. The existence of thiol species in the preparation chamber during the atomic hydrogen cleaning process was confirmed by mass spectrometry, and is thought to result from the liberation of ODT

molecules condensed on the inner surfaces of the chamber from previous SAM depositions. A second possible explanation for the increase in PL intensity deals with the passivation of the GaAs surface and/or near-surface regions by hydrogen atoms [119], [120]. The final plausible explanation for the increased PL efficiency relies on a change in the optical properties at the GaAs interface due to surface roughening [121] that may have occurred as a result of the bombardment with atomic hydrogen radicals during the cleaning process. The possible influence of surface roughing on the PL characteristics of the vapor-deposited monolayers is addressed in the next section.

To probe the origin of the PL enhancement, CA measurements were performed on a GaAs substrate cleaned with atomic hydrogen. The static water CA on a hydrogen-cleaned sample was found to be 95°. While this CA was smaller than that observed on the ODT SAMs (100-102°), it is larger than the CA measured on the untreated substrate (67°), as well as that reported for presumed hydrogen-terminated GaAs surfaces, for which the CAs have been found to be in the range of 70-85° [83]. As suggested by the increased hydrophobicity of the sample surface, the CA data provides support for the hypothesis that the enhancement in PL intensity obtained on the hydrogen-cleaned GaAs sample is due to the formation of a partial ODT monolayer.

3.2.3 Surface Morphology

The surface morphology of the thiol-modified GaAs samples was characterized by means of AFM under ambient laboratory conditions. Since AFM is a convenient means of obtaining a high-resolution visual picture of the surface contours, as well as direct depth information, it can be used to investigate the structure-property relationships of the films [96]. Moreover, structural analysis of the GaAs surface was performed by AFM at various stages of the vapor deposition process in order to deduce if the enhanced change in PL yield

discussed in the previous section was linked to surface roughening caused by atomic hydrogen cleaning. The experimental procedures used to acquire the AFM data are described in Chapter 2.

Figure 3.2 shows AFM images obtained from an untreated GaAs substrate, a sample exposed to the atomic hydrogen cleaning process, as well as samples with a vapor- and solution-deposited SAM. Each image in the figure depicts an area of 1×1 μm^2. The dark depressions on the untreated GaAs substrate are attributed to small defects on the wafer due to polishing of the surface. The

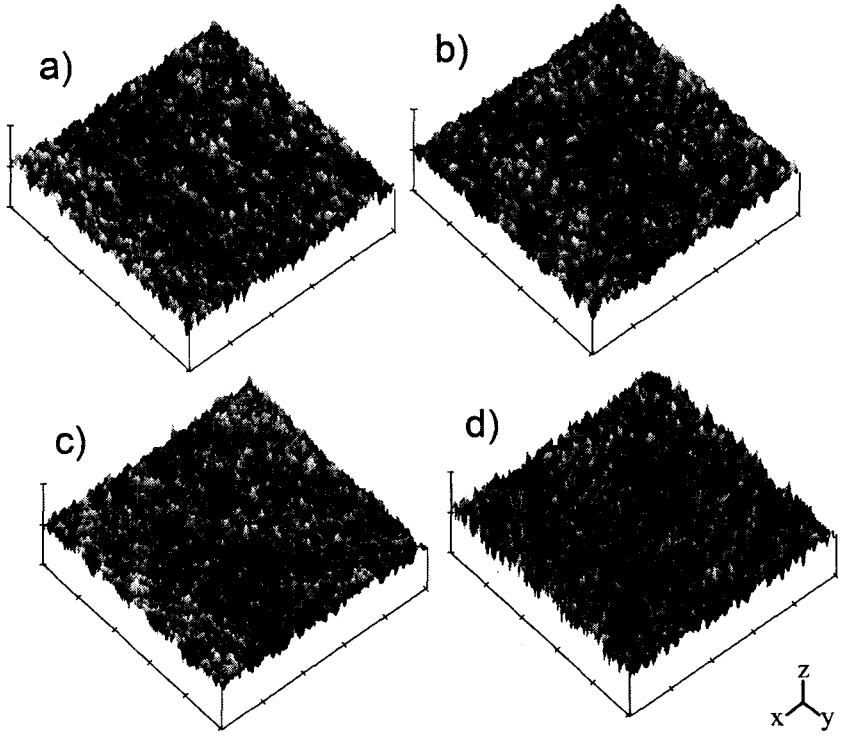

Figure 3.2: **AFM images of GaAs (100) surfaces, a) untreated, b) exposed to the atomic hydrogen cleaning process, c) with a vapor-deposited ODT SAM, and d) with a solution-deposited ODT SAM. (x and y axes: each division corresponds to 0.2 μm, z-axis: each division corresponds to 2.5 nm).**

images demonstrate that the surface morphology of the ODT films is comparable to that of a bare substrate as well as to the hydrogen-cleaned sample in terms of the general physical characteristics. The similarity in the topography between the bare and SAM-functionalized GaAs surfaces is expected given that the adsorption of the thiol molecules closely replicates the geometric contours of the underlying substrate [38], [122]. Furthermore, the topography of the SAM deposited from solution roughly resembles that prepared from vapor phase as no significant difference in the local features is observed.

From the AFM analysis, the rms and average roughness parameters were calculated to quantitatively assess the influence of surface roughness on the properties of the films. As the roughness of the substrate has a bearing on the final structure of the SAMs, with rougher surfaces resulting in less homogeneous, more defect prone films, it is important to determine the quality of the surface on which the monolayers are deposited [122]. The statistical roughness parameters for the samples investigated are presented in Table 3.1. As the data clearly shows, the standard atomic hydrogen surface cleaning procedure does not significantly roughen the GaAs surface topography. In fact, the surface roughness of the hydrogen-cleaned sample is comparable to that of an untreated GaAs substrate, as well as to that of a vapor-deposited ODT SAM. Thus, the observed improvement in the PL intensity obtained on vapor-deposited SAMs is not a consequence of a change in the optical properties at the GaAs surface due to surface roughening. Furthermore, the lower rms and average roughness of the vapor-deposited SAM in comparison to the solution-deposited monolayer implies the formation of a more uniform film with less defects using this preparation technique. The increased surface roughness observed on the solution-deposited SAM can likely be attributed to the wet-etch oxide removal process, which has previously been shown to produce a roughened overlayer on the GaAs surface [83].

Table 3.1: AFM roughness parameters.

Sample	rms roughness (nm, ± 0.02 nm)	Average roughness (nm, ± 0.03 nm)
Untreated GaAs substrate	0.22	0.17
Atomic hydrogen cleaned	0.23	0.18
Vapor-deposited ODT SAM	0.23	0.18
Solution-deposited ODT SAM	0.28	0.23

To further investigate the possible effects of surface roughness caused by the wet chemical procedure on the quality of the resultant SAMs, the standard UV-ozone/HF-etch treatment was performed on a GaAs substrate prior to the vapor deposition of an ODT SAM. Following the preparation treatment, the sample was immediately loaded into the UHV system, along with an untreated reference substrate. Both samples were then cleaned with atomic hydrogen and exposed to a flux of molecular ODT. Upon the completion of the vapor deposition process, the properties of the monolayers were examined by PL measurements. The improvement in PL efficiency obtained for the pretreated sample was closely comparable to that of the reference sample, indicating that the difference in surface roughness between solution- and vapor-deposited SAMs alone does not account for the apparent difference in their passivation properties.

The AFM data in conjunction with the PL measurements indicate that more densely packed films with better surface coverage are produced from vapor than from liquid phase and that the atomic hydrogen cleaning process alone is not responsible for the improved PL. Collectively, the complementary results presented thus far in this chapter imply that PL spectroscopy is more sensitive to the quality of the films when compared to CA analysis, which can be used to indicate the film quality at a more macroscopic level. Thus, PL spectroscopy reveals the differences in the resulting ODT SAM structures whereas CA measurements alone are insufficient in distinguishing between the two growth

methods and cannot serve as the sole characterization method for the determination of variations in molecular density.

3.2.4 SAM Structure and Surface Coverage

The nature of the SAMs deposited from liquid and vapor phase was further investigated by ellipsometry measurements. The application of spectroscopic ellipsometry to the characterization of organic thin films is an effective approach of establishing the thickness and density distribution of organized molecular assemblies [74]. Details regarding the instrumentation and experimental methodology used to acquire the ellipsometric spectra are given in Chapter 2. To describe the optical properties of the SAM samples, a three-phase model consisting of abrupt ambient, SAM, and substrate interfaces was used. In this approach, the organic film was assumed to be compact and homogeneous, based on the conclusions of a substantial number of previous studies on alkanethiol monolayers [123]. The index of refraction for the oxide-free semi-insulating GaAs substrate was obtained by ellipsometry from a freshly HF-etched sample. In the case of the vapor-deposited ODT SAM, a Cauchy dispersion function was used to express the variation in the index of refraction of the ODT monolayer with wavelength, λ, given by: [106]

$$n(\lambda) = A + \frac{B}{\lambda^2} \tag{3.1}$$

where λ is expressed in micrometers, and A and B are the Cauchy coefficients. A Cauchy relationship was applied to simulate the film's optical properties due to the lack of electronic transitions exhibited by alkanethiols in the measurement region, as well as to the slow varying nature of n as a function of λ [74], [124]. The variable Cauchy coefficients were determined by minimizing the mean-square error with the provided regression analysis software. To increase the

validity of the model, realistic physical constraints were imposed on parameters used in the Cauchy dispersion function. For example, the index of refraction of the ODT was maintained at a real value, as alkanethiols are nonabsorbing in the wavelength range of interest [124]. More specifically, the magnitude of the refractive index was permitted to vary in the range of 1.4 to 1.6 on account of the fact that the index of a crystalline monolayer should fall between 1.49 and 1.55, while a value of 1.45 is appropriate for bulk alkanethiols [38].

Figure 3.3 shows the experimental and the model-generated Ψ and Δ spectra for the vapor-deposited SAM sample. The simulated spectra closely resemble the measured results, demonstrating the suitability of the chosen three-phase model. From the iterative fitting procedure, the thickness of the vapor-deposited SAM was determined to be 21 ± 0.4 Å, whereas the Cauchy coefficients were found to be $A = 1.50 \pm 0.03$ and $B = 1.7\times10^{-3} \pm 1.7\times10^{-3}$ μm^2. The large (100%) uncertainty in the computed Cauchy B coefficient can be explained by the correlation between the thickness and index of refraction and by the inherent uniaxial anisotropy of the monolayer [124]. In particular, as a high quality thiol film is composed of an assembly of anisotropic, uniaxially oriented alkyl chains, its index of refraction is best described by a combination of separate components for light polarized parallel and perpendicular to the surface normal. Consequently, when an ideal SAM is described by a Cauchy layer in the model-dependent analysis, different A and B coefficients are expected for light incident at different angles since at each angle the refractive index consists of different relative contributions from its parallel and perpendicular components. While an anisotropic model would be more suitable in describing the optical response of the system, the complex spectral analysis involved would require additional assumptions about the monolayer's characteristics. Additional information concerning the interaction of radiation with the thin film would be required in order to determine the unknown parameters of the model for each angle. Since an accurate knowledge of the optical properties of the adsorbed monolayer is

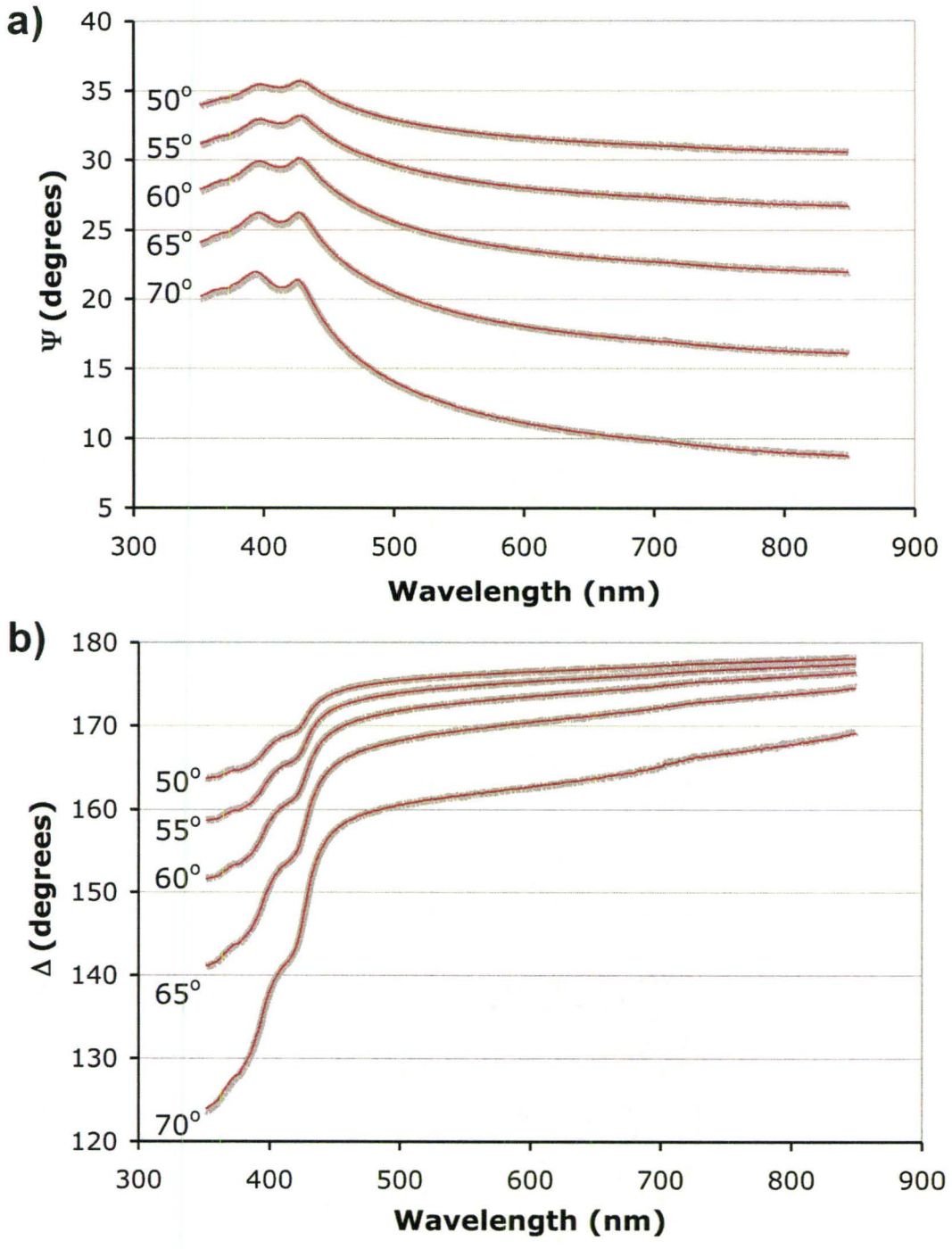

Figure 3.3: **Spectra of ellipsometric parameters a) Ψ and b) Δ of a vapor-deposited ODT SAM on GaAs for various angles of incidence (thick grey line: experimental data, thin red line: model fit).**

unavailable, a basic isotropic model, similar to the one used in this regression analysis, is often adopted to facilitate the interpretation of the ellipsometric data [123], [125], [126]. Nevertheless, the results obtained from this simplified approach are consistent with those adopted in earlier studies [30], [124], [127]. With these limitations in mind, the derived SAM thickness is comparable to the physical length of the octadecyl thiolate molecule (~24.5 Å), suggesting the existence of a well-ordered monolayer on the GaAs surface consisting of densely packed alkyl chains tilted at $31 \pm 2^{\circ}$ from the surface normal.

In an attempt to further increase the agreement between the experimental ellipsometric results and simulated parameters, an ODT/GaAs interface layer was introduced into the model. The optical properties of the interface layer were set to a weighted mean of that of the ODT and the GaAs substrate. However, as the improvement in the goodness of fit was negligible, the interface layer was removed from the model in lieu of the more general framework presented above.

To account for the apparent difference in quality of the monolayers formed from solution, the Bruggeman effective medium approximation (BEMA) [106] was used to describe the properties of the solution-deposited SAM in the three-phase model. The advantage of an ellipsometry analysis involving a BEMA scheme is the ability to characterize the volume fractions of different materials in a composite layer [128]. In this case, the specific BEMA used consisted of two constituents: the adsorbed ODT molecules (volume fraction = f_{ODT}) and a GaAs oxide (volume fraction = f_{ox} = 1- f_{ODT}). The thickness of the resulting solution-deposited film was assumed equal to that of the vapor-deposited SAM, as derived from the aforementioned model, while the variable parameter was the molecular packing density of the ODT. Consequently, the effective refractive index of the monolayer was taken to be a weighted average of the refractive index of the GaAs oxide and the ODT. In this case, the optical constants of the ODT were described

by a Cauchy dispersion formula, with the corresponding parameters determined from the vapor-deposited SAM.

Figure 3.4 shows the experimental and best-fit curves for Ψ and Δ of a film assembled from thiol solution on GaAs. The good agreement between the measured and simulated data implies the film consists of less dense domains of ODT with inclusions of a GaAs oxide. According to the ellipsometric model, the volume fraction of the GaAs oxide in the host medium was 30 ± 0.4 %. It is important to note that this oxide fraction is not an absolute quantity but rather is relative to that of the vapor-deposited SAM, which was assumed to be oxide-free. This assumption concerning the relative quality of the vapor-deposited monolayer was necessary to alleviate problems with cross-correlation between the model-fit parameters in a BEMA framework.

The results of the ellipsometric analysis correspond well to the diminished enhancement in PL intensity observed on SAMs deposited from liquid phase as opposed to those from vapor phase. In the case of vapor-deposited monolayers, the greater surface coverage, provided by a larger number of bonds that were formed between adsorbed ODT molecules and the GaAs substrate, directly translates to the improved passivation provided by these SAMs. On the other hand, the reduced surface coverage observed on the solution-deposited SAMs reflects a lower percentage of ODT-GaAs surface bonds and suggests the formation of oxide at the GaAs surface, thus leading to the reduced passivation. The partial reoxidation of the GaAs surface responsible for the reduced molecular packing density likely occurred during the solution deposition process or immediately after the removal of the sample from the solution into the air ambient.

To test the validity of the ellipsometric analysis, static wetting properties were calculated from the BEMA model in conjunction with Cassie's equation and compared to those measured by CA goniometry. As defined in Chapter 2, the

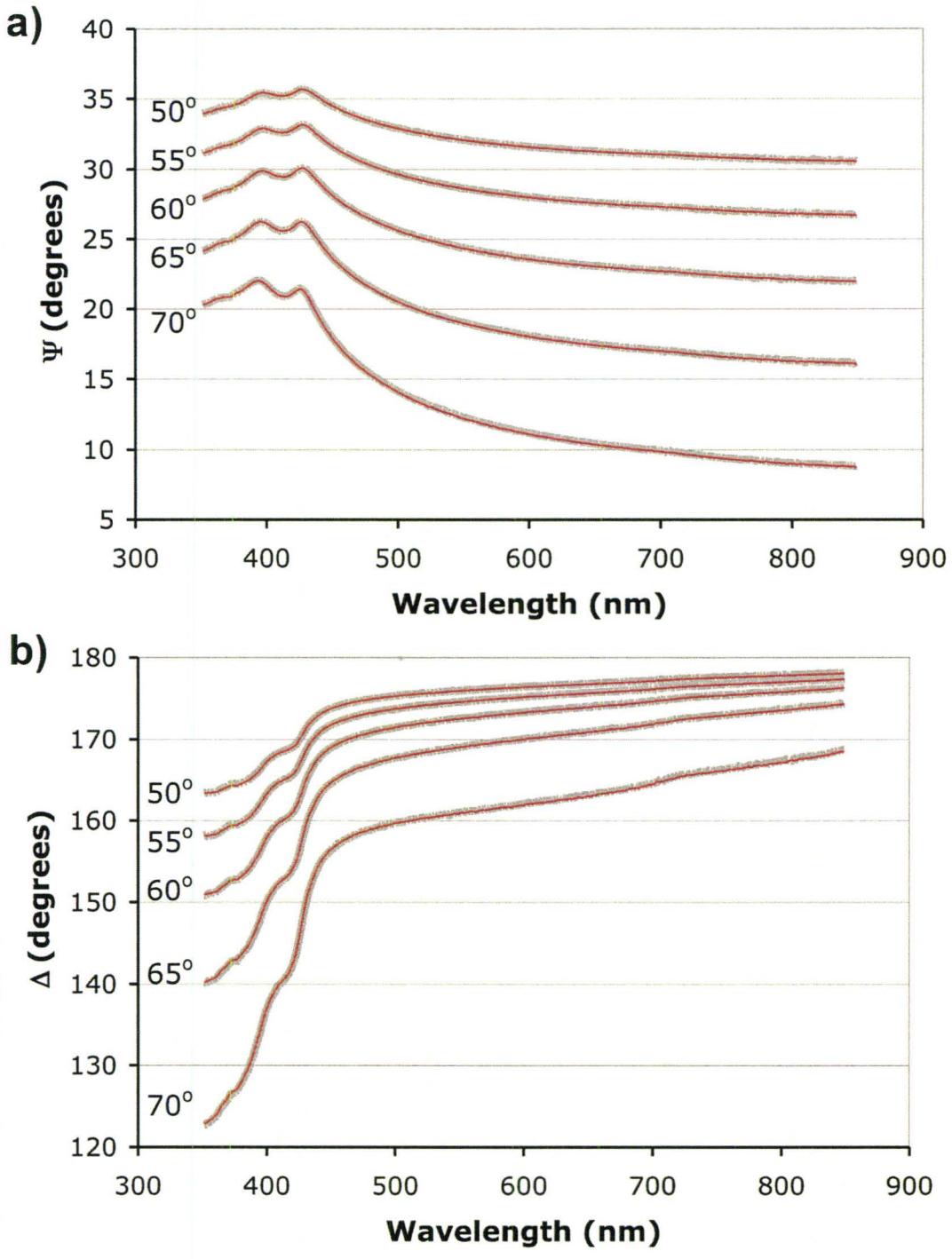

Figure 3.4: **Spectra of ellipsometric parameters a) Ψ and b) Δ of a solution-deposited ODT SAM on GaAs for various angles of incidence (thick grey line: experimental data, thin red line: model fit).**

influence of the monolayer's composition on the measured CA can be described by Cassie's equation, which relates the CA on a heterogeneous surface, θ_{ca}, to the areal fractions, f_1 and f_2, of the two constituents: [74]

$$\cos\theta_{ca} = f_1 \cos\theta_{d1} + f_2 \cos\theta_{d2} \quad \textbf{(3.2)}$$

where θ_{d1} and θ_{d2} are the CAs on the pure films of each component. Substituting the ellipsometrically derived volume fractions of the ODT and GaAs oxide into the equation, along with the measured CAs on the vapor-deposited monolayer and oxidized GaAs substrate, results in an estimated water CA of 92 ± 3° on the solution-deposited SAM. While the predicted CA differs from the experimentally measured value (100 ± 2°), the comparison suggests a tendency of the CA to decrease with decreasing surface coverage of the ODT SAM. Therefore, the difference between the measured water CAs on the vapor- and solution-deposited SAMs (102° versus 100°, respectively) could be interpreted to reflect a statistically significant difference in the packing density of the monolayers.

The apparent discrepancy between the measured CA and that obtained using the ellipsometrically derived parameters in combination with Cassie's equation can be attributed to two factors. First, Cassie's equation is most applicable to a heterogeneous surface which consists of macroscopic single-component domains that act independently [129]. Consequently, it is conceivable that in the case of the solution-deposited SAM, phase segregation did not occur to the extent necessary to create discrete, noninteracting islands of GaAs oxide and ODT large enough to affect the measured CA. Second, the augmented surface roughness of the solution-deposited SAM is also expected to influence the experimentally observed CA, increasing the measured value from that predicted by Cassie's equation [74]. With the previous considerations in mind, the comparison between the experimental and predicted CAs seems to substantiate

the surface coverage results obtained by means of spectroscopic ellipsometry for the ODT SAMs.

3.3 Conclusion

The discussion presented in this chapter examined and compared the properties of ODT monolayers assembled on GaAs substrates from liquid and vapor phases through a variety of complementary surface science techniques. While CA analysis indicated the formation of ordered films by both deposition methods, PL, AFM, and ellipsometry measurements revealed that the overall quality of the resulting SAMs, as well as the attainable surface coverage, depend on the preparation method. In particular, the experimental results showed that PL spectroscopy is more sensitive than CA goniometry in the detection of the variation in the molecular density of the ODT SAMs. The lower SAM coverage, larger surface roughness, and reduced passivation observed on samples prepared from liquid phase could be related to the formation of a partial oxide layer on the GaAs surface as a result of the deposition process. The existence of a partial oxide on the substrate surface suggests a randomized surface structure consisting of a mixture of thiolate molecules and oxide as opposed to a close-packed molecular assembly. To prevent the reoxidation of the GaAs surface and improve the quality of the films, ODT SAMs were formed on the semiconductor surface from vapor phase. A custom-built system was used to attain the desired UHV conditions and clean deposition environment. The resulting SAM structures were found to have greater surface coverage and enhanced passivation properties, as confirmed by ellipsometry and improved PL peak intensity. Additionally, AFM data indicated a smoother topography for the vapor-deposited films. On the basis of these findings, in can be concluded that the structural and chemical properties of the

ODT SAM-GaAs systems are in fact affected by the deposition technique used to prepare the monolayers. Moreover, these results have clearly demonstrated that the preparation of organic SAMs on III-V semiconductors from vapor phase holds promise for a wide range of potential applications that require superior quality organic films.

Chapter 4 Passivation of GaAs by ODT SAMs Deposited from Liquid and Vapor Phases

4.1 Introduction

The passivation of III-V semiconductor surfaces and in particular, GaAs, has been the subject of intensive studies in recent years [51], [130]-[134]. The interest in developing durable passivants is mainly derived from the need to remove the high density of problematic oxide-related surface states that originate from the tendency of the semiconductors to oxidize in ambient conditions. Since the defect states detrimentally affect the electronic and optical properties of the materials, the role of efficient passivants is critical to enhancing the performance of III-V based devices [135]. Although numerous passivation methods have been proposed, ranging from plasma hydrogenation to inorganic sulfidization using wet and dry chemical treatments, poor reproducibility, contamination, and rapid degradation under atmospheric conditions have limited the widespread use of these techniques in the processing and fabrication of devices [120], [130], [136]. Since the degree of passivation has been shown to vary depending on the treatment used to modify the surface, it is necessary to study the efficacy of the proposed passivation method in terms of its suitability for an intended device application. This is of particular importance in the design of an optical PL-based

hybrid biosensor, since the PL response is dictated by the efficiency of the passivation.

One of the more promising approaches to GaAs passivation involves the deposition of organic SAMs on the surface of the semiconductor. The inherent ability of adsorbed monolayers to modify the physical and chemical properties of solid surfaces makes them attractive for the effective control of III-V semiconductors. As alluded to in Chapter 3, alkanethiol-based SAMs have proven to be particularly successful in passivating the electrical activity of unfavorable GaAs dangling bonds through the formation of a well-ordered array of molecules chemically bound to the surface [137]. Consequently, this novel passivation mechanism has demonstrated its relevance as a prospective means of preventing further chemical modification, while at the same time, maintaining the desired electronic properties of the underlying surface, especially in the case of nanoscale device structures for which there is a large surface-to-volume ratio [47].

An important consideration in any surface passivation scheme is the stability of the passivating coatings when exposed to ambient conditions. The passivant must inhibit the regrowth of oxide on the semiconductor surface over a prolonged period of time to be a viable candidate for technological applications [56], [131]. For SAM-based passivants, a key issue pertains to the precise longevity of the treatments under atmospheric conditions as controversial results have been reported for their effectiveness in protecting III-V surfaces against reoxidation, partly due to the range of experimental conditions used to deposit the films across different laboratories [29], [30], [53], [58], [138]-[140]. Hence, it has become increasingly imperative to accurately determine the stability of SAMs prepared by various methods, as well as to develop a better understanding of the reasons underlying the discrepancy in the reliability of the ensuing passivation.

In this chapter, ODT SAMs were assembled on GaAs from solution and from vapor phase and the durability and optoelectronic characteristics of the

resultant monolayers were evaluated over the course of several months by means of CA analysis and PL spectroscopy. Complementary studies using spectroscopic ellipsometry and HRXPS were conducted to correlate the chemical and structural properties of the films to the efficacy of the resulting passivation. As will be discussed later in this chapter, the parametric model used in the analysis of the ellipsometric data expands on the model presented in Chapter 3 and provides a more detailed interpretation of the structural characteristics of the monolayers. The majority of the results discussed in this chapter have been previously published by the author in [141]. Collectively with Chapter 3, the results presented herein suggest that more robust monolayers exhibiting greater surface coverage and therefore, increased passivation and stability characteristics, are assembled from vapor phase.

4.2 Experimental Results

4.2.1 Stability of SAM Passivation

To determine the stability of the passivating films, the PL intensity was measured after leaving the samples under ambient conditions. A thorough description of the PL setup used in the measurements is presented in Chapter 2. Figure 4.1 shows the peak PL intensity as a function of storage time in air for ODT SAMs on semi-insulating GaAs prepared from liquid and vapor phases, as well as that of untreated and atomic hydrogen cleaned GaAs substrates. As indicated in the figure, the PL intensity progressively decreased over the measurement time for all of the treated samples. The time dependence of the PL intensity decay for the vapor-deposited SAM and the atomic hydrogen cleaned sample exhibits temporal characteristics with two different rate components.

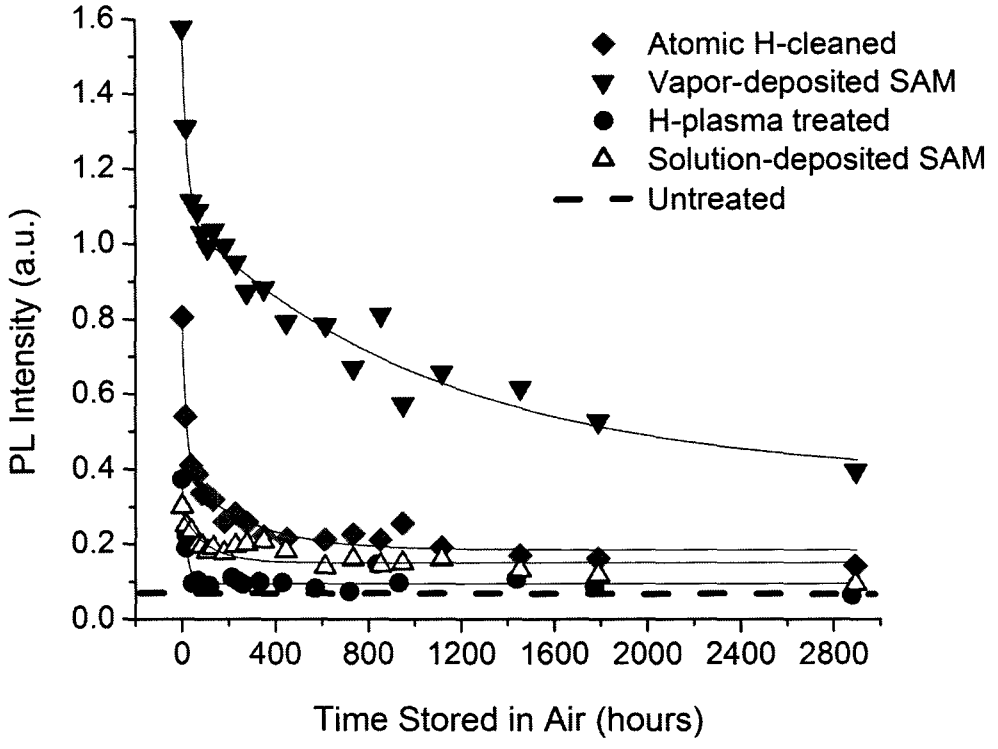

Figure 4.1: **Room temperature peak PL intensity as a function of storage time in air for ODT SAMs on GaAs prepared from liquid and vapor phases, as well as that of untreated and hydrogenated GaAs substrates. The PL data was fitted to exponential decay functions with the fitting results given in Table 4.1.**

Specifically, the decrease in the luminescence signal appears to proceed at a faster rate initially within the first ~100 hours, and then continues at a slower rate with increased exposure to an ambient environment. To highlight this relationship, the PL data was fitted using a least-squares fitting routine to a double exponential decay equation as defined by [142]

$$PL\ Intensity = \alpha_o + A_1 e^{-t/\tau_1} + A_2 e^{-t/\tau_2} \quad (4.1)$$

where t is the storage time in air, A_1 and A_2 are positive fit parameters, and τ_1 and τ_2 are the fast and slow decay time constants, respectively. As demonstrated by the results of the fit analysis presented in Table 4.1, the time constant τ_1 calculated

Table 4.1: Parameters obtained from the fit analysis of the PL decay measurements for the SAM-modified and hydrogenated GaAs samples.

Sample	Curve-fitting equation	Parameters calculated from curve-fitting analysis				
		α_o	A_1	τ_1 (hrs)	A_2	τ_2 (hrs)
Vapor-deposited SAM	$\alpha_o + A_1 e^{-t/\tau_1} + A_2 e^{-t/\tau_2}$	0.37 ± 0.08	0.51 ± 0.06	22 ± 6	0.70 ± 0.07	(1.1± 0.3)×10^3
Atomic hydrogen cleaned	$\alpha_o + A_1 e^{-t/\tau_1} + A_2 e^{-t/\tau_2}$	0.18 ± 0.01	0.41 ± 0.04	17 ± 4	0.21 ± 0.03	(2.7± 0.9)×10^2
Hydrogen plasma treated	$\alpha_o + A_1 e^{-t/\tau_1}$	0.10 ± 0.01	0.28 ± 0.02	17 ± 2	-	-
Solution-deposited SAM	$\alpha_o + A_2 e^{-t/\tau_2}$	0.15 ± 0.01	-	-	0.13 ± 0.02	(1.1± 0.3)×10^2

for the luminescence decay of the vapor-deposited SAM closely resembles that of the atomic hydrogen cleaned sample. As described below, the fast decay (τ_1) can be attributed to the hydrogen passivation, while the slower decay (τ_2) can be explained by ODT passivation.

In an effort to clarify the role of hydrogen in the observed PL enhancement and to eliminate the influence of residual ODT in the vapor deposition chamber, a GaAs substrate was exposed to a hydrogen plasma source in a clean, ODT-free UHV reactor. The processing conditions of the hydrogen plasma treatment were set equivalent to those used for the atomic hydrogen cleaning, in order to achieve an analogous resultant surface. Specifically, the plasma treatment was performed for 10 minutes at an RF (13.56 MHz) power of 350 W applied in the inductively coupled mode, at a pressure of 2.4×10^{-5} Torr, and a substrate temperature of approximately 500°C. As the data in Figure 4.1 shows, the peak PL intensity measured immediately following the plasma treatment increased compared to the untreated substrate. The improvement in PL signal exhibited by the hydrogenated sample is attributed to the passivation of the

dangling bonds and/or near-surface lattice defects in the GaAs substrate by hydrogen atoms. However, with a longer exposure to an ambient atmosphere, the PL yield of the plasma-treated sample rapidly decayed (within about 48 hours) and reverted to nearly the same level as that of an untreated substrate.

To quantify the dynamic characteristics of the PL signal, the time-dependent PL data measured on the hydrogen plasma passivated sample was best fitted to a single exponential equation as given by

$$PL\ Intensity = \alpha_o + A_1 e^{-t/\tau_1} \tag{4.2}$$

where t is the storage time in air, A_1 is a positive fit parameter, and τ_1 is the decay time constant. The results of this analysis are summarized in Table 4.1 and indicate that the partial degree of passivation provided by the hydrogen treatment alone is not successful in stabilizing the GaAs surface for an extended period of time. It is important to note that the time scale (τ_1) over which the PL intensity of the plasma-processed sample degrades coincides within the limits of experimental error with the fast decay rates observed on the atomic hydrogen cleaned sample and the vapor-deposited SAM. The fact that all three of these samples were submitted to a hydrogen treatment suggests the mechanism responsible for the initial decline of the PL signal is the same in all three cases and most likely involves a rapid reduction of the passivation efficacy provided by the hydrogen atoms with increased exposure to air.

Upon closer examination, the experimental data shown in Figure 4.1 reveals that the SAM-modified samples are more stable when compared to the hydrogen plasma-treated sample. In particular, the time required for the PL intensity to decay to 60% of its initial value was 109 hours for the solution-deposited SAM and only about 16 hours for the plasma-treated sample, even though the PL signal initially increased by a larger factor following hydrogen plasma passivation. Clearly, it can be concluded that the relative improvement in

the luminescence efficiency brought about solely by the introduction of hydrogen is short-lived, while the enhancement in PL intensity due to the solution-deposited thiol monolayer, in absence of any hydrogen treatment, is maintained for a longer duration. The apparent long-term stability of the SAM passivated surfaces is believed to result from the formation of robust bonds between the sulfur containing thiols and the GaAs surface, which act as an effective barrier against oxidation of the underlying surface. In the case of the atomic hydrogen cleaned sample, the PL decay data revealed an initial fast decay (τ_1) due to hydrogen passivation, and a slower decay (τ_2). The slower decay can be explained by the deposition of a partial ODT film resulting from residual thiols present in the deposition chamber. The existence of thiol species in the preparation chamber during the atomic hydrogen cleaning process was confirmed by mass spectrometry, and is thought to result from the liberation of ODT molecules condensed on the inner surfaces of the chamber from previous SAM depositions [115].

Another important outcome that can be inferred from the luminescence dynamics deals with the relative stability of the vapor-deposited SAM compared to its solution-deposited counterpart. As shown in Figure 4.1, the magnitude of the PL improvement induced by the SAM was a factor of five greater for vapor deposition when compared to that from solution deposition. After a few hours in an ambient environment, the decay in the luminescence intensity was more pronounced for the vapor-deposited SAM than the solution-deposited SAM. However, with extended ambient exposure time this decay rate decreased significantly. In contrast, the PL signal measured on the monolayer deposited from solution decreased at a more gradual rate initially and then reached a steady-state level after roughly 65 hours in air. This difference in the stability characteristics between the samples can be explained by the variation in the processing conditions used during the deposition of the films. In the case of the vapor-deposited monolayer, the sample was pretreated in atomic hydrogen prior

to the deposition of the thiol film. Consequently, the ensuing passivation of the GaAs surface immediately following the vapor deposition is a product of two distinct passivation methods, namely, hydrogen passivation and ODT SAM passivation. As shown previously in the case of the hydrogen-plasma treated sample, the effects of hydrogen passivation dissipate quickly and thus, are likely responsible for the initial abrupt decrease in the PL intensity of the vapor-deposited sample. With an extended exposure to ambient conditions, the decay in PL yield drastically reduced to a value lower than the rate exhibited by the solution-deposited SAM (see Table 4.1), which suggests that the prolonged enhancement in PL can be attributed to the passivation of the underlying substrate by the organic monolayer. Moreover, after four months in air, the final PL intensity observed on the vapor-deposited SAM was still about a factor of five greater than the intensity measured on the solution-deposited SAM. On the basis of this comparison, the PL results indicate that more stable films with better surface coverage are produced from vapor than from liquid phase and that the hydrogen cleaning process alone is not responsible for the improved PL intensity.

4.2.2 Stability of Surface Organization

To validate the conclusions regarding the stability of the organic films, CA analysis was used to detect the changes in wetting properties on the functionalized semiconductor surfaces brought on by the exposure of the samples to ambient conditions. A description of the experimental methodology used in the measurement of the CAs is provided in Chapter 2. The static water CAs measured on the various GaAs surfaces are summarized in Table 4.2. Immediately after the SAM deposition, the ODT monolayers prepared from liquid and vapor phases demonstrated static water CAs of 100° and 104°, respectively. As mentioned in Chapter 3, water CAs greater than 100° suggest the assembly of high quality ODT monolayers on GaAs surfaces [6], [53], [116]. Consequently, the measured CAs

Table 4.2: Static water CAs measured on GaAs following various treatments and SAM deposition methods. The CAs were measured on [a] newly treated surfaces as well as [b] after being exposed to air for a four month period.

Sample	CA (degrees) (± 2°)	
	Initial[a]	After four months in air[b]
Untreated	73	-
Hydrogen plasma cleaned	62	75
Atomic hydrogen cleaned	95	82
Solution-deposited SAM	100	85
Vapor-deposited SAM	104	98

suggest a similar initial structure for monolayers prepared from liquid and vapor phases, consistent with the existence of uniform films chemically bonded to the GaAs surface. Nevertheless, the small difference between the water CAs on the two SAMs could be interpreted to reflect a statistically significant difference in the packing density of the monolayers, as discussed in Chapter 3. While the CA measured on the atomic hydrogen cleaned sample was smaller than that observed on the ODT SAMs, it is larger than the CA measured on the untreated substrate, as well as that measured on the hydrogen plasma-treated GaAs surface. Thus, the increased hydrophobicity of the sample surface provides support for the hypothesis that the enhancement in PL intensity obtained on the atomic hydrogen cleaned GaAs sample is due in part to the formation of a partial ODT monolayer.

As shown in Table 4.2, the CA of the SAM-modified surfaces decreased after the samples were stored in air for a period of four months. Since the magnitude of the CA depends directly on the quality of the SAM monolayer, the decrease in the CA represents degradation in the film structure with prolonged exposure to the air ambient. Accordingly, the smaller change in the CA observed for the vapor-deposited monolayer compared to that synthesized from solution reflects the superior stability of SAMs prepared under UHV conditions, and is consistent with the PL findings discussed earlier, which show a more gradual

degradation in the film deposited from vapor phase over the course of several months.

4.2.3 Adsorbate-Substrate Bonding Characteristics

To more fully understand the consequences of GaAs passivation by ODT SAMs, the chemical composition of the monolayers deposited from vapor and liquid phases was examined by HRXPS. Details regarding the experimental methods used in the acquisition of the XPS data are given in Chapter 2. Figure 4.2 a) and b) show a comparison of Ga 3d and As 3d core-level spectra, respectively, for GaAs samples which have been untreated, freshly etched in buffered HF, exposed to atomic hydrogen, and modified with an ODT monolayer. The spectrum of the HF-etched GaAs surface was obtained from a sample that was etched for 2.5 minutes in concentrated (~49%) HF, rinsed in deionized water, dried in air, and loaded into the vacuum atmosphere of the XPS instrument within approximately 3 to 5 minutes. Since the etched sample was exposed to the ambient environment for a minimal duration, it was used as a reference standard to which the amount of oxide present at the surface of the other samples was compared. The measured Ga 3d and As 3d spectra were decomposed into several distinct components, with each fitted self-consistently by a pair of characteristic doublets. Peak assignments were made to account for contributions from the bulk Ga and As species, native oxide Ga and As species, elemental Ga and As species, as well as from specific Ga-S and As-S binding components, where applicable. The binding energies associated with the core emissions are summarized in Table 4.3. A survey of recent literature shows that the peak assignments are in agreement with previously reported values [54], [133], [143], [144]. The fitted

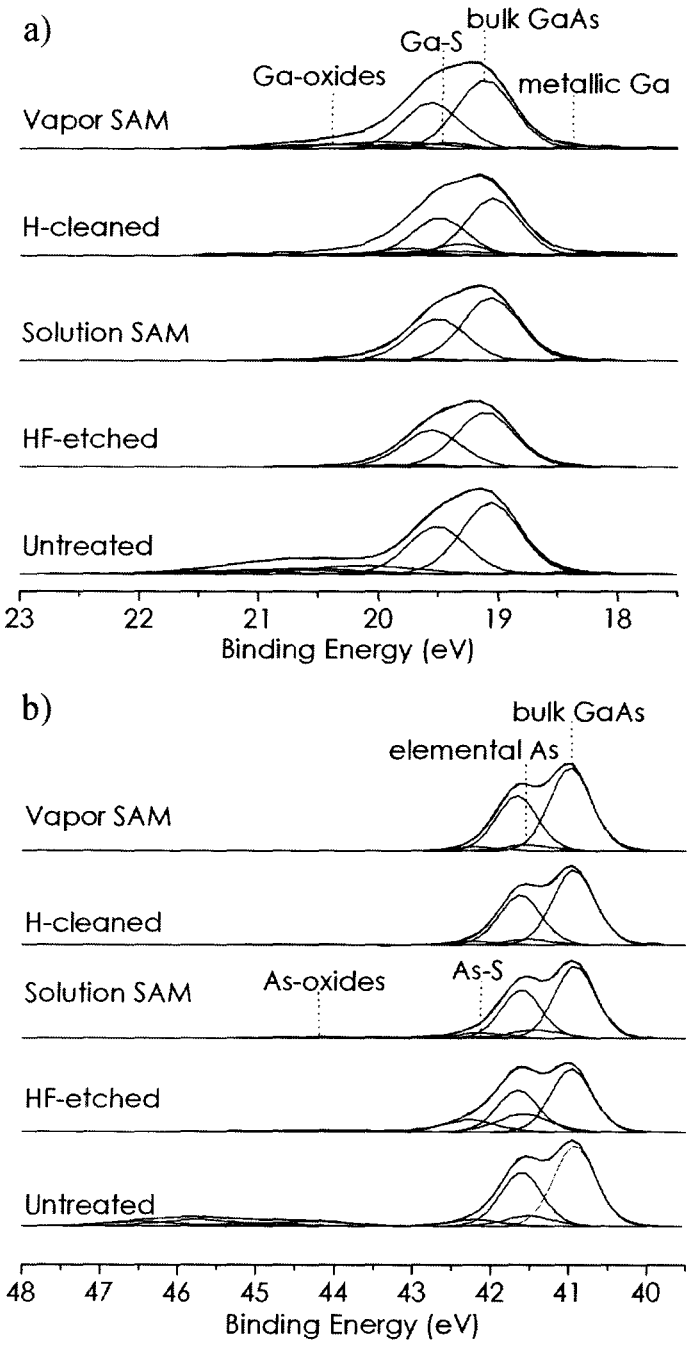

Figure 4.2: **HRXPS spectra of the a) Ga 3d and b) As 3d core levels of GaAs after various treatments and SAM preparation methods recorded at a take-off angle of 90°. The spectra have been offset vertically for clarity and fitted to show the contributions of the component features.**

Table 4.3: Binding energies of different peaks in the Ga 3d and As 3d spectra presented in Figure 4.2 and Figure 4.3. For simplicity, only the energy of the main component in each doublet is reported.

Core level	Binding energy (eV)	Peak assignment
Ga $3d_{5/2}$	19.1 ± 0.2	bulk GaAs
	20.8 ± 0.1	$Ga(OH)_3$
	20.0 ± 0.3	Ga_2O_3
	19.8 ± 0.1	Ga_2O
	18.4 ± 0.2	metallic Ga
	19.5 ± 0.2	Ga-S
As $3d_{5/2}$	40.9 ± 0.1	bulk GaAs
	46.2 ± 0.3	As_2O_5
	44.4 ± 0.4	As_2O_3
	41.5 ± 0.3	elemental As
	42.1 ± 0.1	As-S

spectra overlapped nearly perfectly with the measured spectra in Figure 4.2. Due to the good quality of the fit to the experimental data, some important trends are deduced from the following analysis.

To accentuate the differences between the various surface treatments, the signals from the Ga/As oxides, metallic Ga/elemental As, and Ga-S/As-S components are displayed separately in Figure 4.3. The spectra in Figure 4.3 were multiplied by a factor of five relative to those in Figure 4.2. As shown in Figure 4.3, the untreated GaAs substrate is heavily oxidized at the surface by a native oxide layer consisting of a mixture of Ga- and As-related species. After the etching in HF, the quantity of oxide on the surface was greatly reduced, although it was not entirely eliminated. The incomplete removal of the native oxide layer is likely due to the short exposure of the sample to air during its transfer into the XPS system. Following the deposition of the ODT monolayer from solution, the amount of oxide stayed virtually the same as that measured on the etched material. The fact that the level of oxidation remained unchanged suggests

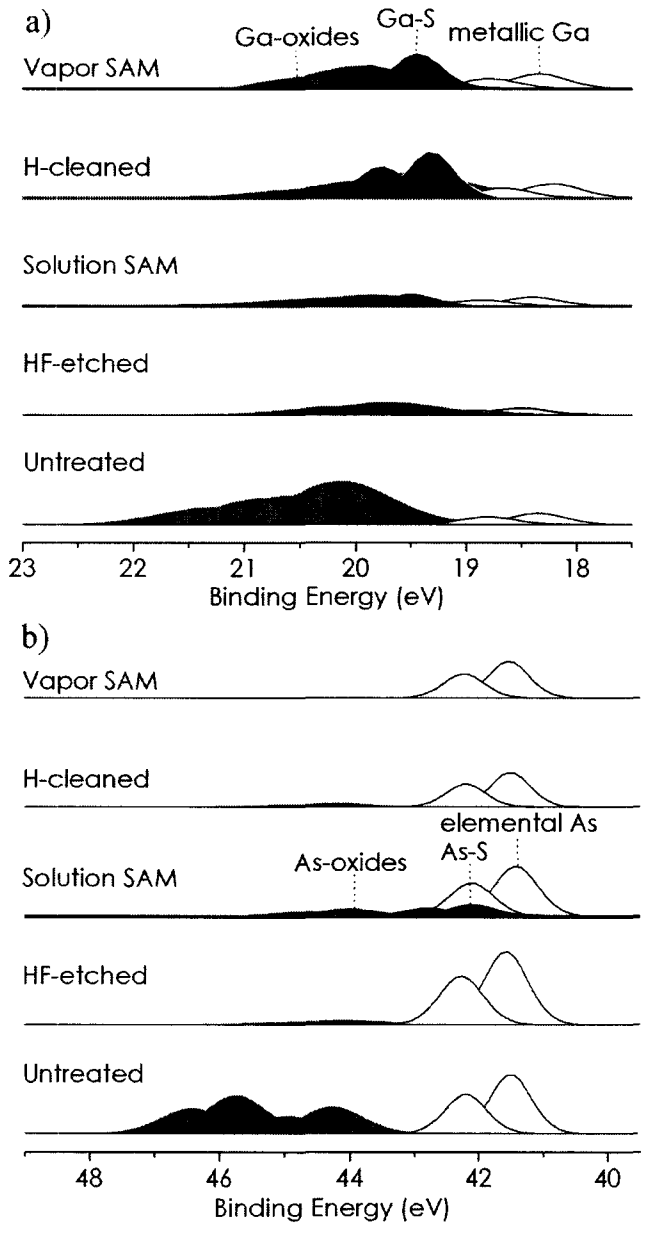

Figure 4.3: **HRXPS spectra of specific a) Ga 3d and b) As 3d core levels of GaAs after various treatments and SAM preparation methods recorded at a take-off angle of 90° (grey doublet: Ga/As oxides, white doublet: metallic Ga/elemental As, black doublet: Ga-S/As-S). The spectra have been offset vertically for clarity. The signals from the Ga/As oxides, metallic Ga/elemental As, and Ga-S/As-S components have been multiplied by a factor of five relative to those shown in Figure 4.2 to accentuate the differences between the curves.**

insufficient etching of the residual oxide by the ammonium hydroxide in the thiol solution. As the presence of oxide species on the sample surface is believed to hinder the formation of the monolayer [145], it is likely that the packing density of the solution-deposited film is less than that of an ideal monolayer formed on an oxide-free surface. On the other hand, the spectra for the vapor-deposited SAM presented in Figure 4.3, show a greater contribution from the Ga oxide component in comparison to that of the HF-etched sample, as well as the total elimination of the As oxide component. Since similar results were obtained for the atomic hydrogen cleaned sample, it is believed that the selective removal of the As oxide species is associated with the exposure of the GaAs surface to atomic hydrogen. Hydrogenation of a GaAs substrate causes a reaction between the incident hydrogen atoms and the native oxide, which leads to a reduction in the concentration of more volatile As species and results in regions of Ga oxide, specifically Ga_2O_3, on the surface [146], [147]. The fact that the Ga oxides tend to remain partially intact following hydrogenation is considered to play a role in preserving the effects of hydrogen passivation [119], [120]. Consequently, as the XPS data indicates, the atomic hydrogen pretreatment was not effective in fully reducing the oxides of Ga, presumably due to the processing conditions used during the treatment, such as substrate temperature and/or insufficient hydrogen dose, which may not have been adequate to completely desorb the Ga_2O_3 [148]. The existence of a non-negligible amount of Ga oxide on the hydrogenated samples suggests that the atomic hydrogen cleaning process can be further optimized to promote the full removal of Ga-like oxides, potentially increasing the coverage of SAMs subsequently deposited on the pretreated surfaces. Alternatively, the Ga-oxide in the spectra of the hydrogen-treated samples can be explained by the short exposure of the samples to the ambient during their transfer into the XPS system. When the GaAs surface is exposed to atomic hydrogen at an elevated temperature, the selective depletion of As-related species occurs, which leads to the production of a Ga-rich overlayer on the resultant surface, as

discussed below. Consequently, the Ga-oxide could have in fact been reduced as a result of the hydrogen treatment and simply reformed rapidly on the ODT-free Ga enriched areas during the short exposure of the samples to air. A method of controlling and monitoring the atomic hydrogen cleaning process involves the introduction of an in-situ characterization technique, such as LEED or Auger electron spectroscopy, during the treatment in order to define the optimal conditions for the cleaning process, as well as to determine the end-point of the oxide removal [90].

Another interesting feature in Figure 4.3 is the appearance of a peak at 18.4 eV in the HRXPS spectra of the hydrogenated samples that can be assigned to elemental Ga generated by the selective depletion of As from the substrates during the hydrogen treatment [119], [148]. Along with the existence of a metallic component, the Ga spectra of the hydrogen-cleaned sample and that of the vapor-deposited SAM reveal a small peak at an energy of 19.5 eV. As this peak was not observed in the spectra of the untreated substrate and the HF-etched sample, it was attributed to the formation of Ga-S bonds on the GaAs surface. This value for the binding energy of Ga-S is in accordance with that previously observed for sulfides on GaAs [133]. The presence of Ga-S bonds in the spectrum of the hydrogen-cleaned sample confirms the formation of a partial ODT film on the sample surface, as speculated above and in Chapter 3. In contrast to the Ga spectra, the As spectra of the hydrogen pretreated samples do not indicate the existence of an As-S binding component. The dominant contribution from the Ga-S bonding and the absence of As-S bonding from the spectrum of the vapor-deposited SAM is expected when the stoichiometry of the surface prior to the film growth is considered. As mentioned previously, the hydrogen-cleaned GaAs surface is depleted of As as a result of the cleaning process and thus, is Ga enriched. Since the deposition of the SAM from vapor phase immediately follows the hydrogen treatment, it is not surprising that the majority of the chemical bonds at the SAM-GaAs interface are Ga-S in nature due to the lack of available As

bonding sites on the cleaned surface. Conversely, the Ga 3d and As 3d spectra of the solution-deposited SAM shown in Figure 4.3 indicate a relatively equal quantity of Ga-S and As-S bonds following ODT modification. This result is also anticipated as previous reports indicate that the chemical etching of GaAs in a dilute HF solution produces a nearly stoichiometric surface termination with a slight excess of As atoms [149]. It should be noted that the HF-etched sample used in the XPS analysis was produced by etching a GaAs substrate in a solution five times more concentrated than that used to clean the sample prior to depositing the SAM from liquid phase. Since the As enrichment on the resultant surface is proportional to the concentration of HF [150], the etched surface in Figure 4.3 is expected to be significantly more As-rich than that used in the solution deposition of the ODT film, which should reflect a more stoichiometric surface composition. Therefore, the XPS data seems to suggest that S-based chemical bonds between the thiolate molecules and the GaAs surface occur at both Ga and As adsorption sites, with the relative abundance of each bonding configuration strongly dependent on the surface composition achieved by the cleaning method used prior to the deposition of the SAM [151]. Moreover, since Ga-S bonds have been reported to be stronger than As-S bonds, the fact that Ga-S bonds are more prevalent in the monolayer deposited from vapor phase is consistent with the increased durability of the SAM, as evident in the PL and CA measurements [66], [133], [152].

A comparison of the C 1s and O 1s spectra of the analyzed samples is given in Figure 4.4. After etching in the HF solution, the C 1s spectrum of the GaAs substrate shows the presence of carbon contamination as defined by the existence of the main hydrocarbon-related peak at a binding energy of 285.0 eV, as well as the formation of a higher energy tail which can be attributed to oxidized carbon species in the form of CO and CO_2 at about 286.5 eV and 289.1 eV, respectively [153]. Contamination of the freshly etched surface by adventitious carbon probably occurred during the transfer of the sample into the XPS

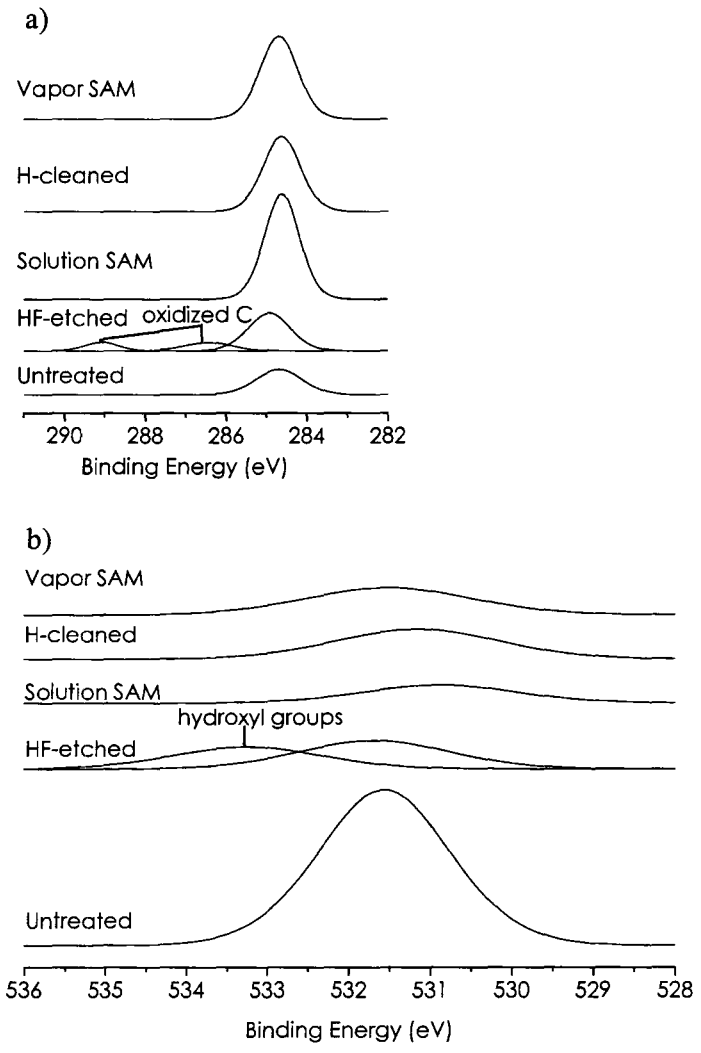

Figure 4.4: **HRXPS spectra of the a) C 1s and b) O 1s core levels of GaAs after various treatments and SAM preparation methods recorded at a take-off angle of 90°. The spectra have been offset vertically for clarity.**

apparatus. On the other hand, the C 1s spectra of the atomic hydrogen cleaned sample as well as those of the SAM-modified samples show a complete absence of oxidized carbon and the distinct presence of a single sharp peak at a binding energy of approximately 284.7 eV, which agrees well with the binding energy reported for C-C/C-H bonds in the backbone of ODT SAMs on GaAs [29], [58].

The lower intensity of the C 1s emission for the hydrogen-cleaned sample when compared to that for the ODT-treated samples signifies the existence of a partial ODT film with a lower surface coverage. In addition, the C 1s peaks of the hydrogen-cleaned and solution-deposited SAM samples are slightly shifted to a lower binding energy with respect to that of the vapor-deposited SAM, which suggests that the carbon atoms exist in an alternate chemical state and likely reflects a more disordered structure for the thiolate molecules on the surfaces of these samples. Moreover, the larger intensity of the C 1s peak observed on the solution-deposited SAM when compared to that of the vapor-deposited SAM may be interpreted in terms of a difference in the tilt angle of the alkyl chains comprising both monolayers. The larger intensity of the C 1s line on the SAM prepared from solution can reflect a thicker monolayer structure and thus, a smaller tilt of the alkyl chains from the surface normal. In contrast, the smaller intensity of the C 1s signal on the vapor-deposited SAM suggests a more canted, thinner film structure with a larger angle between the chain axis and the surface normal. The presumed difference in the orientation of the monolayers relative to the sample surface was verified by spectroscopic ellipsometry as discussed later.

The O 1s spectra shown in Figure 4.4 provide further support for the conclusions deduced from the respective Ga 3d, As 3d, and C 1s spectra. In particular, the O 1s data clearly shows that the amount of surface oxide is significantly diminished following SAM modification and atomic hydrogen cleaning when compared to the level obtained after etching in HF, as well as to the initial level on the untreated GaAs substrate. As this data is consistent with minimal levels of Ga- and As-related oxides in the Ga 3d and As 3d spectra of the SAM-passivated samples, it provides evidence for the previous statement concerning the ability of the films to act as effective barriers against oxidation of the underlying surface. It is interesting to note in Figure 4.4 that in addition to the main oxygen component, the spectrum of the HF-treated sample shows the

existence of hydroxyl groups on the etched GaAs surface, as indicated by the presence of the higher binding energy component at about 533.3 eV [154].

The larger intensity of the O 1s core peak for the hydrogen-cleaned sample when compared to that from the SAM-modified samples coincides with the formation of an island-like ODT coating. Likewise, the slightly larger intensity of the O 1s signal for the vapor-deposited SAM than for the solution-deposited monolayer correlates well with the aforementioned assumption regarding the difference in the tilt angle of the monolayers.

In addition to investigating chemical bonding of the SAMs in the Ga 3d and As 3d energy regions, the adsorption of the thiols to the GaAs substrates was evaluated by examining the S 2p energy region. Figure 4.5 shows the XPS spectra of the SAM-modified surfaces as well as that of the hydrogen-cleaned sample in the vicinity of the S 2p core level. To enhance surface sensitivity of the measurement, an additional set of spectra was acquired at a take-off angle of 30°, measured between the sample surface plane and the entrance to the detector. To distinguish the relative contributions of the main components, the spectra were deconvolved into two main constituents representing signals from the Ga 3s and S 2p levels. Due to limitations in the energy range surveyed, contributions from the As plasmons were not included in the fitting routine. Since the shift in energy between the Ga 3s and S 2p levels is small (~3 eV) there exists a degree of overlap between the peaks which makes the analysis less straightforward. Nevertheless, the appearance of a small doublet at a binding energy of approximately 162 eV is clearly evident in Figure 4.5, consistent with previously reported values for the S $2p_{3/2}$ and S $2p_{5/2}$ components on GaAs [28], [54]. Insufficient resolution and signal-to-noise characteristics of the XPS system prevented unambiguous decomposition of the core peaks into specific Ga-S and As-S chemical states. The aforementioned instrumental limitations

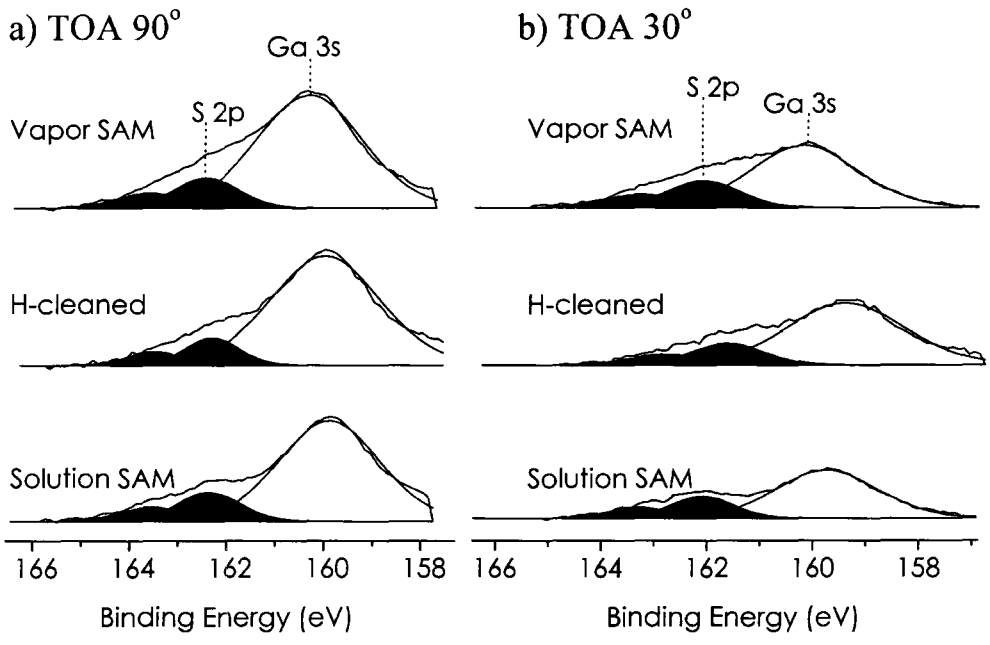

Figure 4.5: HRXPS spectra of the S 2p region for the SAM-modified and hydrogen-cleaned GaAs samples recorded at take-off angles of a) 90° and b) 30°. The spectra have been offset vertically for clarity (TOA: take-off angle) (white peak: Ga 3s, black doublet: S 2p).

notwithstanding, the existence of the S 2p features in the spectra of the ODT-treated samples confirms the formation of direct thiolate bonds with the GaAs surface, as exhibited in the respective Ga 3d and As 3d spectra. Furthermore, the observation of the S 2p peaks in the spectrum of the hydrogen-cleaned sample further substantiates the conclusion that the residual thiols present in the UHV chamber chemically bond to the freshly cleaned substrate.

The nature of the thiolate-GaAs bonds was assessed to a greater extent by reducing the take-off angle of the XPS measurement to 30°. By decreasing the take-off angle of the photoelectrons, the surface sensitivity of the XPS measurement can be increased. As the line-shapes and position of the peaks remained similar to that obtained at the 90° take-off angle, for the sake of brevity, only the spectra in the S 2p region are shown in Figure 4.5 for the hydrogen-cleaned and SAM passivated samples. As expected, the intensity of the S 2p and

Ga 3s peaks decreased concomitantly with the relative decrease in the sampling depth. However, the contribution of S-related features to the overall spectra increased relative to the bulk Ga component, demonstrating that the sulfur headgroups lie closer to the surface immediately above the GaAs interface.

From the integrated intensities of the S 2p, C 1s, and O 1s peaks, the C/S and C/O ratios were derived for each sample and are summarized in Table 4.4. The area intensity ratios were calculated using the appropriate sensitivity factors, assuming that the C 1s and O 1s signals originated entirely from the organic film and oxide regions, respectively. Due to the ambiguity in the curve fitting of the sulfur species along with lateral inhomogeneities of the SAM films, the derived ratios indicate qualitative trends in the depth profile of the surface region and do not provide quantitative information regarding film properties, such as the thickness. Nonetheless, an estimate of the elemental distribution perpendicular to the sample surface can be obtained and provides the basis for a useful model of the molecular architecture. As shown in Table 4.4, the ratio of C/S increased with a reduction of the take-off angle. The attenuation of the S 2p signal can be attributed to the inelastic scattering of the photoelectrons by alkyl chains that are

Table 4.4: Ratios of elements calculated from the integral intensities of the main peaks in the respective angle-dependent XPS spectra.

Sample	Ratio of elements	Take-off angle	
		90°	30°
Atomic hydrogen cleaned	C/S	6.5	9.0
	C/O	1.4	3.0
Solution-deposited SAM	C/S	6.8	12.1
	C/O	3.2	5.2
Vapor-deposited SAM	C/S	5.4	8.3
	C/O	1.6	3.3

oriented away from the GaAs-bound sulfur headgroup toward the surface. As compared to the solution-deposited SAM, the smaller change in the C/S ratio observed on the vapor-deposited SAM and the hydrogen-cleaned substrate implies a larger inclination of the thiolate molecules on the surfaces of these samples. Similarly, at the lower take-off angle, the C/O ratio for each of the samples increased, indicating that, on average, the oxygen atoms lie closer to the GaAs interface than the carbon atoms. These results correlate with the corresponding Ga 3d and As 3d spectra and suggest that despite the pretreatments (e.g. HF-etching or exposure to atomic hydrogen) used to remove the native oxide prior to the deposition of the monolayers, regions of oxide remained on the GaAs surface, which may have perturbed the subsequent anchoring of the thiols. The fact that the presence of residual oxides was observed on films formed from both liquid and vapor phases indicates that the preparation methods used before either deposition technique require further optimization, which may improve the overall quality of the resultant SAMs.

4.2.4 SAM Structure and Surface Coverage

The properties of the monolayers deposited from liquid and vapor phase were further investigated by ellipsometry measurements (the experimental details of the measurements are provided in Chapter 2). To describe the optical properties of the vapor-deposited SAM, a four-phase (ambient/SAM/interface/substrate) model was used based on the surface chemistry deduced from the XPS analysis presented above. Due to the additional insight into the properties of the films afforded by the XPS investigation, the current ellipsometric model is an improvement to the three-phase model discussed in Chapter 3. A porous GaAs interface layer was included in the analysis to represent the hydrogen-induced changes in the optical properties of the surface as a result of the cleaning process. The interface layer accounts for the interaction of atomic hydrogen with the near-

surface regions by means of structural incorporation, surface roughening, defect passivation, and modification of the surface geometry [148], [155], [156]. For layers composed of more than one constituent, the Bruggeman effective medium approximation (BEMA) was used to model the optical properties of the composite layer. The optical constants for the oxide-free semi-insulating GaAs substrate were obtained by ellipsometry from a freshly HF-etched sample. A Cauchy dispersion function was used to describe the wavelength-dependent index of refraction of the thiols, with the appropriate coefficients obtained from previous work [115]. The fitting parameters in each model were determined by minimizing the mean-square error with the provided regression analysis software. Realistic physical constraints were imposed on parameters to further increase the validity of the models. For example, the index of refraction of the ODT was maintained at a real value, as alkanethiols are nonabsorbing in the wavelength range of interest [124].

Figure 4.6 shows the experimental and the model-generated Δ and Ψ spectra for the vapor-deposited SAM sample. A schematic of the corresponding model used to fit the measured spectra is also presented in the figure, along with the respective best-fit layer thicknesses and compositions. As is evident in Figure 4.6, the simulated spectra closely resemble the measured results, demonstrating the suitability of the chosen model as proposed by the XPS analysis. To further emphasize the goodness of the fit, the difference between the experimental and the simulated spectra is reported in Figure 4.7. The observed scatter in the data with the angle of incidence reflects the inherent uniaxial anisotropy of the monolayer as discussed in Chapter 3 [115]. The results of the iterative fitting procedure indicate the presence of a SAM deposited from vapor phase with a thickness of 19.9 ± 0.2 Å and an oxide fraction of 8 ± 2 %. In addition, the best-fit model suggests that the monolayer is formed on a clean GaAs surface covered by a 106 ± 5 Å thick density-deficient-layer, simulated by a mixture of 98.5 ± 0.1 % GaAs and 1.5 ± 0.1 % voids. The existence of a small amount of oxide in the

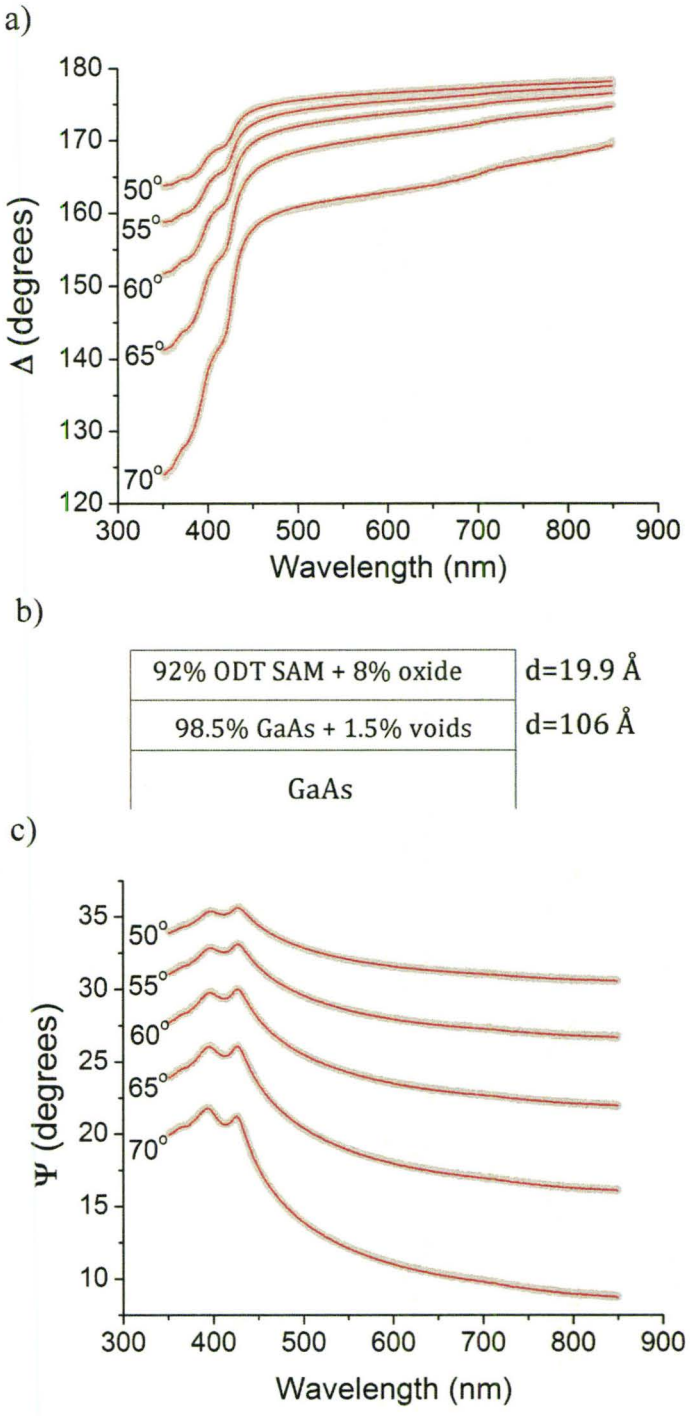

Figure 4.6: **Spectra of ellipsometric parameters a) Δ and c) Ψ of a vapor-deposited ODT SAM on GaAs for various angles of incidence (thick grey line: experimental data, thin red line: model fit). In b) the best-fit BEMA model to the corresponding spectra is shown.**

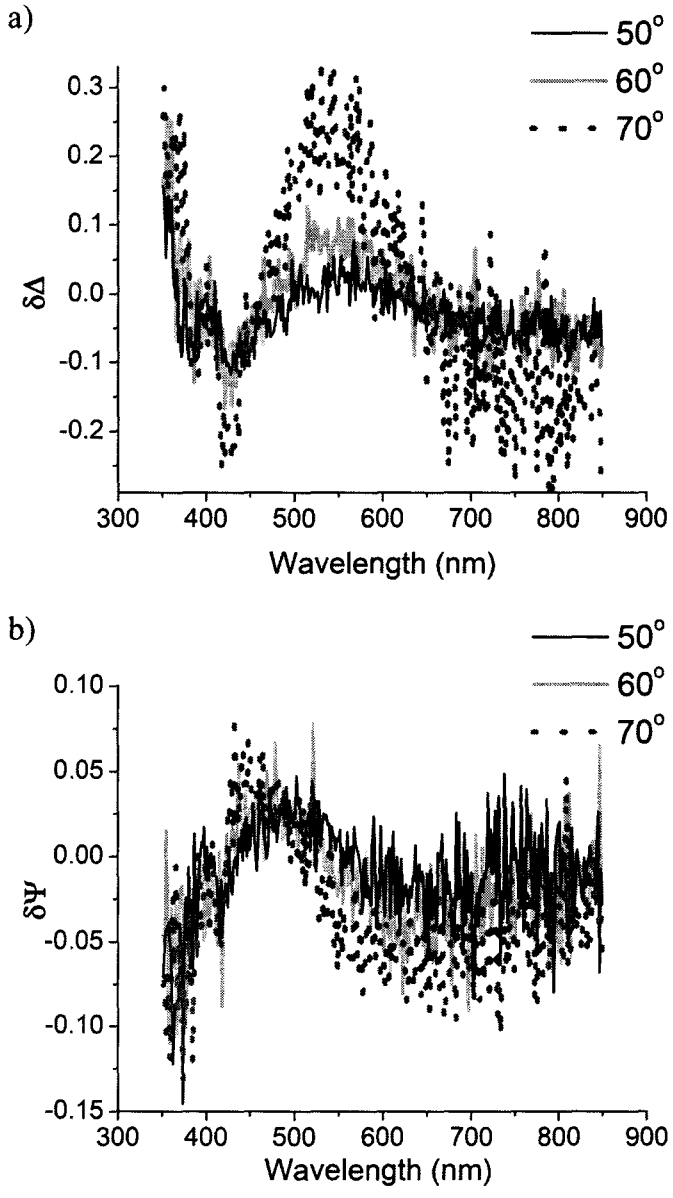

Figure 4.7: Difference spectra (experimental – simulated) of ellipsometric parameters a) Δ and b) Ψ of a vapor-deposited ODT SAM on GaAs for various angles of incidence. For clarity, the spectra at angles of incidence of 55° and 65° have been excluded.

multilayer model is in reasonable accord with the compositional data obtained from the XPS measurements. The presence of a porous interface layer correlates well with the expected interaction of atomic hydrogen with the GaAs substrate

during the oxide removal process. Furthermore, it describes the modification of the optical properties at the surface evoked by the preferential reaction of hydrogen with As and oxygen atoms, which leaves the surface non-stoichiometric and less dense [157]. The ready penetration of GaAs by atomic hydrogen accounts for the augmented thickness of the intermixed phase, as well as for surface roughening that may occur as a result of the treatment [157]. Likewise, the derived thickness of the vapor-deposited SAM is consistent with that reported in earlier studies [30], [124], [127]. The fact that the thickness of the film is smaller than the physical length of the octadecyl thiolate molecule (~24.5 Å), suggests the existence of a well-ordered monolayer on the GaAs surface consisting of densely packed alkyl chains tilted at 36 ± 2° from the surface normal.

An analogous approach to the one described above was adapted to evaluate the spectra of the atomic hydrogen cleaned sample. Figure 4.8 depicts the difference between the ellipsometric data and the results of the regression analysis obtained with the model presented in the figure. The spectroscopic data suggests the formation of more disordered ODT assemblies separated by regions of GaAs oxide (26 ± 3 %) on the surface of the sample. The reduced thickness (15.8 ± 0.1 Å) of the monolayer can likely be explained by a decrease in the tilt of the alkyl chains from the surface normal. Similar to the SAM deposited from vapor phase, the interface layer is modeled reasonably well by a mixture of GaAs and voids, which corresponds to the selective removal of As and oxygen atoms from the GaAs lattice during the exposure to atomic hydrogen.

To account for the apparent distinction in characteristics of the monolayers formed from solution as documented by means of PL spectroscopy and XPS, an alternative four-phase model was used to describe the properties of the solution-deposited SAM. Since the GaAs surface prior to SAM deposition from liquid phase is believed to be nearly stoichiometric, an interface layer was included in

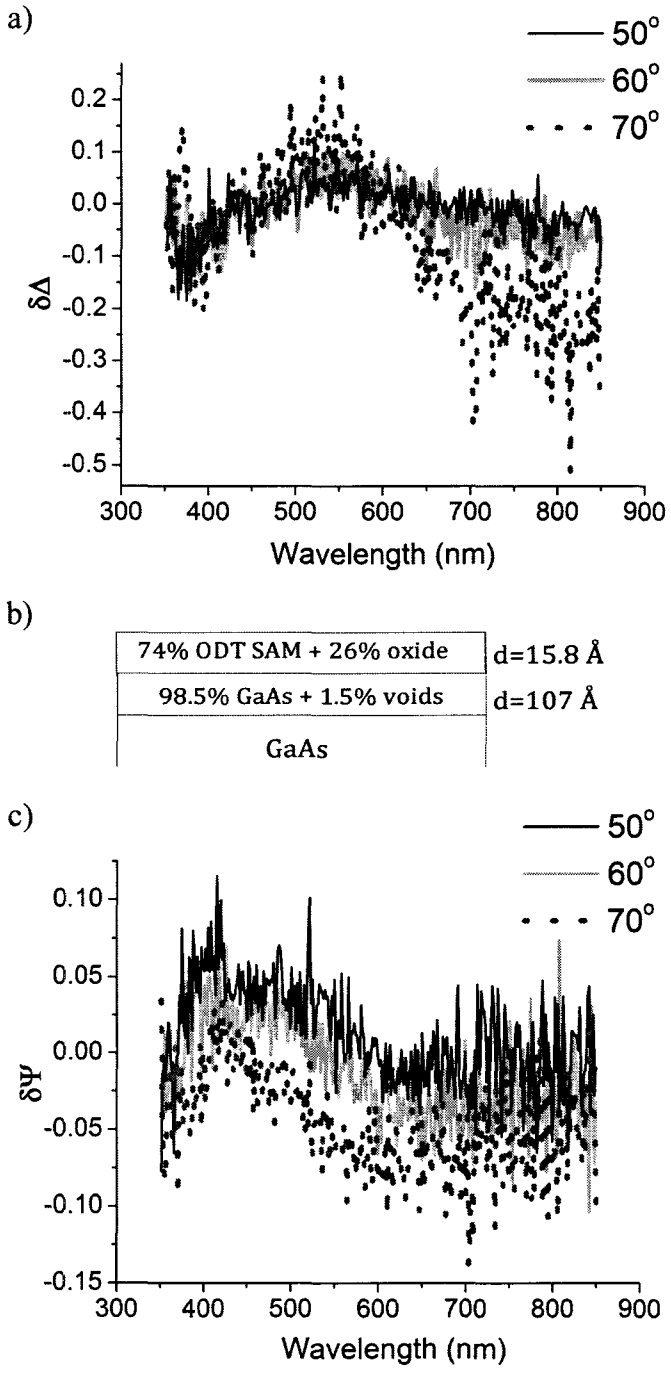

Figure 4.8: **Difference spectra (experimental – simulated) of ellipsometric parameters a) Δ and c) Ψ of an atomic hydrogen cleaned GaAs substrate for various angles of incidence. For clarity, the spectra at angles of incidence of 55° and 65° have been excluded. In b) the best-fit BEMA model to the corresponding spectra is shown.**

the ellipsometric model to allow for the possible formation of a roughened overlayer, which has previously been shown to arise from the wet-etch oxide removal process [83]. As in the case of the vapor-deposited SAM, the effective refractive index of the monolayer was taken to be a weighted average of the refractive index of the GaAs oxide and the ODT, with the optical constants of the latter described by an equivalent Cauchy dispersion formula.

Figure 4.9 shows the difference spectra between the experimental and best-fit curves for Δ and Ψ of a film assembled from the thiol solution on GaAs. The good agreement between the measured and simulated data implies the film consists of less dense thiol domains with inclusions of a GaAs oxide. According to the ellipsometric model, the volume fraction of the GaAs oxide in the host medium was 18 ± 1 %, which is larger than that derived for the vapor-deposited SAM (8 ± 2 %). The best-fit model also indicates that the monolayer is formed on a roughened GaAs overlayer about 1 ± 0.5 Å thick, which is probably formed as a result of the HF-etch used to strip the surface oxide prior to the assembly of the monolayer from solution. Furthermore, the increased thickness of the film of 23 ± 1 Å implies that the alkyl chains in the monolayer are tilted from the surface normal at a smaller angle of 20 ± 2°. Interestingly, this film thickness agrees well with that recently reported for an organized ODT monolayer on GaAs self-assembled from solution under similar preparation conditions [53].

The results of the ellipsometric analysis, along with the experimental XPS data, suggest dissimilar structures for monolayers prepared from liquid and vapor phases. While conventional solution deposition yields a thicker monolayer with the axes of the thiolate molecules oriented nearly perpendicular to the sample surface, the overall coverage of the film is reduced. Conversely, the experimental data for the vapor-deposited monolayer is consistent with the presence of a thinner film composed of a densely packed assembly of molecules tilted more towards the sample surface. The superior characteristics of the vapor-deposited

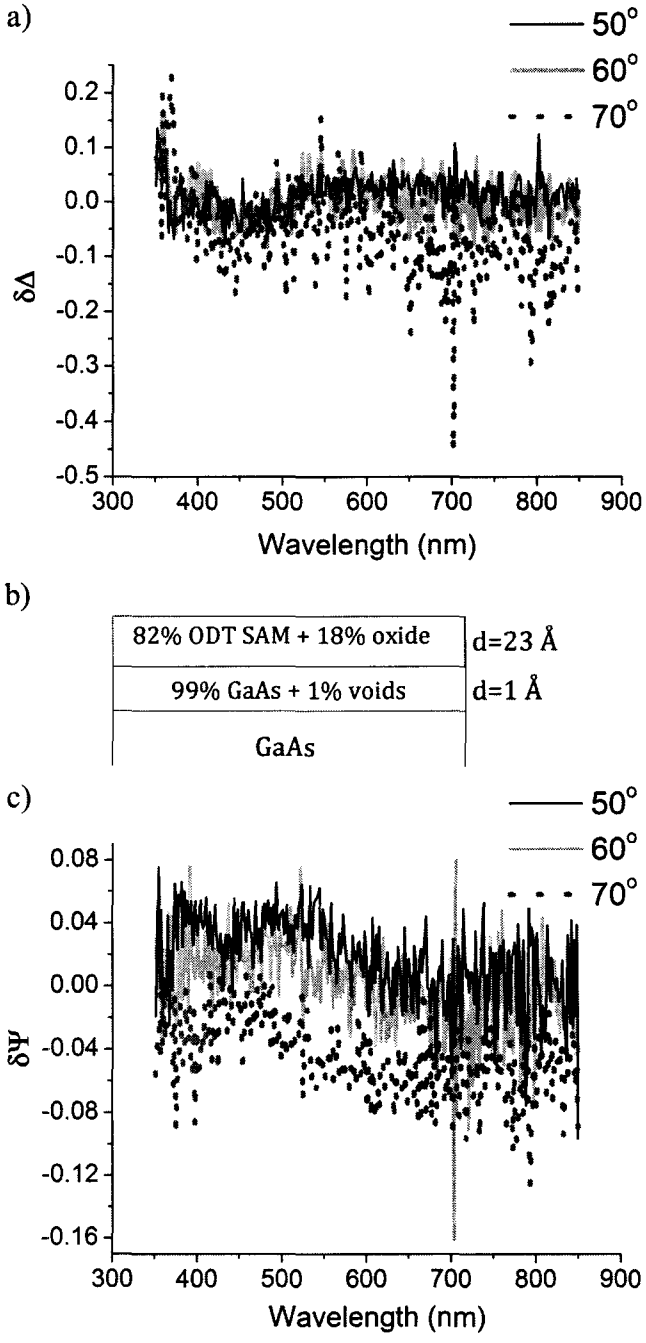

Figure 4.9: **Difference spectra (experimental – simulated) of ellipsometric parameters a) Δ and c) Ψ of a solution-deposited ODT SAM on GaAs for various angles of incidence. For clarity, the spectra at angles of incidence of 55° and 65° have been excluded. In b) the best-fit BEMA model to the corresponding spectra is shown.**

SAM inferred from the ellipsometric simulations correspond well to the larger enhancement in PL intensity observed for the monolayer when compared to that prepared from liquid phase. In the case of a solution-deposited monolayer, the greater oxide content of the SAM is likely related to the existence of weaker As-S bonds at the GaAs surface, which explains the decreased long-term stability of the film with exposure to an ambient environment, as was found through PL and CA analysis. On the other hand, the stronger Ga-S bonds formed between the vapor-deposited SAM and the GaAs substrate are responsible for the greater surface coverage of the film and directly translate to the improved passivation provided by these SAMs.

4.3 Conclusion

The experimental data presented in this chapter suggests that the functionalization of GaAs with ODT SAMs inhibits the oxidization of the surface for an extended period of time and maintains a quality of the interface similar to that achieved via traditional oxide removal procedures. Although well-ordered films were formed from both liquid and vapor phases, PL, CA analysis, and ellipsometry measurements revealed that the overall quality of the resulting SAMs, as well as the long-term durability, depend on the preparation method. Specifically, time-dependent PL and CA analysis of the SAMs when exposed to the ambient environment indicate an increased stability for the vapor-deposited films when compared to the corresponding solution-deposited monolayers, which were shown to be more susceptible to atmospheric conditions over time. The film properties responsible for the difference in the longevity of the resultant surface passivation were further explored by XPS. The attachment of the thiolate molecules to the GaAs surface was shown to proceed through the formation of

chemical bonds as demonstrated by the appearance of the respective emissions in the Ga 3d, As 3d, and S 2p XPS spectra. Moreover, the anchoring of the thiols was observed to occur at both Ga and As adsorption sites and was found to be strongly dependent on the surface termination obtained by the particular oxide removal treatment used prior to the SAM deposition. While both preparation routes produced films with some residual oxide contamination, vapor-deposited SAMs were found to have greater surface coverage and enhanced passivation properties, as confirmed by ellipsometry and improved PL peak intensity. From the XPS results, the superior characteristics of films prepared from vapor phase were linked to the dominant formation of robust Ga-S bonds at the GaAs-SAM interface. Consequently, the preparation of high quality organic SAMs from vapor phase is a promising strategy for the reliable passivation of semiconductor surfaces and a prospective means of enhancing the performance and stability of III-V-based devices. More importantly, the effective passivation of III-V surfaces with organic films is an essential step towards the development of novel biosensors, as discussed in the next chapter.

Chapter 5 Development of a Hybrid Aptamer-GaAs Optical Biosensor

5.1 Introduction

The quest for ultrasensitive biomolecular detection systems has sparked tremendous interest over the last decade not only across a variety of scientific disciplines but also in the technological business sector. Intensive efforts in this area have focused on the development of inexpensive miniature sensors capable of rapidly identifying minute concentrations of a diverse assortment of biological analytes. Some of the more practical applications in which biosensors have shown great potential include medical diagnostics, drug discovery, genomics, forensic examination, food quality control, and in defense against bioterrorism [158]-[161]. A major drawback of most classical biorecognition schemes is the need for labels in the form of fluorescent, chemiluminescent, redox, or radioactive tags, which precludes the use of these devices for real-time monitoring [158]. Consequently, innovative label-free detection methods offer a very promising alternative due to their low cost, facile fabrication, and direct sample readout, as well as elimination of any possible modification of the target species [158].

As mentioned in Chapter 1, the primary architecture of any biosensor consists of two principal components: 1) a biorecognition element used to selectively detect the target species, and 2) a transduction mechanism that translates the biorecognition response to a measurable physical signal [69], [162] -

[164]. While the physical output can manifest itself as an electrical or optical quantity, optical sensors present a few important advantages over their electrical analogs, such as elevated selectivity and specificity, isolation from electromagnetic interference, and the ability to employ novel detection techniques [69]. In an optical biosensing approach, the sensitivity and selectivity of the optical response are partly derived from immobilizing the bioreceptors directly onto the sensor platform, which function to explicitly detect specific analytes by means of certain intrinsic properties [69].

Semiconducting materials composed of III-V compounds provide a desirable combination of electrical, chemical, and optical properties that can be utilized to develop innovative biophotonic devices [165]. GaAs, in particular, affords some unique benefits such as high electron mobility and direct band gap structure that result in an intense PL yield [35], [62]. Since the luminescence response of GaAs is remarkably sensitive to the physical, chemical, and electronic environment at its surface, it can be exploited in the design of state-of-the-art optical biosensors, which couple the advantageous characteristics of GaAs with those of organic biomolecular receptors.

In this chapter, the fabrication and operation of a hybrid GaAs-based optical biosensor are described. The solid-state biosensing platform was prepared by functionalizing a GaAs surface with thiolated aptamer receptors. Single-strand nucleic acids, referred to as aptamers, were selected as the biomolecular recognition element on account of the high affinity and specificity exhibited by these molecules for the target species of interest [166]. Recent progress in the field has shown the enormous potential of aptamer-based molecular recognition in the detection of proteins, peptides, enzymes, antibodies, cells, and other small molecules [167]-[169]. Numerous desirable characteristics of aptamers, such as their ability to be chemically synthesized, high purity, small size, and stability at high temperatures under a variety of buffer conditions, have made these unique molecules extremely attractive alternatives to conventional probes for use in

assays and bioanalytical applications [167]-[169]. Due the intense interest in using aptamers as sensing elements, there are several in-depth reviews on the development of aptamers and aptamer-based technologies that can be consulted for their synthesis and selection techniques, as well as for various analytical methods that employ aptamers [167]-[175].

The implemented detection strategy discussed in this chapter involves a modification in the GaAs PL intensity with the binding of target adenosine 5'-triphosphate (ATP) ligands to the charged aptamer probes immobilized on the substrate surface. From a fundamental perspective, the biorecognition reaction directly affects the surface charge distribution and influences the near-surface depletion width of the semiconductor, resulting in a modified PL response. A quantitative analysis of the measured luminescence data is conducted utilizing Poisson-Boltzmann statistics in conjunction with the dead layer model. The results presented here demonstrate the feasibility of the proposed biorecognition method in providing a simple and effective means of label-free identification of specific biological analytes. These findings have been submitted for publication [176].

5.2 Biofunctionalization Details

ATP, guanosine 5'-triphosphate (GTP), mercaptohexanol (MCH), and NaCl were purchased from Sigma-Aldrich [80] and used as received. Monobasic sodium phosphate and dibasic sodium phosphate used to prepare the phosphate buffer solution (PBS) were purchased from EMD Chemicals [177]. Dithiolthreitol (DTT) and Tris-HCl were purchased from BioShop Canada Inc [178]. The thiol modified and unmodified oligonucleotide-based aptamers were purchased from Integrated DNA Technologies [179]. To ensure a clean environment and

reproducible conditions several precautions similar to those described in Chapter 2 for the liquid deposition of SAMs were used. The water used to prepare all of the solutions as well as that used for rinsing was purified with a Millipore water purification system (resistivity of 18 MΩ-cm) [81]. The 5' terminal end of the aptamers was modified with a hexyldisulfide, which remained intact prior to use and acted as a protective cap. In order to cleave the disulfide bond and liberate the reactive thiol group, the crude oligonucleotides were treated with 10 millimolar DTT in a solution of 50 millimolar Tris-HCl buffer (pH 7.5) and 100 millimolar aqueous NaCl at room temperature. The reduction reaction was accomplished within a period of 1 hour, and the oligonucleotides were precipitated out of the solution by means of ethanol precipitation. Subsequently, the oligonucleotides were purified using standard 10% denaturing polyacrylamide gel electrophoresis. The purified aptamers were then dissolved in ultrapure double distilled water and kept frozen at -20°C until needed. To prepare the final aptamer solutions used in the functionalization of the GaAs substrates, the aptamers were dissolved at the desired concentration into 1 mL PBS in a small autoclaved vial. The concentration and pH of the PBS used to fabricate the samples as well as that used during the PL measurements were 0.2 M and 7.8, respectively.

The GaAs substrates were treated with the aptamers following conventional liquid phase deposition techniques based on GaAs-S chemistry outlined in Chapter 2. First, HF-etched substrates were incubated in 10 μM solutions of aptamer probes (see Table 5.1 for a list of oligonucleotide aptamers used in the study) and PBS for 48 hours at room temperature. Subsequently, the aptamer-modified substrates were rinsed with deionized water, dried with N_2 gas, and treated with a 4 μM solution of MCH in PBS for a period of 1 hour at room temperature. During this processing step, the MCH bonds to unoccupied surface sites surrounding the immobilized probes and removes nonspecifically adsorbed oligonucleotides, thereby orienting the aptamer backbone away from the GaAs surface and promoting the single-point anchoring of individual molecules via the

Table 5.1: Sequences of the oligonucleotide aptamer probes.

Oligonucleotide	Sequence
T10ATP	5'-HS-TTTTTTTTTTACCTGGGGGAGTATTGCGGA GGAAGGT-3'
MUT10ATP	5'-HS-TTTTTTTTTTACCTGTGGGAGTATTGCGTAG GAAGGT-3'
T5ATP	5'-HS-TTTTTACCTGGGGGAGTATTGCGGAGGAAG GT-3'
T20ATP	5'-HS-TTTTTTTTTTTTTTTTTTTACCTGGGGGAGT ATTGCGGAGGAAGGT-3'
T30ATP	5'-HS-TTTTTTTTTTTTTTTTTTTTTTTTTTTTTACC TGGGGGAGTATTGCGGAGGAAGGT-3'
non-thiolated T10ATP	5'-TTTTTTTTTTACCTGGGGGAGTATTGCGGAGGA AGGT-3'

thiolate headgroup [180], [181]. The overall effect of the MCH treatment is an improved aptamer film structure that helps to increase the subsequent efficiency of biorecognition [180], [181]. Following the reaction, the samples were rinsed with deionized water and dried in N_2 gas.

The assay treatment of aptamer-modified GaAs surfaces was conducted in a 1 millimolar solution of ATP in PBS. To promote the biomolecular recognition, the samples were heated to approximately 70°C for 1 minute, and allowed to cool to room temperature for 2 hours. A portion of the aptamer-modified sample was treated with a noncognate ligand GTP in a 1 millimolar PBS solution under the same conditions as outlined above for ATP. ATP (GTP) molecules do not bind to the MUT10ATP (T10ATP) receptors. The use of ATP and GTP was therefore used to validate the specificity of the detection process.

All of the previously mentioned reactions were carried out in a nitrogen-purged glove-box with oxygen and moisture levels below 1 part per million to avoid reoxidation of the freshly etched sample surface, which would otherwise occur in an air ambient. Moreover, to prevent the regrowth of the GaAs native

oxide, each solution was purged with N_2 gas for 5 minutes to remove any dissolved oxygen before the sample was introduced.

Immediately following the biorecognition process, PL measurements were conducted on each sample to determine the suitability of optical transduction as a platform for biosensing assays. Luminescence spectra were recorded at room temperature using a home-built apparatus described in Chapter 2. To maintain the conditions necessary for biorecognition, the PL measurements were conducted through a thin glass microscope cover slip used to contain a small volume of liquid at the surface of each sample (approximately 2 μL). With the exception of the ATP- and GTP-treated samples, the liquid used during the PL measurement was PBS. In the case of the ATP- and GTP-treated samples, a 2 μL drop of the ATP- or GTP-PBS solution, respectively, was used for the measurement.

Since the absorption length of the laser radiation in GaAs is approximately 250 nm [103], the laser beam is absorbed close to the top of the sample surface [182]. Consequently, the intensity of the resulting PL signal is strongly controlled by the surface properties and hence, can be exploited to indicate the presence of specific analytes immobilized near this region. As in the case of the standard SAM-passivated samples, prior to each PL measurement of the aptamer-modified samples, the PL system was tested by obtaining PL from a reference sample consisting of a highly doped untreated n-type GaAs substrate to confirm reproducibility between PL measurements. As discussed in Chapter 2, the use of a reference standard in this way ensured that any influence of the PL apparatus on the obtained PL results (such as changes in incident laser power) was negligible. On each sample, PL was collected from three different locations and averaged to account for any non-uniformity in the surface properties. The typical variation in peak PL intensity across the surface of each sample was approximately 10%.

5.3 Experimental Results

Figure 5.1 a) and b) show room temperature PL spectra of the T10ATP aptamer-treated GaAs samples as well as that of an untreated GaAs substrate. The peak PL intensity occurred at a wavelength of approximately 872 nm, corresponding to the band gap of GaAs. As indicated in Figure 5.1 a), the peak PL intensity following deposition of the aptamer molecules (sample referred to as T10ATP and MUT10ATP, respectively) is quenched compared to the untreated substrate. The observed decrease in the PL intensity upon exposure to the thiolated oligonucleotides is attributed to the bending of the energy bands at the GaAs surface due to the adsorption of the negatively charged molecules. The resultant negative charge depletes electrons from the near-surface region of the GaAs semiconductor, effectively increasing the band bending and the width of the depletion region [35]. Since light-generated charge carriers created within a distance on the order of the depletion width do not contribute to the luminescence signal, an increase in depletion width corresponds to a decrease in the measured PL intensity [183]. It is important to note that in previous studies, the modification of GaAs substrates with self-assembled monolayers of basic long-chain alkanethiols has resulted in an enhanced luminescence yield, presumably due to the passivation of mid-gap surface states through the formation of sulfur-GaAs bonds [115], [184]. Thus, the observed PL quenching suggests that the band bending caused by the considerable negative charge of the aptamers dominates any passivation effect generated as a result of the thiolate bond used to tether the molecules to the semiconductor surface. On the other hand, in the presence of the target ATP molecules, the peak luminescence intensity of the T10ATP modified sample (referred to as ATP+T10ATP) increased appreciably while the intensity of the mutated MUT10ATP sample (referred to as ATP+MUT10ATP) did not change (see Figure 5.1 b)). Moreover, there was no change observed in the peak

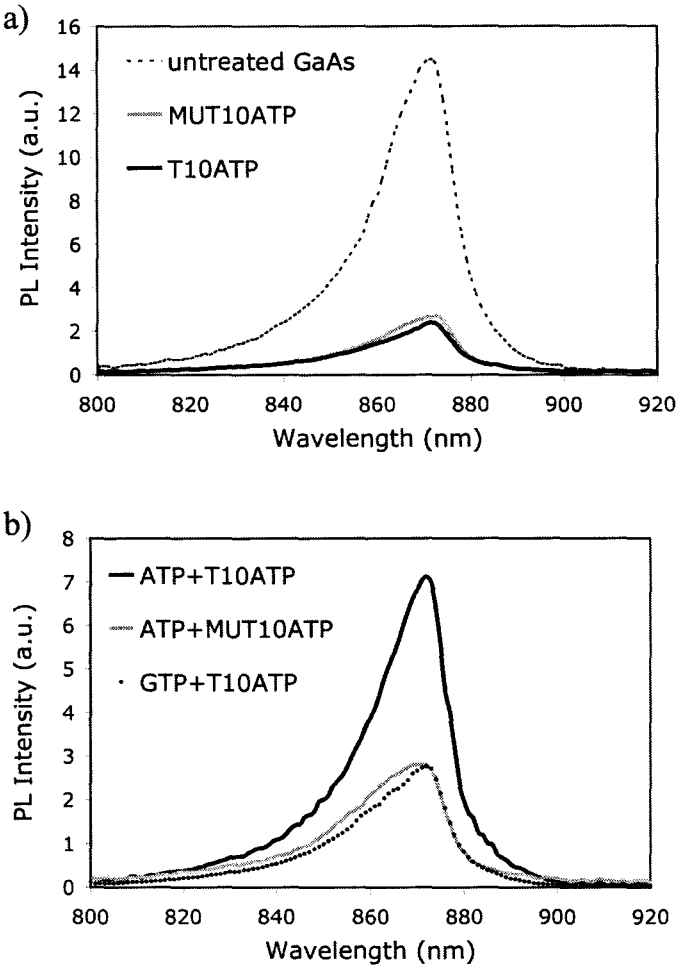

Figure 5.1: Room temperature PL spectra of the T10ATP aptamer-treated GaAs samples as well as that of an untreated substrate: a) following the initial probe functionalization and b) after exposure to the ATP or GTP solution.

PL intensity of the T10ATP modified sample in the presence of GTP molecules (referred to as GTP+T10ATP).

The enhanced PL signal of the ATP+T10ATP sample demonstrates the successful recognition of the target ATP ligands by the T10ATP receptors. During the formation of ATP-aptamer complexes, the aptamer probes fold through self-complementary pairing and adopt a tertiary structure simulating a stem-and-loop

[185]. The increase in PL intensity as a result of the ATP-aptamer complex formation corresponds to a decrease in the width of the GaAs depletion region due to a change in the charge distribution at the sample surface. The lack of change in the PL intensity observed on the ATP+MUT10ATP and GTP+T10ATP samples is consistent with the fact that the ATP (GTP) molecules do not bind to the MUT10ATP (T10ATP) receptors, respectively. A schematic of the proposed mechanism responsible for the biorecognition-facilitated change in the GaAs surface properties is depicted in Figure 5.2 a) and b). In the absence of ATP, the aptamer assembly adopts a configuration where the molecules are tilted toward the substrate surface at a substantial angle with respect to the surface normal (Figure 5.2 a)). Following the binding of the ATP, the conformational transformation forces the immobilized aptamers toward a stabilized, upright position (Figure 5.2 b)). The reorientation of the probes with target sensing effectively reduces the charge density near the GaAs interface by increasing the width over which the total aptamer charge is distributed, resulting in the measured PL enhancement.

Additional evidence that the observed PL enhancement is a direct consequence of successful biorecognition is provided by the control experiments performed using the mutant aptamer MUT10ATP and the noncognate GTP ligands (see Figure 5.1 b)). In strict contrast to the non-mutated aptamers, the mutant counterparts cannot fold in the presence of the ATP ligands due to a base mismatch and thus are rendered unreactive to the target species. Consequently, no change in the measured PL intensity was observed following the exposure of the MUT10ATP sample to ATP. Similarly, since the GTP molecules cannot trigger a structural change in the aptamer receptors, the addition of GTP to the T10ATP-functionalized sample had no effect on the luminescence signal of the underlying substrate, as depicted in Figure 5.1 b). The outcome of the former control experiment verifies that the PL enhancement was indeed induced by the conformational transformation of aptamer probes upon ATP capture, while the

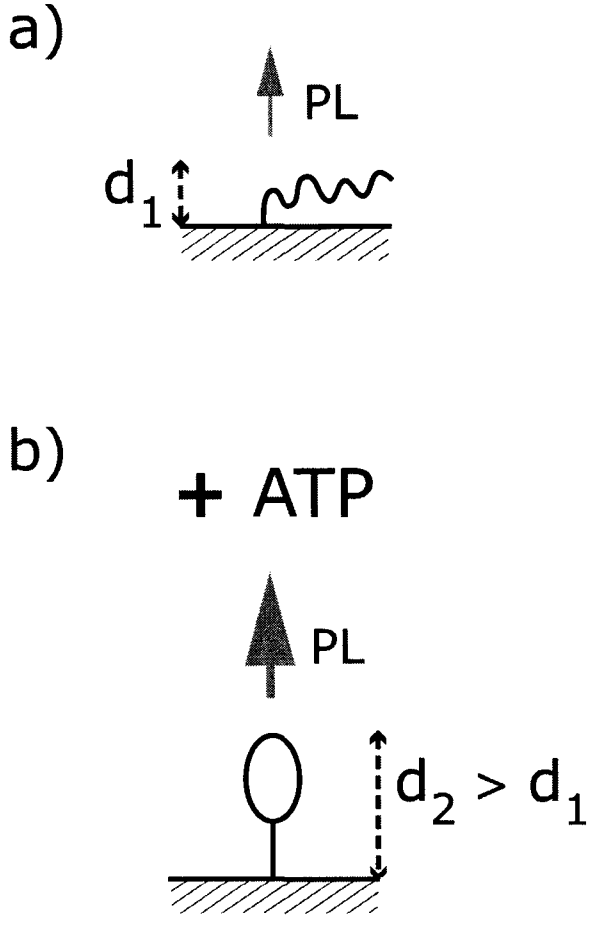

Figure 5.2: Schematic representation of the proposed mechanism responsible for the biorecognition-facilitated change in the GaAs luminescence: a) prior to the target sensing, b) after the binding of the target ATP ligands.

results of the latter control experiment confirm the inherent specificity of the target detection owing to the ability of the sensor to accurately discriminate ATP from GTP.

To investigate the bonding characteristics of the aptamer probes on a semiconductor surface, an oligonucleotide sequence without the thiol anchor was employed. Since direct bonding of the aptamers to the surface via the base moieties is detrimental to biorecognition, it is crucial from the perspective of

sensitivity to minimize the extent of base-GaAs interactions [180]. Figure 5.3 compares the PL spectra of GaAs samples functionalized with the standard thiolated T10ATP, non-thiolated T10ATP, as well as that of an untreated substrate. Evidently, no appreciable change in the PL intensity was observed following the treatment of the surface with the non-thiolated strands. The lack of affinity for GaAs exhibited by the aptamer backbone provides evidence that the thiolate endgroup is responsible for anchoring the probes to the semiconductor surface with an orientation beneficial to target sensing.

An important characteristic of any biosensor design is the reversibility of the signaling mechanism (i.e. the removal of the target analyte from the probe functionalized surface) which allows for the regeneration of the sensor platform and provides a means for real-time detection of specific target analytes [186], [187]. The regeneration potential of the proposed biosensor was investigated by measuring the PL signal after the dissociation of the aptamer-ATP complexes. The dissociation reaction was performed by immersing the ATP-modified

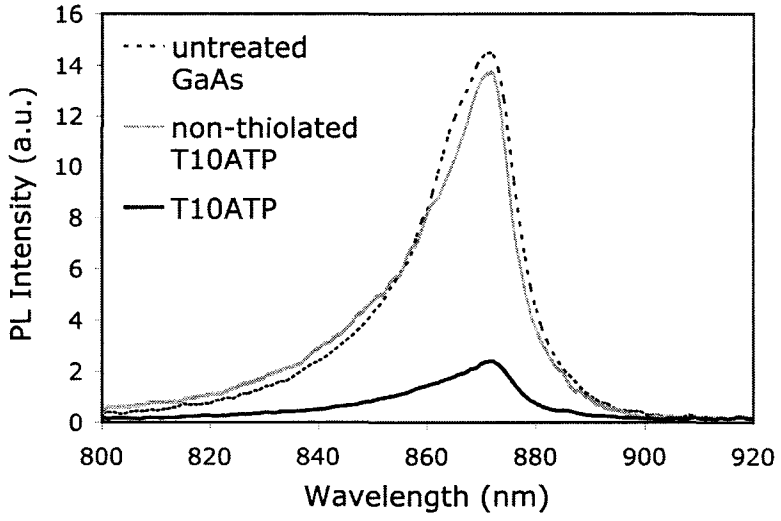

Figure 5.3: PL spectra of GaAs substrates modified with thiolated T10ATP, non-thiolated T10ATP, as well as that of an untreated substrate.

T10ATP sample in PBS for 2 minutes at 70°C and subsequently rinsing the surface with copious amounts of warm PBS. Since thiolated DNA on GaAs has been previously shown to be relatively stable in boiling water for a period of 5 minutes [61], a temperature of 70°C was selected for the reaction in order to facilitate the successful dissociation of the ATP-aptamer complexes while simultaneously preserving the aptamer functionalized surface.

In order to ensure that the ATP molecules were fully dissociated from the aptamer probes, the preceding procedure was repeated three consecutive times, after which the sample was dried with N_2 gas. Figure 5.4 illustrates the room temperature PL spectra of the dissociated sample (denoted as (ATP+T10ATP)-ATP), as well as that of the original T10ATP sample, the ATP-modified T10ATP sample, and an untreated GaAs substrate. As outlined in the figure, the baseline

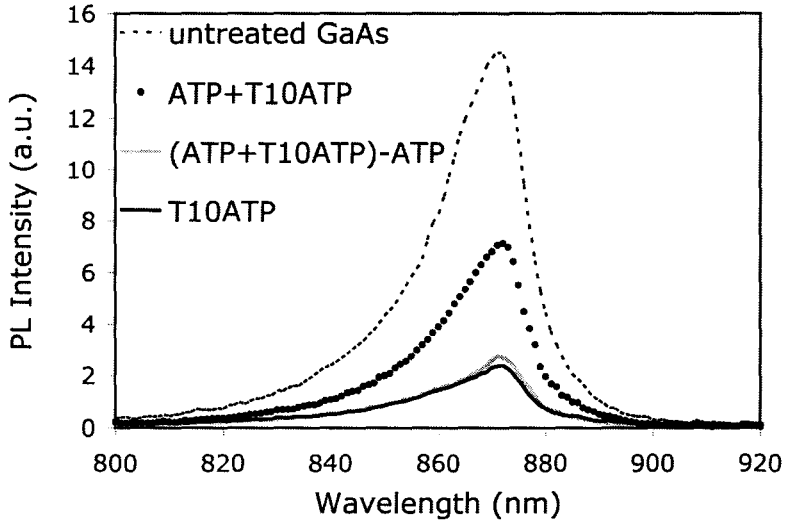

Figure 5.4: A comparison of room temperature PL spectra of an ATP-treated T10ATP sample before and after dissociation (denoted as ATP+T10ATP and (ATP+T10ATP)-ATP, respectively), a T10ATP sample, and an untreated GaAs substrate.

PL signal of the aptamer-modified sample was restored close to the original strength following the denaturation reaction, implying a change in the aptamer conformation back to the initial ligand-free orientation. The reversibility of the specific interaction between aptamer receptors and the ATP target, as suggested by the PL response, demonstrates the suitability of the hybrid organic-semiconductor platform for use in real-time biosensing applications.

The sensitivity of the device to charged oligonucleotides was further evaluated by measuring the PL response of the GaAs-based biosensor to aptamers of varying strand lengths. To synthesize the additional aptamer sequences the length of the thymine-based linker was modified. Specifically, three linker lengths consisting of 5-mer, 20-mer, and 30-mer segments of sequential thymine bases were examined in addition to the 10-mer thymine-linked T10ATP aptamer discussed above (see Table 5.1 for a full description of the oligonucleotide sequences studied). Figure 5.5 a) shows the relative change in the peak PL intensity of the oligonucleotide-modified samples as a function of the aptamer probe length. For the purpose of comparison, the PL data from the previously described T10ATP sample is also included in the figure. Clearly, the decrease in the PL intensity observed following the initial aptamer functionalization of the substrates increases with the thymine spacer length. This trend in the PL signal is attributed to an increase in the negative charge density with the length of the aptamer strands, which in turn leads to an expansion of the semiconductor depletion width. Moreover, following the detection of the ATP target, the relative change in the luminescence signal is greater for longer probe sequences as indicated in Figure 5.5 b). The relationship between the PL response with biorecognition and the aptamer strand length is consistent with the sensing mechanism suggested earlier. Since the magnitude of the PL enhancement observed upon the formation of ATP-aptamer complexes is proportional to the aptamer length, it supports the conclusion that the underlying mechanism responsible for the PL response involves a ligand-dependent conformational

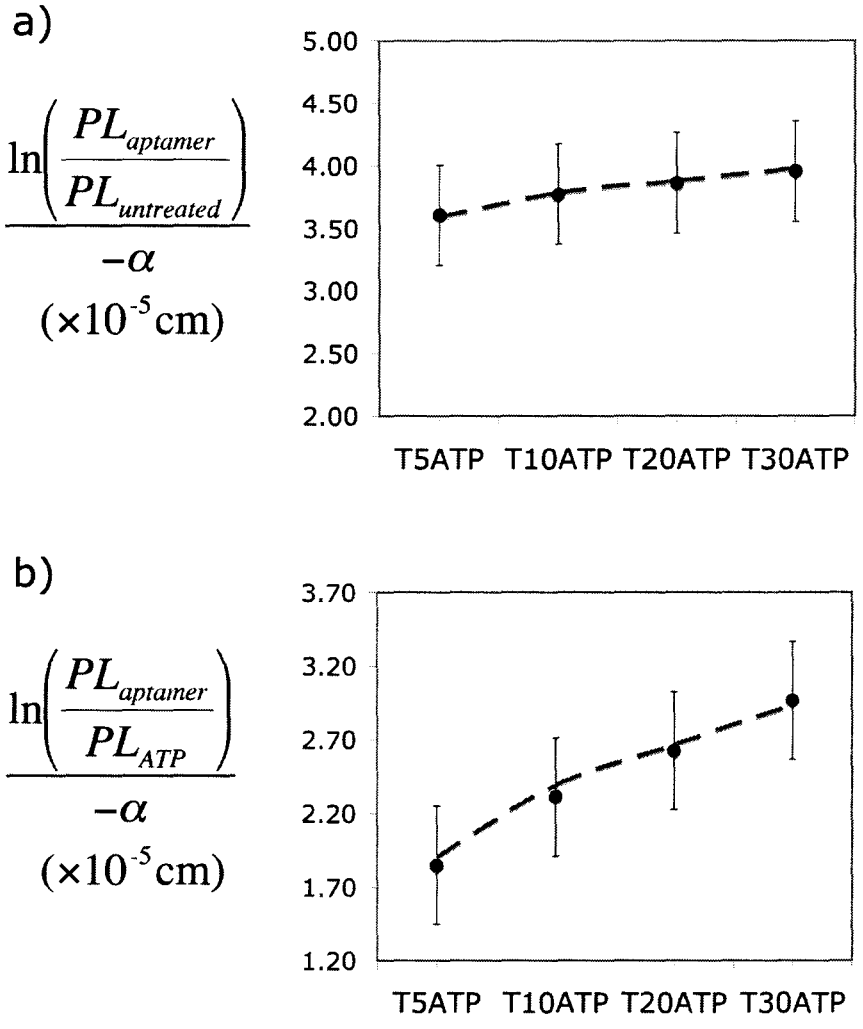

Figure 5.5: **Relative change in the peak PL intensity of the oligonucleotide-modified GaAs samples as a function of the aptamer probe length: a) PL yield of the aptamer functionalized sample relative to that of an untreated substrate, b) PL yield of the aptamer functionalized sample relative to that exposed to the ATP assay solution. The data reflect the natural logarithm of the specified PL ratios divided by the GaAs absorption coefficient, α (experimental data: •, model fit: – – –). The error bars correspond to the standard deviation of the PL measurements obtained at three different locations on the surface of each sample.**

transition of the aptamer molecules, which modifies the thickness of the aptamer layer as a function of the molecular length. Another important feature reflected in Figure 5.5 a) and b) is the sensitivity of the luminescence to the local environment at the GaAs surface, which remains responsive to recognition events across the entire range of probe lengths investigated.

To quantitatively describe the change in the measured PL signal of the system, Poisson-Boltzmann statistics in conjunction with the dead layer model were employed. This model assumes that a near-surface region in the semiconductor on the order of the depletion layer is nonemissive (i.e. no PL is emitted) because of the absence of radiative recombination [183]. This nonemissive layer is also referred to as a dead layer. To be consistent with similar models and simplify the analysis, the aptamer film was represented as a planar porous membrane of finite thickness consisting of oligonucleotide strands in contact with an electrolyte solution.

From an electrostatic perspective, a fundamental aspect of the system under consideration is the variation in the potential profile across the aptamer-functionalized semiconductor and the ionic electrolyte. Since the electrolyte solution functions as a bulk reservoir of mobile ions, it has a considerable effect on the potential at the semiconductor surface [188]. As the system reaches equilibrium, the charged molecules within the permeable membrane work to simultaneously attract the surrounding counterions (i.e. ions with an opposite electric charge to the membrane) while expelling the nearby coions (i.e. ions with the same electric charge as the membrane) by means of strong Coulomb forces. Due to the highly localized nature of the charges in the membrane, the countercharge attributed by the electrolyte ions in the vicinity of the semiconductor consists of an excess of counterions and a deficit of coions. This charge balancing process leads to a redistribution of the ions as well as a corresponding change in the potential across the aptamer layer and the neighboring electrolyte solution. In the latter aptamer-free region, the potential

profile with respect to the neutral bulk electrolyte for the planar geometry, $\psi_{electrolyte}$, is mediated by the one dimensional Poisson-Boltzmann equation, as given by [188]

$$\frac{d^2\psi_{electrolyte}(x)}{dx^2} = \frac{2zqn_0}{\varepsilon_0\varepsilon_e}\sinh\left(\frac{zq\psi_{electrolyte}(x)}{kT}\right) \tag{5.1}$$

where z and n_0 are the valence and concentration of the anions and cations in the symmetrical electrolyte, ε_0 is the relative permittivity of free space, ε_e is the dielectric constant of the electrolyte, q is the fundamental electron charge, k is the Boltzmann constant, and T is the temperature. The above expression stems from a combination of Poisson's equation, which relates the potential around an electrolyte ion to the space charge density of the surrounding ionic atmosphere, and Boltzmann's law, which governs the distribution of ions in the solution [189]. Similarly, in the region adjacent to the semiconductor surface, the potential distribution across the aptamer membrane, $\psi_{membrane}$, satisfies the charge-modified Poisson-Boltzmann equation, which is expressed as [190]

$$\frac{d^2\psi_{membrane}(x)}{dx^2} = \frac{2zqn_0}{\varepsilon_0\varepsilon_m}\sinh\left(\frac{zq\psi_{membrane}(x)}{kT}\right) - \frac{vqN_m}{\varepsilon_0\varepsilon_m} \tag{5.2}$$

The first term in Equation (5.2) is derived from the permeation of the mobile electrolyte ions through the porous membrane, where ε_m is the dielectric constant in the membrane, while the last term is associated with the fixed negative charges on the aptamer molecules and the potential that forms across the membrane to compensate the diffusion of the ions along the developing concentration gradient [191]. The fixed charge embedded in the membrane is assumed to be uniformly distributed at a volume density of N_m as given by

$$N_m = \frac{N\rho}{d_{1,2} \cdot \pi r^2} \tag{5.3}$$

where N is the number of charges per strand (each oligonucleotide base contributes a single negative charge of valency, ν = -1), d_1 (d_2) is the average membrane thickness before (after) binding of the target ATP ligands (see Figure 5.2), and r is the probe radius (equal to approximately 1 nm) [192]. ρ is the coverage of aptamer probes on the semiconductor surface ranging between 1, in the case of the maximum attainable surface coverage (corresponding to $1/\pi r^2$), and 0, in the case of an aptamer-free surface (i.e. $0 \leq \rho \leq 1$).

In the case of the semiconductor region, Poisson's equation along with the fundamental expressions for the charge carrier concentrations combine to give the GaAs surface potential, ψ_0, relative to the equilibrium bulk position as defined by [35]

$$\frac{d^2\psi_0(x)}{dx^2} = \frac{q}{\varepsilon_0 \varepsilon_{GaAs}}\left(2n_i \sinh\left(\frac{q}{kT}(\psi - \phi_F)\right) + N_d\right) \tag{5.4}$$

where ε_{GaAs} is the GaAs dielectric constant, n_i is the intrinsic carrier concentration of the GaAs, ψ is the potential across the semiconductor depletion region, and N_d is the extrinsic doping concentration of the semiconductor substrate. In the above equation, the relative Fermi energy, ϕ_F, represents the position of the Fermi level with respect to the intrinsic level of the semiconductor, which is defined as the middle of the band gap [35]. Solving the set of coupled nonlinear second order differential equations specified in (5.1)-(5.4) for the electrostatic potential requires the use of boundary conditions. The primary boundary condition originates from the requirement that the potential must be continuous across the three distinct material regions [188]. The second boundary condition stems from the fact that the potential must vanish within the bulk of the electrolyte solution

and the semiconductor [188]. The final boundary condition that must be fulfilled follows from the necessity for overall charge neutrality (i.e. that the charge at the semiconductor surface must equal and oppose the total charge in the aptamer membrane and the electrolyte solution) [188]. A self-consistent solution to the proposed model subject to the above boundary conditions was determined by using Comsol Multiphysics software [193].

As the aforementioned theory predicts, the adsorption of the charged aptamer probes at the GaAs interface modifies the surface potential through the manifestation of band bending. Since the surface potential effectively controls the thickness of the nonemissive layer within the near-surface region of the GaAs, it also directly influences the PL characteristics of the material system. To interpret the response of the luminescence signal to the variation in the surface potential, a dead layer model was employed. The model assumes that light-generated charge carriers created within a distance on the order of the depletion width are prevented from recombining radiatively by means of an electric field and thus do not contribute to the PL signal [183]. A quantitative expression of the model is provided by the following relation [194]

$$\frac{PL_{modified}}{PL_{untreated}} = e^{-\alpha \Delta D} \tag{5.5}$$

where $PL_{\text{untreated}}$ and PL_{modified} are the peak PL intensities of the band-to-band radiative transitions before and after the biological modification, respectively, ΔD is the corresponding change in the thickness of the nonemissive dead layer, and $\alpha = \alpha_{\text{probe}} + \alpha_{\text{PL}}$ (where α_{probe} and α_{PL} are the absorption coefficients for the incident and emitted radiation). Under the experimental conditions used in this study, α_{probe} and α_{PL} were 4×10^4 cm^{-1} (at a wavelength of 632 nm) [182] and 7.5×10^3 cm^{-1} (at the GaAs band gap wavelength) [195], respectively. Since the thickness of the dead layer is approximately equal to the depletion width at the

semiconductor surface [194], the change in the dead layer thickness can also be defined as [35]

$$\Delta D \approx \Delta W = W_{modified} - W_{untreated} \tag{5.6}$$

where

$$W_{untreated,\,modified} = \left[\frac{2\varepsilon_{GaAs}\varepsilon_0 \left(\psi_{0,\,untreated,\,modified} - \frac{kT}{q} \ln\left(\frac{N_c}{N_d} \right) \right)}{q} \left(\frac{1}{N_d} \right) \right]^{1/2} \tag{5.7}$$

In the above equations, $W_{\text{untreated}}$ and W_{modified} are the widths of the surface depletion region before and after the biological functionalization, expressed in terms of the respective surface potentials, $\psi_{0,\,\text{untreated}}$ and $\psi_{0,\,\text{modified}}$, and N_c is the effective density of states at the conduction band minimum.

Substituting Equations (5.6) and (5.7) into Equation (5.5) along with the necessary constants and material parameters results in a relationship between the change in the PL intensity and the variation in the surface potential obtained by the modification of the GaAs substrate with the charged biological species. The applicable material parameters used in the computation are summarized in Table 5.2. It should be noted that a dielectric constant of 1.77, equal to that of water (pH 7, 25°C) at optical frequencies, was used for the bulk electrolyte solution as well as the aptamer membrane (i.e. $\varepsilon_e = \varepsilon_m = 1.77$) [196], [197]. Assigning the same value in the two regions is only a first order approximation since it is likely that the dielectric constant is altered in the vicinity of the charged aptamer probes [190]. However, since the influence of the dielectric constant on the response of the biosensor modeled in this study as well as that of a similar field-effect biosensor was found to be minor [162], this approximation is considered sufficient for the purpose of this investigation.

Table 5.2: Material parameters used in the modeling computation.

Parameter	Value (units)
GaAs dielectric constant, ε_{GaAs}	13.2
Intrinsic carrier concentration, n_i	2×10^6 (cm^{-3})
Impurity carrier concentration, N_d	3×10^8 (cm^{-3})
Relative Fermi energy, ϕ_F	0.13 (eV)
Effective density of states, N_c	4.35×10^{17} (cm^{-3})
GaAs absorption coefficient at the incident wavelength, α_{probe}	4×10^4 (cm^{-1})
GaAs absorption coefficient at the PL wavelength, α_{PL}	7.5×10^3 (cm^{-1})
Electrolyte pH	7.8
Electrolyte dielectric constant, ε_e	1.77
Ionic concentration, n_0	0.2 (mol/l)
Valence of electrolyte ions, z	±1
Membrane dielectric constant, ε_m	1.77
Valence of membrane charges, ν	-1

Figure 5.5 shows the results of the theoretical model whereby the experimental data is fitted using the previously described Poisson-Boltzmann statistics in combination with the dead layer model as defined in Equations (5.1) to (5.7). A fit to the data was obtained by varying the thickness of the membrane (d_1, d_2) and the surface coverage, ρ, of the aptamer probes. The probe coverage was assumed to remain the same before and after ATP sensing.

As illustrated in Figure 5.5, good agreement exists between the measurements (represented by the filled circles) and the calculated values (represented by the dashed line). The results of the computation indicate that, in the absence of ATP, the molecular membrane is best described by a very thin layer consisting of aptamer probes lying nearly flat on the GaAs surface. Assuming a cylindrical rod geometry for each aptamer molecule, a length of 0.34 nm between each oligonucleotide base pair [192], and a 1.2 nm long hexanethiol anchor [198], the simulated membrane thickness corresponds to an average molecular tilt angle of 20 ± 4° with respect to the GaAs surface for all aptamers considered. It should be noted that while this simplistic tilt angle is meant to

provide some physical insight into the typical orientation of the aptamers, the actual molecules likely adopt different tilt angles and resemble randomly oriented collapsed coils [199]. Nevertheless, the relatively flat orientation of the aptamer probes is in accord with that reported for a similar system of DNA oligomers on GaAs, which showed the nearly parallel alignment of DNA molecules to the semiconductor interface by means of grazing incidence x-ray scattering [200]. Moreover, the computed data reveals that the immobilized aptamer molecules occupy approximately 0.1% of the theoretical maximum surface coverage based on the area of a single molecule (i.e. maximum surface coverage = $1/(\pi r^2)$). It should be noted that due to the bulky nature of the molecules, the maximum attainable surface density of the aptamer probes is limited by the dimensionality of the molecules rather than the number of available bonding sites on the GaAs surface. The low packing density of the aptamer probes can be attributed to a number of factors. First, the kinetics of the adsorption process can produce an equilibrium probe density that is less than the total number of available surface bonding sites [162]. Second, the relatively sparse distribution of the aptamer molecules may reflect steric effects that hinder the formation of a closely packed structure [201]. Third, the MCH treatment of the aptamer modified surface may partially be responsible for the low surface density as previous studies have shown that DNA-modified surfaces exposed to MCH can result in more loosely packed layers when compared to untreated surfaces [198]. Finally, the electrostatic repulsion that exists between the phosphate moieties of adjacent aptamers may contribute to the low surface coverage of the probes on the GaAs surface [202]. Regardless of the mechanism responsible for the low probe density, a large separation between individual aptamer probes is actually advantageous in sensing applications as it facilitates a more rapid detection response [203]. Moreover, the aptamer probe density of approximately 3.2×10^{14} m^{-2} derived from the model is comparable to that reported in the literature for oligonucleotides immobilized on a variety of substrates such as Au, glass, SiO_2, and Si_3N_4 which

show densities between 10^{12}–10^{18} m^{-2} [180], [181], [198], [204]-[208]. As indicated by the wide range of densities, the coverage of surface-bound oligonucleotides is greatly influenced by the substrate material as well as by the immobilizing chemistry. Thus, it is likely that the density of aptamer molecules adsorbed on GaAs can be optimized by adjusting the relevant deposition parameters, as discussed in Chapter 6 [208].

Subsequent to the biorecognition process, the simulated results obtained with the present model affirm that the aptamer probes adopt a different conformation in which the molecules are erect in a stem-loop structure through the self-complementary pairing of several bases at both ends (see Figure 5.2). As hypothesized earlier, this target-induced structural configuration is accompanied by an increase in the thickness of the aptamer membrane, which in turn leads to a reduction in the negative charge density at the GaAs interface and a decrease in the depletion width. The resulting effect is consistent with the PL enhancement observed after the introduction of the ATP target. The agreement between the quantitative model and the experimental data was achieved assuming a membrane thickness, d_2, corresponding to a vertical orientation of the ATP-aptamer complexes, demonstrating the probe chain length dependent nature of the signal response.

Furthermore, the simulated and experimental results can be rationalized by considering the relationship between the orientation of the aptamer molecules and the ionic screening effect of the electrolyte. Prior to ATP sensing, the charge on the aptamer molecules is only partially screened by the nearby counterions, owing to the nearly flat orientation of the aptamer probes with respect to the GaAs surface which may preclude the counterions from completely surrounding the molecules. On the other hand, following the ATP detection, the vertical alignment of the ATP-aptamer complexes allows the molecules to be fully surrounded by the electrolyte ions which aids in effectively screening the aptamer charge.

5.4 Conclusion

The present study demonstrates the feasibility of using GaAs in conjunction with thiolated aptamers in the development of novel hybrid biosensors for the label-free detection of ATP. The implemented sensing mechanism takes advantage of the ultrasensitive nature of the GaAs PL emission to the local environment at its surface. Specifically, the ensuing PL response is linked to a change in the conformation of the charged aptamer bioreceptors with binding of the target ATP ligands. Since the aptamer probes are directly immobilized on the GaAs substrate, the resulting conformational transition alters the surface charge distribution and therefore, the width of the nonemissive depletion region. Varying the length of the aptamer probes revealed a relationship between the biorecognition stimulated luminescence and the aptamer strand length, with longer probes eliciting a larger PL enhancement upon ATP binding. Results of several control experiments indicate the high sensitivity and selectivity of the developed biosensor in identifying ATP. Modeling the performance data by means of Poisson-Boltzmann statistics in combination with the dead layer model showed a good correlation between the structural characteristics of the aptamer assembly and the PL yield of the underlying substrate. Collectively, these results indicate the promise of the proposed biosensing strategy for use in real-time applications requiring a simple and rapid means of detection. Moreover, the present hybrid scheme is also very attractive in terms of its potential for integration with innovative nanotechnologies in the construction of portable devices capable of sensing ultralow concentrations of target biomolecules.

Chapter 6 Conclusions and Future Work

6.1 Summary

In the preliminary chapters of the present study, an introductory review on the subject of self-assembly and the various analytical techniques utilized throughout the work were presented. In the following experimental sections, the chemical, structural, and optical properties of self-assembling alkanethiol monolayers deposited on GaAs substrates from liquid and vapor phases were compared and contrasted. The SAMs prepared from solution were formed by incubating the substrate in a dilute millimolar ODT-ethanol solution, while vapor-deposited monolayers were prepared from vapor phase transport of ODT in a custom-built UHV system. Characterization of the resulting SAMs was conducted with numerous surface science tools including CA analysis, PL spectroscopy, AFM, spectroscopic ellipsometry, and HRXPS. The comparative investigation was motivated by the potential of vapor deposition in the synthesis of high quality, reproducible, and scalable organic thin films on semiconductor surfaces for a wide variety of technological applications.

Static water CA measurements of the ODT monolayers indicated the successful formation of organized monolayers by both preparation routes. In contrast, PL spectroscopy, AFM, and ellipsometry measurements showed differences in the optical and structural properties of SAMs prepared from liquid and vapor phases. Specifically, room temperature luminescence results indicated

that the enhancement in PL intensity of GaAs upon exposure to the thiols was, on average, a factor of two greater for vapor-deposited SAMs compared to their solution-deposited analogs. Similarly, as illustrated via AFM, the surface roughness of the vapor-deposited monolayers was found to be lower in comparison to the solution-deposited monolayers, implying the formation of more uniform films with fewer defects. These observations were further supplemented by spectroscopic ellipsometry measurements in conjunction with a three-phase analytical model, which revealed an oxide content of approximately 30% greater in SAMs formed from liquid phase as opposed to those formed from vapor phase. Collectively, the data presented in Chapter 3 demonstrates that more densely packed monolayers exhibiting greater surface coverage and increased passivation are assembled from vapor phase on GaAs substrates. The lower SAM coverage and reduced passivation observed on samples prepared from liquid phase was attributed to the formation of a partial oxide layer on the GaAs surface as a result of the deposition process. Moreover, the results presented illustrate the particular sensitivity of each analytical technique to the specific characteristics of the monolayers. In particular, the data implies that PL spectroscopy is more sensitive to the quality of the films when compared to CA analysis, which can be used to indicate the film quality at a more macroscopic level.

Chapter 4 detailed an examination of the chemical bonding characteristics and stability of the SAMs deposited on GaAs substrates from vapor and liquid phases. The data presented implies that the modification of GaAs substrates with ODT SAMs prevents the reoxidization of the surface for a prolonged period of time and maintains an interfacial quality comparable to that achieved with conventional oxide removal techniques. Time-dependent PL and CA analysis indicated that the long-term durability of the SAMs was related to the specific preparation method used to deposit the films. Specifically, the PL intensity was found to progressively decrease over time for all of the treated samples exposed to air. The time dependence of the PL intensity decay for the vapor-deposited SAM

exhibited temporal characteristics with two different rate components: an initial fast rate constant proceeded by a slower rate constant with increased exposure to an ambient environment. On the other hand, the decay in the luminescence intensity of solution-deposited SAM showed a single, more gradual rate constant. This difference in the stability of the two samples was explained by the experimental conditions used to synthesize the films. In the case of the vapor-deposited SAM, the resultant GaAs passivation is a product of two different passivation techniques, namely, hydrogen passivation, which stems from the atomic hydrogen pretreatment utilized to remove the native oxide, and SAM passivation. While the effects of hydrogen passivation were observed to dissipate quickly and thus, were deemed responsible for the initial fast PL decay, passivation of the underlying substrate by the organic monolayer produced a prolonged effect, as described by the second slower decay constant. Since the solution-deposited film was prepared without the use of atomic hydrogen, the passivation of the GaAs surface was created solely by the SAM modification, and thus could be represented by a single decay constant. Moreover, after a period of four months in air, the luminescence yield observed on the vapor-deposited monolayer was shown to be about a factor of five greater than that of the solution-deposited monolayer. Similarly, a time-dependent CA analysis showed a smaller degradation in the CA for the vapor-deposited monolayer following a four month exposure to ambient conditions compared to the SAM synthesized from solution. Consequently, the PL results in conjunction with the CA data demonstrated that more stable films are produced from vapor than from liquid phase, which were shown to be more susceptible to atmospheric conditions over time.

By way of HRXPS measurements, the attachment of the thiolate molecules to the GaAs substrates was observed to occur through the formation of chemical bonds at both Ga and As surface sites, as confirmed by the manifestation of the relevant emissions in the Ga 3d, As 3d, and S 2p spectra. Additionally, the percentage of each bonding configuration was shown to be dictated by the surface

termination produced via the cleaning and oxide removal processes used prior to the deposition of the monolayer. While films deposited by either method revealed signs of some residual oxide contamination, SAMs prepared under UHV conditions were found to exhibit greater surface coverage and enhanced passivation properties, as confirmed by spectroscopic ellipsometry and improved PL yield. In particular, a four-phase ellipsometric model fitted to the experimental data indicated the formation of a thicker monolayer from liquid phase consisting of the thiolate molecules oriented nearly perpendicular to the GaAs surface at a reduced surface coverage. On the contrary, the ellipsometric simulations of the vapor-deposited film indicated the existence of a thinner assembly of closely packed chains tilted more towards the substrate surface. From the HRXPS results, the superior properties of SAMs synthesized from vapor phase were related to the formation of stronger Ga-S bonds at the GaAs interface. Collectively, the results of Chapter 3 and Chapter 4 indicate that SAMs prepared from vapor phase deposition have more optimal characteristics compared to monolayers prepared from solution. These results represent the first systematic investigation concerning the characterization of alkanethiol SAMs deposited on GaAs surfaces from liquid and vapor phases.

In the final experimental chapter of this thesis, the relevance of thiolated SAMs in development of novel analytical biosensing devices was investigated. In particular, the design and performance of a label-free hybrid GaAs-aptamer biosensor were outlined. The implemented detection strategy combines the high affinity of thiolated biofunctional monolayers for semiconductors with the sensitivity of the GaAs PL emission to the local atmosphere at its surface. To fabricate the devices, GaAs substrates were chemically modified with thiol-derivatized oligonucleotide aptamers following conventional condensed-phase deposition techniques and exposed to the target ATP biomolecules. The resulting modification in the PL intensity was attributed to a specific biorecognition interaction between aptamer receptors and the ATP target and, more importantly,

6.2 Outlook

Alkanethiol SAMs adsorbed on solid inorganic surfaces have been a widely studied topic of interest for a number of years. Although these archetypal compounds are commonly used to model the concept of self-assembly, the complex nature of SAM formation has limited the thorough understanding of the precise structures and processes involved on the molecular level, especially in the case where less conventional materials such as semiconductors are used as growth supports. The intricacies associated with alkanethiol-based adsorbate-substrate systems are much more complicated than once believed and many questions regarding the detailed quantitative properties of these systems have yet to be conclusively answered. While progress towards a qualitative understanding of self-organization and interfacial interactions has been made, a unified picture of the structure-property relationships of SAMs remains unresolved. Thus, to achieve the full potential of alkanethiol monolayers in applications ranging from classical areas of technology to more novel areas such as those associated with interfacing biorelated devices, future investigations will need to address the remaining fundamental issues. This section of the thesis will suggest some directions for future research in this area, with emphasis on the important role of thiolated SAMs in development of innovative biotechnologies. To narrow the focus, the following discussion will be subdivided into four main points: 1) optimization of the vapor deposition process, 2) surface engineering of SAMs after formation, 3) enhancement of the aptamer-GaAs biosensor and model, and 4) development of SAM-based nanostructured optical biosensors.

6.2.1 Optimization of the Vapor Deposition Process

The results presented throughout this work show the vapor deposition of organothiolate SAMs on compound semiconductors has numerous benefits

compared to liquid phase deposition, including improved passivation properties, increased stability, and greater surface coverage. However, as discussed in Chapter 4, the atomic hydrogen pretreatment used prior to the vapor deposition was insufficient in fully removing the native oxide from the GaAs surface. The reason behind the incomplete desorption of the oxide layer is likely the experimental parameters used during the treatment, such as substrate temperature and/or insufficient hydrogen dose. Since the existence of oxide contamination on the semiconductor surface limits the ultimate coverage of the monolayer, it is advantageous to optimize the atomic hydrogen cleaning procedure along with the subsequent vapor phase deposition process in order to promote the full removal of the oxide species as well as the assembly of a highly dense, defect-free monolayer. By carefully altering the preparation conditions including those related to the temperature, time, and reactant dose, and consistently characterizing the resulting SAM structures, an optimal set of control parameters can be identified which leads to the formation of reproducible and complete single-domain films on GaAs surfaces.

An attractive way to determine the appropriate processing conditions is through the use of in-situ diagnostic techniques, such as LEED, STM, spectroscopic ellipsometry, and Auger electron spectroscopy. For instance, LEED or STM can be used during the cleaning and deposition treatments to image the sample surface as well as the various film structures [72], [92]. Similarly, a non-intrusive method like in-situ ellipsometry can be applied to monitor the evolution of the film formation in real-time [209]. Thus, by retrofitting the UHV deposition system used in this work with a suitable analytical surface science tool, the most favorable processing parameters along with the treatment end-points can be accurately defined in order to improve the surface coverage of the SAMs, as well as the relevant film properties.

6.2.2 Surface Engineering of SAMs after Formation

To fully exploit the advantageous properties of the vapor-deposited SAMs for a variety of applications, it is valuable to functionally modify the films following their formation on the GaAs substrates. The post-preparation modification of SAMs is especially important in the development of biologically active architectures where the functional moieties are physically large and complex [49]. Since the synthesis of thiol molecules exhibiting different terminal functionalities is generally difficult and time consuming, numerous approaches have previously been developed for modifying the exposed surfaces of monolayers after their assembly [49]. Functionalization of the vapor-deposited alkanethiol monolayers on GaAs surfaces following their preparation offers some key advantages. First, it relies on the use of well-established processing reactions and thus simplifies the overall sample preparation procedures [49]. Second, it permits the incorporation of ligands into the films that are otherwise incompatible with UHV synthesis techniques [49]. Third, it enables the rapid modification of several samples with a variety of engineered functionalities and provides a central design flexibility, both at the molecular and material levels [49]. Fourth, it reduces the overall amount of functional groups that is required, which often lowers the fabrication costs especially in the case of more expensive biological molecules [49]. Lastly, the post-formation modification of the SAMs derived from vapor phase maintains the characteristics of the underlying monolayer at the semiconductor interface [49]. This latter point is very important as thiol monolayers assembled from gas phase were shown throughout this work to possess properties that were distinctly superior to those exhibited by films prepared from liquid phase. Thus, for example, by experimentally exploring various strategies of functionally tailoring the composition of the preformed vapor-deposited SAMs, the density of biorecognition elements can potentially be increased on the GaAs biosensor platform described in Chapter 5.

6.2.3 Enhancement of the Hybrid Aptamer-GaAs Optical Biosensor and Model

One of the main objectives of this work was to construct SAM-based assays for optical GaAs biosensors. While this goal was realized from a proof-of-concept perspective, as discussed in Chapter 5, future work needs to be undertaken before this system can be utilized in a broader range of applications. For instance, an in-depth study which details the structural characteristics of the aptamer assemblies as well as their optical and chemical properties should be conducted in order to develop an understanding of the interactions that occur at the aptamer-GaAs interface. To this end, XPS analysis can be performed to deduce the elemental composition of the outermost layers on the semiconductor surface. Depth profiling of the aptamer films can be achieved by varying the angle of the XPS measurements, thus revealing the position of the various biological species as a function of distance from the surface. Similarly, AFM can be utilized to define the surface topography of the functionalized samples by providing a direct image of the surface structure. Supplementary characterization techniques such as spectroscopic ellipsometry and near-edge x-ray absorption fine structure (NEXAFS) spectroscopy can be applied to examine the thickness of the resultant aptamer films as well as the molecular orientation and ordering. Information obtained by several complementary surface science tools can be used to quantitatively determine the surface coverage of the adsorbed aptamer molecules and compare it to that previously calculated from the theoretical model presented in Chapter 5. The effects of the various treatments (i.e. MCH, dissociation, analyte detection) on the aptamer surface coverage should also be examined in the same manner. Moreover, to obtain a comprehensive description of the mechanisms involved in the operation of the biosensor it would be constructive to characterize the properties of the aptamer-GaAs samples before and after the analyte sensing. In particular, by investigating the changes in the film thickness and molecular orientation of the aptamer probes with the introduction of the ATP

target, the structure-switching abilities of the signaling aptamers can be verified along with the proposed mechanism responsible for the observed changes in the PL signal.

In addition to fully characterizing the system from a materials science standpoint, another avenue along which future research could proceed involves the sensitivity of the hybrid biosensor to different environmental factors and their influence on the sensor's optical properties. Several different parameters can potentially affect the sensitivity and reliability of the aptamer-GaAs biosensor, including the electrolyte strength, pH of the solution, temperature, and probe density [210]. Hence, a rigorous study that accounts for the effects of these variables on the sensitivity will likely arrive at an optimum set of parameters that ensures the best detection response from the sensor platform. Another aspect of the system that should be addressed is the sensitivity of the biosensor to the concentration of the target analyte. Specifically, by progressively varying the analyte concentration, the performance of the sensor with respect to the response signal can be profiled and the minimum effective concentration required for unambiguous detection can be identified. Likewise, since the target analyte was dispersed in carefully prepared 'clean' synthetic solutions in this study, it would be useful to discern the selectivity of the proposed biosensing strategy under more realistic conditions in which the analyte exists in solution with other biomolecules. The presence of the target analyte in close proximity to other biological species simulates conditions found in living systems. The operation of the biosensor in this environment would demonstrate the potential of the device for studying cellular processes.

The theoretical model used in the analysis of the luminescence data acquired from the aptamer-GaAs biosensor is another area that deserves further consideration in future studies. While the simple model discussed in Chapter 5 captures the essential phenomena that define the sensor's functions and provides good insight into the fundamental mechanisms involved in the operation of the

sensor, several basic assumptions were necessary for its development which may inadvertently underestimate the effects of various processes. To provide a more realistic interpretation of the system characteristics, an advanced description of the biosensor is necessary. A preliminary approach to this task should begin with modifying the sensor's physical structure. In the present one-dimensional model, the negative charges supplied by the aptamer probes were assumed to be delocalized and distributed over a continuum spanning the width of the membrane region. In reality, however, the charges are spatially localized along the length of the aptamer molecules and the previous approximation is primarily applicable to cases where the probes are densely assembled. This limitation in the model can be overcome by exposing the molecular structure of the probes and representing the aptamer membrane as a two-dimensional array composed of discrete aptamer molecules [211]. Besides modifying the physical characteristics of the aptamer layer, additional factors that should be incorporated into future models include the possible existence of surface oxide species, condensation of ions along the aptamer backbone, and the adsorption of ions on the GaAs surface [211]. The presence of superfluous ions within the vicinity of the semiconductor surface would alter the equilibrium charge distribution and thus the simulated potential profile associated with the biorecognition response.

6.2.4 Development of SAM-Based Nanostructured Optical Semiconductor Biosensors

An attractive prospect of using SAMs in combination with GaAs and other III-V semiconductors is in the construction of ultrasensitive label-free nanostructured biosensors with specifically tailored properties. The nanometer scale is particularly important in biological applications on account of the fact that the dimensions of most bulky biomolecules and sub-cellular structures are generally in the range of 1 to 1000 nm [212]. The results obtained with the planar

biosensor discussed in Chapter 5 demonstrate the applicability of this system to the selective detection of specific analytes. Thus, the target of future studies should entail adapting this concept to the design of new assays based on the SAM-functionalization of nanoscaled structures. A particularly promising strategy involves the development of a miniature aptamer-GaAs NW optical biosensor. A schematic of the proposed sensing platform is illustrated in Figure 6.1. In this design, an alkanethiol SAM is used as a bonding layer to immobilize charged aptamer probes on the surface of vertically aligned GaAs NWs arranged in an array on a solid support. As in the case of the planar geometry, the introduction of the ATP target triggers a direct transformation in the conformation of the probes and the formation of the aptamer-ATP complexes. This biomolecular recognition event is accompanied by a change in the charge density at the surface of the NW transducers and a resultant modification in NW luminescence. The small, elongated structure of the NWs results in a high surface-to-volume ratio that augments the role of surface states and provides an enhancement in the responsiveness of the PL signal to fluctuations in the surface charge density. Altering the sensor geometry from a planar to a NW-based configuration takes advantage of the size effects and overcomes the sensitivity limitations imposed by the former design. Specifically, the change in the potential profile induced by the folding of the aptamers with ATP binding occurs in the bulk of the NW as opposed to only in the near-surface region of the planar substrate. Consequently, similar devices composed of semiconductor NWs have been shown to be capable of detecting ultralow concentrations of bioaffinitive agents [213]. Similarly, theoretical calculations have shown that NW sensors possess improved performance characteristics compared to planar configurations in terms of sensitivity to external stimuli and response time [213]. Furthermore, the

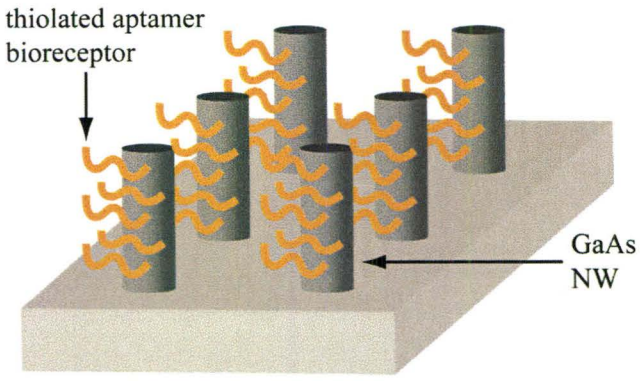

Figure 6.1: Schematic depiction of the proposed aptamer-GaAs NW optical biosensor. The vertically aligned NWs are modified using thiolate chemistry with an aptamer functionalized SAM which acts as the sensing layer.

combination of freestanding NWs with optical transduction is also advantageous compared to more traditional FET-based approaches since it circumvents the difficulties associated with the formation of NW-electrode interconnects and facilitates scalable and reproducible manufacturing.

Utilization of SAM-modified GaAs NWs can potentially translate into state-of-the-art optical assays that expand on current techniques of detection and diagnostic screening. By integrating NW sensing arrays with novel MEMS and microfluidic networks, all-inclusive devices can be realized and implemented to develop a new paradigm for the label-free monitoring of biological processes. In principle, the fact that all the constituent elements, including the optical excitation source and detector can be derived from III-V materials provides for the possibility of a single chip architecture (see Figure 6.2). These comprehensive lab-on-a-chip systems represent a final product from the point of view of several individually linked analytical components capable of automatically acquiring, processing, detecting, and qualifying target analytes within a sample fluid. The attainment of such a complete hybrid organic-semiconductor biosensor is the

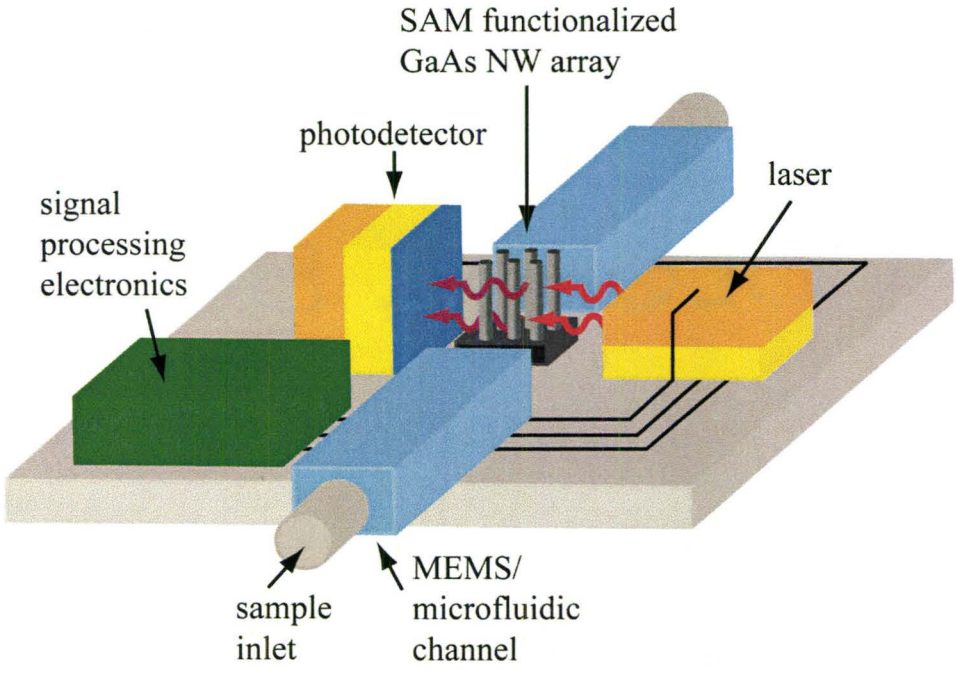

Figure 6.2: Novel hybrid SAM-NW optical lab-on-a-chip biosensor [Adapted from [214]].

ultimate goal of the present research since it would provide a cost-effective means of rapid and sensitive detection in a compact portable package. While much work remains to be completed before this long-standing goal is fully realized, this study has shown the considerable promise of alkanethiol SAMs on GaAs surfaces combined with PL-based sensing for the development of highly integrated analytical sensors. The favorable performance characteristics of this innovative hybrid platform present new perspectives in terms of the widespread applications in miniaturized molecular diagnostics and monitoring. The findings presented in this thesis form a strong foundation for the continued development and optimization of novel biosensor technologies consisting of functionalized-SAM bioreceptors immobilized on III-V semiconductor transducers.

Appendix A

Permission for Reproduction of Published Work

The American Institute of Physics has granted me permission to reproduce the following articles in my thesis. I hereby grant an irrevocable, nonexclusive license to McMaster University and the National Library of Canada to reproduce the material as part of the thesis.

1. H. Budz and R. LaPierre, J. Vac. Sci. Technol. A 26, 1425 (2008).
2. H. Budz, M. Biesinger, and R. LaPierre, J. Vac. Sci. Technol. B 27, 637 (2009).
3. H. A. Budz, M. Ali, Y. Li, and R. R. LaPierre, accepted for publication on Apr. 7, 2010 in J. Appl. Phys.

Permission from the American Institute of Physics

AMERICAN INSTITUTE OF PHYSICS LICENSE TERMS AND CONDITIONS

Mar 16, 2010

This is a License Agreement between Hanna Budz ("You") and American Institute of Physics ("American Institute of Physics") provided by Copyright Clearance Center ("CCC"). The license consists of your order details, the terms and conditions provided by American Institute of Physics, and the payment terms and conditions.

All payments must be made in full to CCC. For payment instructions, please see information listed at the bottom of this form.

License Number	2390860186202
License date	Mar 16, 2010
Licensed content publisher	American Institute of Physics
Licensed content publication	Journal of Vacuum Science & Technology A
Licensed content title	Properties of octadecanethiol self-assembled monolayers deposited on GaAs from liquid and vapor phases
Licensed content author	H. A. Budz, R. R. LaPierre
Licensed content date	Nov 1, 2008
Volume number	26
Issue number	6
Type of Use	Thesis/Dissertation
Requestor type	Author (original article)
Format	Print and electronic
Portion	Excerpt (> 800 words)
Will you be translating?	No
Title of your thesis / dissertation	Growth and Characterization of Self-Assembled Monolayers on GaAs for use in Optical Biosensing Applications
Expected completion date	Jun 2010
Estimated size (number of pages)	150
Total	0.00 USD

Terms and Conditions

American Institute of Physics -- Terms and Conditions: Permissions Uses

American Institute of Physics ("AIP") hereby grants to you the non-exclusive right and license to use and/or distribute the Material according to the use specified in your order, on a one-time basis, for the specified term, with a maximum distribution equal to the number that you have

ordered. Any links or other content accompanying the Material are not the subject of this license.

1. You agree to include the following copyright and permission notice with the reproduction of the Material: "Reprinted with permission from [FULL CITATION]. Copyright [PUBLICATION YEAR], American Institute of Physics." For an article, the copyright and permission notice must be printed on the first page of the article or book chapter. For photographs, covers, or tables, the copyright and permission notice may appear with the Material, in a footnote, or in the reference list.
2. If you have licensed reuse of a figure, photograph, cover, or table, it is your responsibility to ensure that the material is original to AIP and does not contain the copyright of another entity, and that the copyright notice of the figure, photograph, cover, or table does not indicate that it was reprinted by AIP, with permission, from another source. Under no circumstances does AIP, purport or intend to grant permission to reuse material to which it does not hold copyright.
3. You may not alter or modify the Material in any manner. You may translate the Material into another language only if you have licensed translation rights. You may not use the Material for promotional purposes. AIP reserves all rights not specifically granted herein.
4. The foregoing license shall not take effect unless and until AIP or its agent, Copyright Clearance Center, receives the Payment in accordance with Copyright Clearance Center Billing and Payment Terms and Conditions, which are incorporated herein by reference.
5. AIP or the Copyright Clearance Center may, within two business days of granting this license, revoke the license for any reason whatsoever, with a full refund payable to you. Should you violate the terms of this license at any time, AIP, American Institute of Physics, or Copyright Clearance Center may revoke the license with no refund to you. Notice of such revocation will be made using the contact information provided by you. Failure to receive such notice will not nullify the revocation.
6. AIP makes no representations or warranties with respect to the Material. You agree to indemnify and hold harmless AIP, American Institute of Physics, and their officers, directors, employees or agents from and against any and all claims arising out of your use of the Material other than as specifically authorized herein.
7. The permission granted herein is personal to you and is not transferable or assignable without the prior written permission of AIP. This license may not be amended except in a writing signed by the party to be charged.
8. If purchase orders, acknowledgments or check endorsements are issued on any forms containing terms and conditions which are inconsistent with these provisions, such inconsistent terms and conditions shall be of no force and effect. This document, including the CCC Billing and Payment Terms and Conditions, shall be the entire agreement between the parties relating to the subject matter hereof.

This Agreement shall be governed by and construed in accordance with the laws of the State of New York. Both parties hereby submit to the jurisdiction of the courts of New York County for purposes of resolving any disputes that may arise hereunder.

Gratis licenses (referencing $0 in the Total field) are free. Please retain this printable license for your reference. No payment is required.

If you would like to pay for this license now, please remit this license along with your payment made payable to "COPYRIGHT CLEARANCE CENTER" otherwise you will be invoiced within 48 hours of the license date. Payment should be in the form of a check or money order referencing your account number and this invoice number RLNK10751813.
Once you receive your invoice for this order, you may pay your invoice by credit card. Please follow instructions provided at that time.

Make Payment To:
Copyright Clearance Center
Dept 001
P.O. Box 843006
Boston, MA 02284-3006

If you find copyrighted material related to this license will not be used and wish to cancel, please contact us referencing this license number 2390860186202 and noting the reason for cancellation.

Questions? customercare@copyright.com or +1-877-622-5543 (toll free in the US) or +1-978-646-2777.

AMERICAN INSTITUTE OF PHYSICS LICENSE TERMS AND CONDITIONS

Mar 16, 2010

This is a License Agreement between Hanna Budz ("You") and American Institute of Physics ("American Institute of Physics") provided by Copyright Clearance Center ("CCC"). The license consists of your order details, the terms and conditions provided by American Institute of Physics, and the payment terms and conditions.

All payments must be made in full to CCC. For payment instructions, please see information listed at the bottom of this form.

License Number	2390860052298
License date	Mar 16, 2010
Licensed content publisher	American Institute of Physics
Licensed content publication	Journal of Vacuum Science & Technology B
Licensed content title	Passivation of GaAs by octadecanethiol self-assembled monolayers deposited from liquid and vapor phases
Licensed content author	H. A. BudzM. C. BiesingerR. R. LaPierre
Licensed content date	Mar 1, 2009
Volume number	27
Issue number	2
Type of Use	Thesis/Dissertation
Requestor type	Author (original article)
Format	Print and electronic
Portion	Excerpt (> 800 words)
Will you be translating?	No
Title of your thesis / dissertation	Growth and Characterization of Self-Assembled Monolayers on GaAs for use in Optical Biosensing Applications
Expected completion date	Jun 2010
Estimated size (number of pages)	150
Total	0.00 USD

Terms and Conditions

American Institute of Physics -- Terms and Conditions: Permissions Uses

American Institute of Physics ("AIP") hereby grants to you the non-exclusive right and license to use and/or distribute the Material according to the use specified in your order, on a one-time basis, for the specified term, with a maximum distribution equal to the number that you have

ordered. Any links or other content accompanying the Material are not the subject of this license.

1. You agree to include the following copyright and permission notice with the reproduction of the Material: "Reprinted with permission from [FULL CITATION]. Copyright [PUBLICATION YEAR], American Institute of Physics." For an article, the copyright and permission notice must be printed on the first page of the article or book chapter. For photographs, covers, or tables, the copyright and permission notice may appear with the Material, in a footnote, or in the reference list.
2. If you have licensed reuse of a figure, photograph, cover, or table, it is your responsibility to ensure that the material is original to AIP and does not contain the copyright of another entity, and that the copyright notice of the figure, photograph, cover, or table does not indicate that it was reprinted by AIP, with permission, from another source. Under no circumstances does AIP, purport or intend to grant permission to reuse material to which it does not hold copyright.
3. You may not alter or modify the Material in any manner. You may translate the Material into another language only if you have licensed translation rights. You may not use the Material for promotional purposes. AIP reserves all rights not specifically granted herein.
4. The foregoing license shall not take effect unless and until AIP or its agent, Copyright Clearance Center, receives the Payment in accordance with Copyright Clearance Center Billing and Payment Terms and Conditions, which are incorporated herein by reference.
5. AIP or the Copyright Clearance Center may, within two business days of granting this license, revoke the license for any reason whatsoever, with a full refund payable to you. Should you violate the terms of this license at any time, AIP, American Institute of Physics, or Copyright Clearance Center may revoke the license with no refund to you. Notice of such revocation will be made using the contact information provided by you. Failure to receive such notice will not nullify the revocation.
6. AIP makes no representations or warranties with respect to the Material. You agree to indemnify and hold harmless AIP, American Institute of Physics, and their officers, directors, employees or agents from and against any and all claims arising out of your use of the Material other than as specifically authorized herein.
7. The permission granted herein is personal to you and is not transferable or assignable without the prior written permission of AIP. This license may not be amended except in a writing signed by the party to be charged.
8. If purchase orders, acknowledgments or check endorsements are issued on any forms containing terms and conditions which are inconsistent with these provisions, such inconsistent terms and conditions shall be of no force and effect. This document, including the CCC Billing and Payment Terms and Conditions, shall be the entire agreement between the parties relating to the subject matter hereof.

This Agreement shall be governed by and construed in accordance with the laws of the State of New York. Both parties hereby submit to the jurisdiction of the courts of New York County for purposes of resolving any disputes that may arise hereunder.

Gratis licenses (referencing $0 in the Total field) are free. Please retain this printable license for your reference. No payment is required.

If you would like to pay for this license now, please remit this license along with your payment made payable to "COPYRIGHT CLEARANCE CENTER" otherwise you will be invoiced within 48 hours of the license date. Payment should be in the form of a check or money order referencing your account number and this invoice number RLNK10751811.
Once you receive your invoice for this order, you may pay your invoice by credit card. Please follow instructions provided at that time.

Make Payment To:
Copyright Clearance Center
Dept 001
P.O. Box 843006
Boston, MA 02284-3006

If you find copyrighted material related to this license will not be used and wish to cancel, please contact us referencing this license number 2390860052298 and noting the reason for cancellation.

Questions? customercare@copyright.com or +1-877-622-5543 (toll free in the US) or +1-978-646-2777.

Dear Dr. Budz:

Thank you for requesting permission to reproduce material from American Institute of Physics publications.

Permission is granted – subject to the conditions outlined below – for the following:

H. A. Budz, M. Ali, Y. Li, and R. R. LaPierre,
"Photoluminescence Model for a Hybrid Aptamer-GaAs Optical Biosensor", Manuscript #: JR09-7058R, accepted for publication on Apr. 7, 2010 in J. Appl. Phys.

To be used in the following manner:

Reproduced as part of your Ph.D. thesis at McMaster University entitled, "Growth and Characterization of Self-Assembled Monolayers on GaAs for use in Optical Biosensing Applications."

1. The American Institute of Physics grants you the right to reproduce the material indicated above on a one-time, non-exclusive basis, solely for the purpose described. Permission must be requested separately for any future or additional use.

2. This permission pertains only to print use and its electronic equivalent, including CD-ROM or DVD.

3. The following copyright notice must appear with the material: "The following article has been accepted by [Name of Journal]."

Full citation format is as follows: Author names, journal title, Vol. #, Page #, (Year of publication). For an article, the copyright notice must be printed on the first page of the article or book chapter. For figures, photographs, covers, or tables, the notice may appear with the material, in a footnote, or in the reference list.

4. This permission does not apply to any materials credited to sources other than the copyright holder.

Please let us know if you have any questions.

Sincerely,
Susann Brailey

Begin forwarded message:

From: Hanna Budz <budzha@mcmaster.ca>
Date: April 7, 2010 8:02:55 AM CDT
To: jap-edoffice@aip.org
Subject: Permission for Reproduction of Accepted Work

Dear Sir/Madam,

I am completing a Ph.D. thesis at McMaster University entitled, "Growth and Characterization of Self-Assembled Monolayers on GaAs for use in Optical Biosensing Applications ". I would like your permission to reprint sections of the following manuscript recently accepted for publication in the Journal of Applied Physics in my thesis:

1. H. A. Budz, M. Ali, Y. Li, and R. R. LaPierre, "Photoluminescence Model for a Hybrid Aptamer-GaAs Optical Biosensor", Manuscript #: JR09-7058R, accepted for publication on Apr. 7, 2010 in J. Appl. Phys.

Please note that I am the first author of the above manuscript.

I am also requesting that you grant irrevocable, nonexclusive licence to McMaster University and to the National Library of Canada to reproduce this material as part of the thesis. Proper acknowledgement of your copyright of the reprinted material (including title, authors, date, and publisher) will be given in the thesis.

If these arrangements meet with your approval, please let me know.

Thank you very much,

Hanna Budz

Ph.D. Candidate
Department of Engineering Physics
McMaster University
1280 Main Street West
Hamilton, ON, L8S 4L7
email: budzha@mcmaster.ca

~~~~~~~~~~~

Office of the Publisher, Journals and Technical Publications
Rights & Permissions
American Institute of Physics
Suite 1NO1
2 Huntington Quadrangle
Melville, NY 11747-4502
516-576-2268 TEL
516-576-2450 FAX
rights@aip.org
~~~~~~~~~~~

References

[1] A. Ulman, Chem. Rev. 96, 1533 (1996).

[2] H. Kuhn and A. Ulman, in *Thin Films: Organic Thin Films and Surfaces*, edited by A. Ulman, Vol. 20 (Academic Press, San Diego, USA, 1995).

[3] A. Duwez, Journal of Electron Spectroscopy and Related Phenomena 134, 97 (2004).

[4] B. Bhushan, A. Kulkarni, V. Koinkar, M. Boehm, L. Odoni, C. Martelet, and M. Belin, Langmuir 11, 3189 (1995).

[5] R. Maboudian, Sur. Sci. Rep. 30, 207 (1998).

[6] C. Kirchner, M. George, B. Stein, W. Parak, H. Gaub, and M. Seitz, Adv. Funct. Mater. 12, 266 (2002).

[7] K. Xiao, Y. Liu, Y. Guo, G. Yu, L. Wan, and D. Zhu, Appl. Phys. A 80, 1541 (2005).

[8] M. Schvartzman, V. Sidorov, D. Ritter, and Y. Paz, Semicond. Sci. Technol. 16, L68 (2001).

[9] M. Schvartzman, V. Sidorov, D. Ritter, and Y. Paz, J. Vac. Sci. Technol. B 21, 148 (2003).

[10] K. Moumanis, X. Ding, J. Dubowski, and E. Frost, J. Appl. Phys. 100, 034702 (2006).

[11] T. Sai and A. Raychaudhuri, J. Phys. D 40, 3182 (2007).

[12] O. Azzaroni, M. Fonticelli, G. Benítez, P. Schilardi, R. Gago, I. Caretti, L. Vazquez, and R. Salvarezza, Adv. Mater. 16, 405 (2004).

[13] C. Bruinink, M. Peter, M. de Boer, L. Kuipers, J. Huskens, and D. Reinhoudt, Adv. Mater. 16, 1086 (2004).

[14] M. Zharnikov and M. Grunze, J. Vac. Sci. Technol. B 20, 1793 (2002).

[15] G. Baralia, A. Pallandre, B. Nysten, and A. Jonas, Nanotechnology 17, 1160 (2006).

[16] P. DiMilla, J. Folkers, H. Biebuyck, R. Haerter, G. Lopez, and G. Whitesides, J. Am. Chem. Soc. 116, 2225 (1994).

[17] C. Erdelen, L. Haeussling, R. Naumann, H. Ringsdorf, H. Wolf, J. Yang, M. Liley, J. Spinke, and W. Knoll, Langmuir 10, 1246 (1994).

[18] N. Chaki, M. Aslam, J. Sharma, and K. Vijayamohanan, Proc. Indian Acad. Sci. (Chem. Sci.) 113, 659 (2001).

[19] W. Senaratne, L. Andruzzi, and C. Ober, Biomacromolecules 6, 2427 (2005).

[20] O. Chailapakul, L. Sun, C. Xu, and R. Crooks, J. Am. Chem. Soc. 115, 12459 (1993).

[21] E. Thoden van Velzen, J. Engbersen, P. de Lange, J. Mahy, and D. Reinhoudt, J. Am. Chem. Soc. 117, 6853 (1995).

[22] S. Dong and J. Li, Bioelectroch. Bioener. 42, 7 (1997).

[23] R. Nyquist, A. Eberhardt, L. Silks, Z. Li, X. Yang, and B. Swanson, Langmuir 16, 1793 (2000).

[24] S. Flink, F. van Veggel, and D. Reinhoudt, Adv. Mater. 12, 1315 (2000).

[25] M. Yu, N. Bovet, C. Satterley, S. Bengio, K. Lovelock, P. Milligan, R. Jones, D. Woodruff, and V. Dhanak, Phys. Rev. Lett. 97, 166102 (2006).

[26] C. Vericat, M. Vela, G. Benitez, J. Gago, X. Torelles, and R. Salvarezza, J. Phys. Cond. Mat. 18, R867 (2006).

[27] S. Mendoza, I. Arfaoui, S. Zanarini, F. Paolucci, and P. Rudolf, Langmuir 23, 582 (2007).

[28] Y. Jun, X. Zhu, J. Hsu, Langmuir 22, 3627 (2006).

[29] S. Ye, G. Li, H. Noda, K. Uosaki, and M. Osawa, Surf. Sci. 529, 163 (2003).

[30] K. Adlkofer and M. Tanaka, Langmuir 17, 4267 (2001).

[31] H. Lim, C. Carraro, and R. Maboudian, Langmuir 20, 743 (2004).

[32] S. Lodha and D. Janes, J. Appl. Phys. 100, 024503 (2006).

[33] Y. Huang, X. Duan, Q. Wei, and C. Lieber, Science 291, 630 (2001).

[34] L. Mohaddes-Ardabili, L. Martinez-Miranda, J. Silverman, A. Christou, L. Salamanca-Riba, M. Al-Sheikhly, W. Bentley, and F. Ohuchi, Appl. Phys Lett. 83, 192 (2003).

[35] B. Streetman and S. Banerjee, *Solid State Electronic Devices*, 5th ed., (Prentice Hall, Upper Saddle River, USA, 2000).

[36] I. Langmuir, J. Am. Chem. Soc. 39, 1848 (1917).

[37] D. Zerulla, in *Encyclopedia of Nanoscience and Nanotechnology*, edited by H. Nalwa, Vol. 9 (American Scientific Publishers, Stevenson Ranch, USA, 2004).

[38] A. Ulman, An Introduction to Ultrathin Organic Films: From Langmuir-Blodgett to Self-Assembly, (Academic Press, Boston, USA, 1991).

[39] K. Blodgett, J. Am. Chem. Soc. 57, 1007 (1935).

[40] W. Bigelow, E. Glass, and W. Zisman, J. Colloid Sci. 1, 513 (1946).

[41] E. Shafrin and W. Zisman, J. Colloid Sci. 4, 571 (1949).

[42] P. Laibinis, B. Palmer, S. Lee, and G. Jennings, in *Thin Films: Organic Thin Films and Surfaces*, edited by A. Ulman, Vol. 20 (Academic Press, San Diego, USA, 1995).

[43] W. Bigelow, E. Glass, and W. Zisman, J. Colloid Sci. 2, 563 (1947).

[44] F. Schulman and W. Zisman, J. Colloid Sci. 7, 465 (1952).

[45] R. Nuzzo and D. Allara, J. Am. Chem. Soc. 105, 4481 (1983).

[46] C. Bain, E. Troughton, Y. Tao, J. Evall, G. Whitesides, and R. Nuzzo, J. Am. Chem. Soc. 111, 321 (1989).

[47] K. Adlkofer, E. Duijs, F. Findeis, M. Bichler, A. Zrenner, E. Sackmann, G. Abstreiter, and M. Tanaka, Phys. Chem. Chem. Phys. 4, 785 (2002).

[48] T. Tanzer, P. Bohn, I. Roshchin, L. Greene, and J. Klem, Appl. Phys. Lett. 75, 2794 (1999).

[49] J. Love, L. Estroff, J. Kriebel, R. Nuzzo, and G. Whitesides, Chem. Rev. 105, 1103 (2005).

[50] Y. Gu, Z. Lin, R. Butera, V. Smentkowski, and D. Waldeck, Langmuir 11, 1849 (1995).

[51] O. Dassa, V. Sidorov, Y. Paz, and D. Ritter, J. Electrochem. Soc. 153, G91 (2006).

[52] C. McGuiness, D. Blasini, J. Masejewski, S. Uppili, O. Cabarcos, D. Smilgies, and D. Allara, ACS Nano, ACS Nano 1, 30 (2007).

[53] C. McGuiness, A. Shaporenko, C. Mars, S. Uppili, M. Zharnikov, and D. Allara, J. Am. Chem. Soc. 128, 5231 (2006).

[54] C. McGuiness, A. Shaporenko, M. Zharnikov, A. Walker, and D. Allara, J. Phys. Chem. C 111, 4226 (2007).

[55] X. Ding, K. Moumanis, J. Dubowski, L. Tay, N. Rowell, J. Appl. Phys. 99, 054701 (2006).

[56] X. Ding and J. Dubowski, Proc. of SPIE 5713 (SPIE, Bellingham, USA, 2005), 545.

[57] G. Marshall, F. Bensebaa, and J. Dubowski, J. Appl. Phys. 105, 094310 (2009).

[58] D. Wieliczka, X. Ding, and J. Dubowski, J. Vac. Sci. Technol. A 24, 1756 (2006).

[59] Q. Hang, F. Wang, P. Carpenter, D. Zemlyanov, D. Zakharov, E. Stach, W. Buhro, and D. Janes, Nano Lett. 8, 49 (2008).

[60] S Lodha, P Carpenter, D Janes, J. Appl. Phys. 99, 024510 (2006).

[61] Y. Ye, A. Wong, and U. Krull, Proc. of SPIE 5969, 59690L (2005).

[62] X. Ding, K. Moumanis, J. Dubowski, E. Frost, and E. Escher, Appl. Phys. A 83, 357 (2006).

[63] B. Kobrin and J. Chinn, Russian Vacuum Technology Journal 16, 133 (2006).

[64] P. Holloway and G. McGuire, eds., Handbook of Compound Semiconductors: Growth, Processing, Characterization, and Devices, (Noyes Publications, Park Ridge, USA, 1995).

[65] O. Voznyy and J. Dubowski, J. Phys. Chem. B 110, 23619 (2006).

[66] O. Voznyy and J. Dubowski, J. Phys. Chem. C 112, 3726 (2008).

[67] S. Donev, N. Brack, N. Paris, P. Pigram, N. Singh, and B. Usher, Langmuir 21, 1866 (2005).

[68] G. Urban, Meas. Sci. Technol. 20, 012001 (2009).

[69] P. Prasad, *Introduction to Biophonotics*, (Wiley-Interscience, Hoboken, USA, 2003).

[70] L. Gorton, ed., *Biosensors and Modern Biospecific Analytical Techniques*, Vol. 40 (Elsevier, Amsterdam, The Netherlands, 2005).

[71] A. Rasooly and K. Herold, eds., *Biosensors and Biodetection: Methods and Protocols*, Vol. 503 (Humana Press, New York, USA, 2009).

[72] F. Schreiber, Prog. Surf. Sci. 65, 151 (2000).

[73] A. Ulman, ed., *Thin Films: Self-Assembled Monolayers of Thiols*, Vol. 24 (Academic Press, San Diego, USA, 1998).

[74] A. Ulman, *Characterization of Organic Thin Films*, (Butterworth-Heinemann, Stoneham, USA, 1995).

[75] Wafer Technology Ltd, 34 Maryland Road., Tongwell, Milton Keynes, Bucks, MK15 8HJ, United Kingdom, http://www.wafertech.co.uk/.

[76] R. LaPierre, B. Robinson, and D. Thompson, Appl. Surf. Sci. 90, 437 (1995).

[77] W. Ranke, J. Finster, and H. Kuhr, Surf. Sci. 187, 112 (1987).

[78] S. Lunt, G. Fiyba, P. Santangelo, and N. Lewis, J. Appl. Phys. 70, 7449 (1991).

[79] T. Baum, S. Ye, and K. Uosaki, Langmuir 15, 8577 (1999).

[80] Sigma-Aldrich, 3050 Spruce Street, St. Louis, MO 63103, USA, http://www.sigmaaldrich.com/.

[81] Millipore, 290 Concord Road, Billerica, MA 01821, USA, http://www.millipore.com/.

[82] R. Driad, Z. Lu, S. Laframboise, D. Scansen, W. McKinnon, and S. McAlister, Jpn. J. Appl. Phys 38, 1124 (1999).

[83] S. Adachi and D. Kikuchi, J. Electrochem. Soc. 147, 4618 (2000).

[84] Vacuum Atmospheres Company, 4652 W Rosecrans Ave., Hawthorne, CA 90250, USA, http://www.vac-atm.com/.

[85] Y. Ke, S. Milano, X. Wang, N. Tao, and Y. Darici, Surf. Sci. 415, 29 (1998).

[86] O. Dannenberger, M. Buck, and M. Grunze, J. Phys. Chem. B 103, 2202 (1999).

[87] D. Karpovich, H. Schessler, and G. Blanchard, in *Thin Films: Self-Assembled Monolayers of Thiols*, edited by A. Ulman, Vol. 24 (Academic Press, San Diego, USA, 1998).

[88] K. Adlkofer, W. Eck, M. Grunze, and M. Tanaka, J. Phys. Chem. B 107, 587 (2003).

[89] Veeco Instruments Inc., Terminal Drive, Plainview, NY 11803, USA, http://www.veeco.com/.

[90] Veeco, Application Note No. 3/98 (online), September 1998, (http://www.veeco.com/pdfs/appnotes/98sept_ahs_78.pdf) (accessed September 13, 2008).

[91] N. Razek, K. Otte, T. Chasse, D. Hirsch, A. Schindler, F. Frost, and B. Rauschenbach, J. Vac. Sci. Technol. A 20, 1492 (2002).

[92] D. Zerulla and T. Chasse, Langmuir 18, 5392 (2002).

[93] M. Ohring, *Materials Science of Thin Films*, 2nd ed., (Academic Press, San Diego, USA, 2002).

[94] J. Siepmann and I. McDonald, in *Thin Films: Self-Assembled Monolayers of Thiols*, edited by A. Ulman, Vol. 24 (Academic Press, San Diego, USA, 1998).

[95] G. Barnes and I. Gentle, *Interfacial Science – An Introduction*, (Oxford University Press, Oxford, UK, 2005).

[96] G. Liu, S. Xu, and S. Cruchon-Dupeyrat, in *Thin Films: Self-Assembled Monolayers of Thiols*, edited by A. Ulman, Vol. 24 (Academic Press, San Diego, USA, 1998).

[97] G. Friedbacher, in *Surface and Thin Film Analysis*, edited by H. Bubert and H. Jenett, (Wiley-VCH, Weinheim, Germany, 2002).

[98] D. Schroder, *Semiconductor Material and Device Characterization*, 2nd ed., (John Wiley and Sons, New York, USA, 1998).

[99] K. Westra and D. Thomson, J. Vac. Sci. Technol. B 13, 344 (1995).

[100] E. Gadelmawla, M. Koura, T. Maksoud, I. Elewa, and H. Soliman, J. Mater. Process. Technol. 123, 133 (2002).

[101] Olympus, Japan, http://probe.olympus-global.com/en/.

[102] J. Pankove, *Optical Processes in Semiconductors*, (Dover Publications, Inc., New York, USA, 1975).

[103] L. Pavesi and M. Guzzi, J. Appl. Phys. 75, 4779 (1994).

[104] Sciencetech Inc., 60 Meg Drive, London, ON N6E 3T6, Canada, http://www.sciencetech-inc.com/.

[105] H. Tompkins and W. McGahan, *Spectroscopic Ellipsometry and Reflectometry*, (Wiley-Interscience, New York, USA, 1999).

[106] H. Tompkins, *A User's Guide to Ellipsometry*, (Academic Press, Boston, USA, 1993).

[107] R. Azzam and N. Bashara, *Ellipsometry and Polarized Light*, (North-Holland Publishing Company, Amsterdam, The Netherlands, 1977).

[108] J. A. Woollam Co., Inc., 645 M Street, Suite 102, Lincoln, NE 68508-2243, USA, http://www.jawoollam.com/.

[109] B. Ratner and D. Castner, in *Surface Analysis – The Principal Techniques*, edited by J. Vickerman and I. Gilmore, 2nd ed. (John Wiley and Sons, Chichester, UK, 2009).

[110] D. Briggs and J. Grant, eds., *Surface Analysis by Auger and X-ray Photoelectron Spectroscopy*, (John Wiley and Sons, Chichester, UK, 2003).

[111] V. Nefedov, *X-ray Photoelectron Spectroscopy of Solid Surfaces*, (VSP BV, Zeist, The Netherlands, 1988).

[112] H. Bubert and J. Riviere, in *Surface and Thin Film Analysis*, edited by H. Bubert and H. Jenett, (Wiley-VCH, Weinheim, Germany, 2002).

[113] Casa Software Ltd., http://www.casaxps.com/.

[114] A. Ulman, ed., Thin Films: Organic Thin Films and Surfaces: Directions for the Nineties, Vol. 20 (Academic Press, San Diego, USA, 1995).

[115] H. Budz and R. LaPierre, J. Vac. Sci. Technol. A 26, 1425 (2008).

[116] O. Nakagawa, S. Ashok, C. Sheen, J. Martensson, and D. Allara, Jpn. J. Appl. Phys. 30, 3759 (1991).

[117] A. Green, W. Spicer, J. Vac. Sci. Technol. 11, 1061 (1993).

[118] A. Zangwill, *Physics at Surfaces*, (Cambridge University Press, Cambridge, UK, 1988).

[119] E. Yoon, R. Gottscho, V. Donnelly, and H. Luftman, Appl. Phys. Lett. 60, 2681 (1992).

[120] R. Gottscho, B. Preppernau, S. Pearton, A. Emerson, K. Giapis, J. Appl. Phys. 68, 440 (1990).

[121] R. Hey, I. Gorbunova, M. Ramsteiner, M. Wassermeier, L. Daweritz, and K. Ploog, J. Cryst. Growth 175-176, 1167 (1997).

[122] A. Abdelghani, Mater. Lett. 50, 73 (2001).

[123] F. Bordi, M. Prato, O. Cavalleri, C. Cametti, M. Canepa, and A. Gliozzi, J. Phys. Chem. B 108, 20263 (2004).

[124] J. Shi, B. Hong, A. Parikh, R. Collins, D. Allara, Chem. Phys. Lett. 246, 90 (1995).

[125] L. Richter, C. Yang, P. Wilson, C Hacker, R. van Zee, J. Stapleton, D. Allara, Y. Yao, and J. Tour, J. Phys. Chem. B 108, 12547 (2004).

[126] S. Mark, N. Sandhyarani, C. Zhu, C. Campagnolo, and C. Batt, Langmuir 20, 6808 (2004).

[127] S. Lodha, D. Janes, Fourth IEEE Conference on Nanotechnology, (2004 IEEE-NANO proceedings, USA) p. 278.

[128] H. Fujiwara, *Spectroscopic Ellipsometry: Principles and Applications*, (John Wiley and Sons, Chichester, UK, 2007).

[129] C. Bain, J. Evall, and G. Whitesides, J. Am. Chem. Soc. 111, 7155 (1989).

[130] G. Bruno, P. Capezzuto, and M. Losurdo, Vacuum 57, 189 (2000).

[131] M. Kang and H. Park, Jpn. J. Appl. Phys. 40, 4454 (2001).

[132] S. Anantathanasarn, and H. Hasegawa, Appl. Surf. Sci. 190, 343 (2002).

[133] S. Arabasz, E. Bergignat, G. Hollinger, and J. Szuber, Vacuum 80, 888 (2006).

[134] C. Ashby, K. Zavadil, A. Baca, P. Chang, B. Hammons, and M. Hafich, Appl. Phys. Lett. 76, 327 (2000).

[135] K. Butcher, R. Egan, T. Tansley, and D. Alexiev, J. Vac. Sci. Technol. B 14, 152 (1996).

[136] M. Kang, J. Kim, and H. Park, Jpn. J. Appl. Phys. 39, 7003 (2000).

[137] S. Lunt, P. Santangelo, and N. Lewis, J. Vac. Sci. Technol. B 9, 2333 (1991).

[138] J. Dorsten, J. Maslar, and P. Bohn, Appl. Phys. Lett. 66, 1755 (1995).

[139] H. Ohno, M. Motomatsu, W. Mizutani, and H. Tokumoto, Jpn. J. Appl. Phys. 34, 1381 (1995).

[140] K. Remashan and K. Bhat, Thin Solid Films 342, 20 (1999).

[141] H. Budz, M. Biesinger, and R. LaPierre, J. Vac. Sci. Technol. B 27, 637 (2009).

[142] T. Hou, C. Greenlief, S. Keller, L. Nelen, and J. Kauffman, Chem. Mater. 9, 3181 (1997).

[143] C. Wagner, A. Naumkin, A. Kraut-Vass, J. Allison, C. Powell, and J. Rumble, NIST X-ray Photoelectron Spectroscopy Database, The Measurement Services Division of the National Institute of Standards and Technology [Online]. August 27, 2007, http://srdata.nist.gov/xps (accessed August 25, 2008).

[144] S. Ghosh, M. Biesinger, R. LaPierre, P. Kruse, J. Appl. Phys. 101, 114322 (2007).

[145] Y. Gu, and D. Waldeck, J. Phys. Chem. B 102, 9015 (1998).

[146] C. Hamilton, S. Hicks, B. Vogele, J. Marsh, and J. Aitchison, Electronics Letters 31, 1393 (1995).

[147] M. Yamada, Y. Ide, and K. Tone, Jpn. J. Appl. Phys. 31, L1157 (1992).

[148] M. Losurdo, P. Capezzuto, and G. Bruno, Thin Solid Films 313-314, 501 (1998).

[149] A. Chanda, S. Verma, and C. Jacob, Bulletin of Materials Science 30, 561 (2007).

[150] D. Gräf, M. Grundner, D. Lüdecke, and R. Schulz, J. Vac. Sci. Technol. A 8, 1955 (1990).

[151] J. Shin, K. Geib, and C. Wilmsen, J. Vac. Sci. Technol. B 9, 2337 (1991).

[152] H. Sik, Y. Feurprier, C. Cardinaud, G. Turban, and A. Scavenne, J. Electrochem. Soc. 144, 2106 (1997).

[153] I. Gouzman, M. Dubey, M. Carolus, J. Schwartz, and S. Bernasek, Surf. Sci. 600, 773 (2006).

[154] M. Rei Vilar, J. El Beghdadi, F. Debontridder, R. Artzi, R. Naaman, A. Ferraria, and A. Botelho do Rego, Surf. Interface Anal. 37, 673 (2005).

[155] M. Kuball, M. Kelly, P. Santos, and M. Cardona, Phys. Rev. B 50, 8609 (1994).

[156] G. Bruno, P. Capezzuto, and M. Losurdo, Phys. Rev. B 54, 17175 (1996).

[157] P. Snyder, N. Ianno, B. Wigert, S. Pittal, B. Johs, and J. Woollam, J. Vac. Sci. Technol. B 13, 2255 (1995).

[158] J. Fritz, E. Cooper, S. Gaudet, P. Sorger, and S. Manalis, Proceedings of the National Academy of Sciences (PNAS 2002), 99, 14142 (2002).

[159] J. Lu, G. Getz, E. Miska, E. Alvarez-Saavedra, J. Lamb, D. Peck, A. Sweet-Cordero, B. Ebert, R. Mak, A. Ferrando, J. Downing, T. Jacks, H. Horvitz, and T. Golub, Nature 435, 834 (2005).

[160] H. Berney, J. West, E. Haefele, J. Alderman, W. Lane, and J. Collin, Sensors and Actuators B 68, 100 (2000).

[161] S. Hashsham, L. Wick, J. Rouillard, E. Gulari, and J. Tiedje, Biosens. Bioelectron. 20, 668 (2004).

[162] M. Deen, M. Shinwari, and P. Selvaganapathy, Proc. 26th IEEE International Conference on Microelectronics (MIEL 2008), Nis, Serbia, 307 (2008).

[163] C. Berggren, P. Stalhandske, J. Brundell, and G. Johansson, Electroanalysis 11, 156 (1999)

[164] P. Bergveld, Sensors and Actuators A 56, 65 (1996).

[165] F. Seker, K. Meeker, T. Kuech, and A. Ellis, Chem. Rev. 100, 2505 (2000).

[166] H. Hasegawa, K. Taira, K. Sode, and K. Ikebukuro, Sensors 8, 1090 (2008).

[167] S. Balamurugan, A. Obubuafo, S. Soper, and D. Spivak, Anal. Bioanal. Chem. 390, 1009 (2008).

[168] A. Cheng, D. Sen, and H. Yu, Bioelectrochemistry 77, 1 (2009).

[169] S. Tombelli, M. Minunni, and M. Mascini, Biosens. Bioelectron. 20, 2424 (2005).

[170] S. Song, L. Wang, J. Li, J. Zhao, and C. Fan, TrAC Trends Anal. Chem. 27, 108 (2008).

[171] T. Mairal, V. Ozalp, P. Sanchez, M. Mir, I. Katakis, and C. O 'Sullivan, Anal. Bioanal. Chem. 390, 989 (2008).

[172] D. Proske, M. Blank, R. Buhmann, and A. Resch, Appl. Microbiol. Biotechnol. 69, 367 (2005).

[173] C. Hamula, J. Guthrie, H. Zhang, X. Li, and X. Le, TrAC Trends Anal. Chem. 25, 681 (2006).

[174] J. Lee, H. So, E. Jeon, H. Chang, K. Won, and Y. Kim, Anal. Bioanal. Chem. 390, 1023 (2008).

[175] N. Rupcich, W. Chiuman, R. Nutiu, S. Mei, K. Flora, Y. Li, and J. Brennan, J. Am. Chem. Soc. 128, 780 (2006).

[176] H. A. Budz, M. Ali, Y. Li, and R. R. LaPierre, accepted for publication on Apr. 7, 2010 in J. Appl. Phys.

[177] EMD Chemicals, 2695 North Sheridan Way, Suite 200, Mississauga, ON L5K 2N6, Canada, http://www.emdserono.ca/en/index_en.html.

[178] BioShop Canada Inc, 4060 Fairview Street, Burlington, ON L7L 4Y8, Canada, http://www.bioshopcanada.com/.

[179] Integrated DNA Technologies, 1710 Commercial Park, Coralville, IA 52241, Canada, http://www.idtdna.com/Home/Home.aspx.

[180] N. Tercero, K. Wang, P. Gong, and R. Levicky, J. Am. Chem. Soc. 131, 4953 (2009).

[181] C. Lee, P. Gong, G. Harbers, D. Grainger, D. Castner, and L. Gamble, Anal. Chem. 78, 3316 (2006).

[182] D. Aspnes and A. Studna, Phys. Rev. B 27, 985 (1983).

[183] T. Kuech, A. Ellis, R. Brainard, K. Kepler, D. Moore, E. Winder, and G. Lisensky, J. Chem. Educ. 74, 680 (1997).

[184] H. Budz, M. Biesinger, R. LaPierre, J. Vac. Sci. Technol. B 27, 637 (2009).

[185] C. Lin and D. Patel, Chem. Biol. 4, 817 (1997).

[186] K. Kepler, G. Lisensky, M.Patel, L. Sigworth, and A. Ellis, J. Phys. Chem. 99, 16011 (1995).

[187] D. Moore, K. Meeker, and A. Ellis, J. Am. Chem. Soc. 118, 12997 (1996).

[188] J. Israelachvili, *Intermolecular and Surface Forces*, 2nd ed., (Academic Press, New York, USA, 1992).

[189] H. Strathmann, Membrane Science and Technology Series, 9: Ion-Exchange Membrane Separation Processes, (Elsevier, Boston, USA, 2004).

[190] D. Landheer, G. Aers, W. McKinnon, M. Deen and J. Ranuarez, J. Appl. Phys. 98, 044701 (2005).

[191] J. Lyklema, *Fundamentals of Interface and Colloid Science*, Vol. II, (Academic Press, San Diego, USA, 1995).

[192] M. Hughes, Nanoelectromechanics in Engineering and Biology, (CRC Press, New York, USA, 2003).

[193] COMSOL Inc., 744 Cowper Street, Palo Alto, CA, 94301, USA, http://www.comsol.com/.

[194] R. Hollingsworth and J. Sites, J. Appl. Phys. 53, 5357 (1982).

[195] U. Keil, J. Hvam, S. Tautz, S. Dankowski, P. Kiesel, and G. Dohler, Appl. Phys. Lett. 70, 72 (1997).

[196] R. Aroca, *Surface-enhanced Vibrational Spectroscopy*, (John Wiley & Sons, Inc, Chichester, UK, 2006).

[197] M. Boyle, J. Mitra, and P. Dawson, Nanotechnology 20, 1 (2009).

[198] G. McEwen, F. Chen, and A. Zhou, Anal. Chim. Acta 643, 26 (2009).

[199] W. Zhao, W. Chiuman, J. Lam, S. McManus, W. Chen, Y. Cui, R. Pelton, M. Brook, and Y. Li, J. Am. Chem. Soc 130, 3610 (2008).

[200] L. Mohaddes-Ardabili, L. J. Martinez-Miranda, L. Salamanca-Riba, A. Christou, J. Silverman, W. Bentley, and M. Al-Sheikhly, J. Appl. Phys. 95, 6021 (2004).

[201] R. Brainard, C. Paulson, D. Saulys, D. Gaines, T. Kuech, and A. Ellis, J. Phys. Chem. B 101, 11180 (1997).

[202] E. Huang, M. Satjapipat, S. Han, and F. Zhou, Langmuir 17, 1215 (2001).

[203] A. Peterson, R. Heaton, and R. Georgiadis, Nucl. Acids Res. 29, 5163 (2001).

[204] D. Kim, Y. Jeong, H. Lyu, H. Park, H. Kim, J. Shin, P. Choi, J. Lee, G. Lim, and M. Ishida, Jpn. J. Appl. Phys. 42, 4111 (2003).

[205] W. Michel, T. Mai, T. Naiser, and A. Ott, Biophys. J. 92, 999 (2007).

[206] F. Fixe, H. Branz, N. Louro, V. Chu, D. Prazeres, and J. Conde, Nanotechnology 16, 2061 (2005).

[207] T. Sakata, M. Kamahori, and Y. Miyahara, Jpn. J. Appl. Phys. 44, 2854 (2005).

[208] T. Sakata, M. Kamahori, and Y. Miyahara, Mat. Sci. Eng. C 24, 827 (2004).

[209] M. Godin, P. Williams, V. Tabard-Cossa, O. Laroche, L. Beaulieu, R. Lennox, and Peter Grutter, Langmuir 20, 7090 (2004).

[210] M. Shinwari, M. Deen, and P. Selvaganapathy, IET Circuits Devices Syst. 2, 158 (2008).

[211] M. Shinwari and M. Deen, Processing of the IEEE Microsystems and Nanoelectronics Research Conference (MNRC 2008), 185 (2008).

[212] L. Bauer, N. Birenbaum, and G. Meyer, J. Mater. Chem. 14, 517 (2004).

[213] Z. Gao, A. Agarwal, A. Trigg, N. Singh, C. Fang, C. Tung, Y. Fan, K. Buddharaju, and J. Kong, Anal. Chem. 79, 3291 (2007).

[214] Private communication from Dr. Qiyin Fang: Dept of Engineering Physics, McMaster University.